

Evaluation of Primary Flight Display Enhancements for Improving General Aviation Safety

by

Daniel R. Craig

S.B., Aerospace Engineering
Massachusetts Institute of Technology, 2003

SUBMITTED TO THE DEPARTMENT OF AERONAUTICS AND ASTRONAUTICS
IN PARTIAL FULFILLMENT OF THE REQUIREMENTS FOR THE DEGREE OF

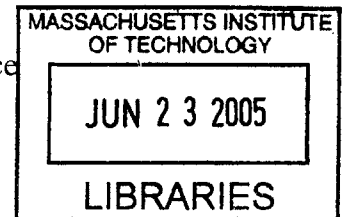
MASTER OF SCIENCE IN AERONAUTICS AND ASTRONAUTICS
AT THE
MASSACHUSETTS INSTITUTE OF TECHNOLOGY

2005 [unclear]

© 2005 Daniel R. Craig. All rights reserved.

The author hereby grants to MIT the permission to reproduce
and to distribute publicly paper and electronic
copies of this thesis document in whole or in part.

1st copy



Signature of Author: _____
Daniel R. Craig
Department of Aeronautics and Astronautics
May 2005

Certified by: _____
Prof. R. John Hansman
Professor of Aeronautics and Astronautics
Thesis Supervisor

Accepted by: _____
Prof. Jaime Peraire
Professor of Aeronautics and Astronautics
Chair, Committee on Graduate Students

EVALUATION OF PRIMARY FLIGHT DISPLAY ENHANCEMENTS FOR IMPROVING GENERAL AVIATION SAFETY

by

Daniel R. Craig and R. John Hansman

Abstract

The information architecture of general aviation cockpits is shifting from one of independent mechanical instruments to one of digital sensors, common databuses, and liquid crystal displays. This integrated architecture presents an opportunity to improve general aviation safety through enhancements to the flight display utilizing the data, computing power, and display capabilities available on a modern integrated cockpit.

A study of general aviation accident causes identified takeoff and climbout, stall, and spatial disorientation as potential root causes that could be addressed with enhancements to the Primary Flight Display of an integrated general aviation cockpit. To address these accident causes, four prototype enhancements were designed, implemented on a PFD, and flight tested in a single-engine general aviation aircraft.

A Takeoff Performance Monitor prototype demonstrated the usefulness of automating the published takeoff distance calculation required of, but seldom performed by, pilots and also showed that performance deficiencies as small as a 10% reduction in power can be detected within the first few seconds immediately after throttle-up. The prototype was also able to predict takeoff distance in real-time within 200 feet by 55 knots using a simple acceleration model.

A Dynamic Stall and V-Speeds prototype calculated stall speeds, best angle of climb speed, best rate of climb speed, and best glide speed given the current flight conditions and marked them on the airspeed indicator. Subject pilots reported the speeds aided in maintaining awareness of stall margin and optimal performance conditions.

An Angle of Attack Estimator that used a speed-based method and an angle-based method to compute the angle of attack using only the data available on the PFD without additional sensors was prototyped along with two means of display; a traditional angle of attack gauge and a Pitch Limit Indicator. Both estimator methods were compared to an angle of attack vane during a series of maneuvers. It was shown that a speed-based angle of attack estimator along with the pitch limit indicator is a useful stall avoidance aid.

Finally, an Unusual Attitude Alerting prototype provided specific verbal cues over the intercom when pitch or roll limits were exceeded to aid a pilot in recovery from unusual attitudes. Subject pilots preferred alerts that commanded the recovery maneuver over alerts that informed the pilot of the attitude but left the recovery procedure to the pilot, and preferred both to alerts that simply told the pilot to recover without specific information about the attitude.

Thesis Supervisor: R. John Hansman

Title: Professor of Aeronautics and Astronautics

Acknowledgements

This work was supported by the National Aeronautics and Space Administration/Federal Aviation Administration Joint University program under grant number FAA 95-G-017 and by the Avidyne Corporation. The authors wish to thank the participants in the program for their valuable feedback and advice.

The authors would also like to thank Steve Jacobson, Chris Fay, Ryan Berk, and Michael McPartland of Avidyne Corp. for their insight and guidance in designing and developing enhancements on a PFD. Thanks also to Mike Keirnan of Avidyne and Erik Kohlman of Florida Institute of Technology for their guidance and assistance in flight testing. Thanks also to Dave Rathbun of Cirrus Design Corp., Tony DiLemma of Forte RTS, and Elbie Mendenhall of EM Aviation, LLC for their assistance in designing and building an angle of attack vane. Lastly, thanks to Miriam Lezak of Avidyne and Jennie Lott for their assistance in editing and proofreading.

Table of Contents

CHAPTER 1	INTRODUCTION	15
1.1	EVOLUTION OF THE COCKPIT INFORMATION ARCHITECTURE	15
1.2	FLIGHT ACCIDENT TRENDS AND OPPORTUNITIES FOR IMPROVEMENT	18
1.2.1	<i>Stall Accidents</i>	19
1.2.2	<i>Takeoff and Climbout Accidents</i>	20
1.2.3	<i>Spatial Disorientation</i>	21
CHAPTER 2	THESIS OVERVIEW	23
2.1	BASELINE SYSTEM	23
2.2	PROTOTYPE FEATURES	25
2.3	FLIGHT TEST IMPLEMENTATION	27
2.4	FLIGHT TEST EVALUATIONS	29
CHAPTER 3	TAKEOFF PERFORMANCE MONITOR.....	33
3.1	ANATOMY OF A TAKEOFF	33
3.1.1	<i>Phases of a Takeoff</i>	34
3.1.2	<i>Acceleration and Speed in the Ground Roll</i>	35
3.2	TAKEOFF ACCIDENT CAUSES.....	37
3.2.1	<i>Exceeding Performance Limits</i>	38
3.2.2	<i>Deficient Performance Takeoff</i>	39
3.3	PREVIOUS TAKEOFF SAFETY METHODS.....	41
3.3.1	<i>Previous Takeoff Performance Monitor Research</i>	42
3.4	PROTOTYPE TAKEOFF PERFORMANCE MONITOR DESIGN	44
3.4.1	<i>Prototype Takeoff Performance Monitor Architecture</i>	44
3.4.2	<i>Runway Selector</i>	46
3.4.3	<i>Published Takeoff Distance</i>	46
3.4.4	<i>Real-time Takeoff Prediction</i>	47
3.4.5	<i>Takeoff Monitor Display Design</i>	48
3.5	TAKEOFF PERFORMANCE MONITOR FLIGHT TESTS.....	50
3.6	FLIGHT TEST RESULTS.....	51
3.6.1	<i>Examples of Data Plots</i>	52
3.6.2	<i>Published Takeoff Distances</i>	55
3.6.3	<i>Observing Steady Deficiencies Through Acceleration</i>	56
3.6.4	<i>Observing Discrete Deficiencies Through Acceleration</i>	58
3.6.5	<i>Real-time Takeoff Distance Prediction</i>	59
3.6.6	<i>Reconstructed Takeoff Distance Predictor</i>	61
3.7	CONCLUSIONS.....	65
CHAPTER 4	DYNAMIC STALL AND V-SPEEDS.....	67
4.1	SPEEDS RELEVANT TO FLIGHT	67
4.1.1	<i>Stall Speed</i>	67
4.1.2	<i>Climb Speeds</i>	69
4.1.3	<i>Best Glide Speed</i>	72
4.2	EXISTING V-SPEED INDICATORS.....	74
4.3	PROTOTYPE V-SPEED SYSTEM DESIGN.....	75
4.3.1	<i>Stall Speeds</i>	75
4.3.2	<i>Climb and Glide Speeds</i>	77
4.4	V-SPEED FLIGHT TESTS	77
4.5	FLIGHT TEST RESULTS	78

4.5.1	<i>Dynamic Stall Speed Maneuvers</i>	79
4.5.2	<i>Climb Speed Maneuvers</i>	88
4.5.3	<i>Glide Speed Maneuvers</i>	89
4.6	CONCLUSIONS	90
CHAPTER 5 ANGLE OF ATTACK ESTIMATOR		93
5.1	ANGLE OF ATTACK AND STALL	93
5.2	PREVIOUS ANGLE OF ATTACK SYSTEMS	94
5.3	PROTOTYPE ANGLE OF ATTACK ESTIMATORS	95
5.3.1	<i>Speed-based Estimator</i>	95
5.3.2	<i>Angle-based Estimator</i>	97
5.4	PROTOTYPE ANGLE OF ATTACK DISPLAYS	99
5.5	ANGLE OF ATTACK FLIGHT TESTS	100
5.6	FLIGHT RESULTS	101
5.6.1	<i>Constant Speed, Constant Altitude</i>	101
5.6.2	<i>Acceleration and Deceleration at Constant Altitude</i>	102
5.6.3	<i>Power-off Stalls and Slow Flight</i>	104
5.6.4	<i>Abrupt Pull Up/Push Down</i>	108
5.6.5	<i>Steep Turns</i>	108
5.6.6	<i>Chandelle</i>	109
5.6.7	<i>Lazy-8</i>	110
5.6.8	<i>Pilot Feedback on the Pitch Limit Indicator and AOA Gauge</i>	111
5.7	CONCLUSION	112
CHAPTER 6 UNUSUAL ATTITUDE ALERTING		113
6.1	SPATIAL DISORIENTATION	113
6.2	AUDIO ALTERING	115
6.3	PROTOTYPE UNUSUAL ATTITUDE ALERTING	116
6.4	UNUSUAL ATTITUDE ALERTING FLIGHT TESTS	117
6.5	FLIGHT TEST RESULTS	118
6.5.1	<i>Unusual Attitude Maneuvers</i>	118
6.5.2	<i>Pilot Feedback</i>	121
6.6	CONCLUSION	121
CHAPTER 7 SUMMARY OF CONCLUSIONS		123
APPENDIX A – PREVIOUS TAKEOFF MONITOR DISPLAYS		125
WORKS CITED		127

List of Figures

Figure 1: Cockpit information architecture of the “Steam Gauge Era” 16

Figure 2: Early generation integrated cockpit architecture..... 16

Figure 3: Data architecture in an integrated glass cockpit..... 17

Figure 4: Next generation integrated cockpit architecture..... 18

Figure 5: Fatal Stall/Spin Accident Phases of Flight, 1991-2000 [2]..... 19

Figure 6: Altitudes of Fatal Stall Spin Accidents, 1991-2000. 80% of all stall/spin accidents occur at or below traffic pattern altitude, 1000 ft AGL [2]..... 20

Figure 7: Accident causes for single-engine fixed-gear in 2002 [3]..... 21

Figure 8: VFR Spatial Disorientation Accidents from 1994-2003, sorted by Meteorological Conditions, Day/Night, and Pilot’s Instrument Rating [6]..... 22

Figure 9: Baseline Avidyne Primary Flight Display..... 24

Figure 10: Prototype Display Components..... 26

Figure 11: Flight Test System Setup..... 27

Figure 12: Screenshot of the flight test telemetry software 28

Figure 13: Experimental Cirrus SR22 N753CD used for test flights, with angle of attack vane mounted on the boom of a modified wingtip 29

Figure 14: The five forces acting on an airplane during takeoff..... 34

Figure 15: The five phases of a takeoff⁶ 34

Figure 16: Acceleration as speed increases during the phases of takeoff..... 36

Figure 17: Takeoff Accident Causes, 2000 [9]..... 37

Figure 18: Pilot’s Operating Handbook takeoff distance table for a Cirrus SR22 at 3400 pounds gross weight..... 39

Figure 19: Consistent loss of acceleration during a takeoff ground roll..... 40

Figure 20: Discrete loss in acceleration during a takeoff ground roll..... 41

Figure 21: Real-time Takeoff Performance Monitor Architecture 45

Figure 22: Runway Selector scoring algorithm 46

Figure 23: Real-time takeoff distance prediction method..... 47

Figure 24: Predicting the acceleration at rotation based on current speed and acceleration 48

Figure 25: Takeoff Monitor in four situations. 1) POH values displayed, but no real-time prediction yet 2) Real-time prediction marked by inverted "V" 3) Runway flashes yellow for Caution 4) Runway flashes red for Warning..... 50

Figure 26: Takeoff 1, Distance vs. Time Plot..... 52

Figure 27: Takeoff 1, Airspeed and Ground Speed vs. Time Plot..... 53

Figure 28: Takeoff 1, Acceleration vs. Airspeed Plot 54

Figure 29: Takeoff 1, Acceleration vs. Time Plot 55

Figure 30: Actual takeoff distances for each steady power takeoff with the published takeoff distance for the wind reported before the takeoff..... 56

Figure 31: Acceleration plots for 100%, 90%, and 70% power settings 57

Figure 32: Peak accelerations for steady power takeoffs, two for each power setting 58

Figure 33: Discrete drop in power at 50 KCAS..... 59

Figure 34: GPS positions recorded when the aircraft was at the hold short line for runway 9L 60

Figure 35: Position and Predicted Liftoff Distance vs. Time plot for 90% Power, Steady, Takeoff 4.....	62
Figure 36: Distance vs. Time plot for 60% Power, Steady, Takeoff 5.....	63
Figure 37: Position and Predicted Takeoff Distances during discrete performance deficiency takeoff.....	64
Figure 38: Difference between Predicted Distances and Actual Takeoff Distances vs. the airspeed when the predictions were made during all ten steady power takeoffs. By 55 KCAS, the predicted distance is generally within 200 feet of the actual takeoff distance.	65
Figure 39: During a turn, more lift is required to support the weight and the centripetal force.	68
Figure 40: Flaps-down stall speed increasing with bank angle	69
Figure 41: V-Speeds in the Cirrus SR22 Pilot's Operating Handbook	70
Figure 42: V-Speeds for a Cirrus SR22 changing over density altitude, at maximum gross weight, as interpolated from the pilot's operating handbook. Best Glide Speed, V_G , does not change with density altitude.	72
Figure 43: Published Best Glide Speeds from a Cirrus SR22 Pilot's Operating Handbook	72
Figure 45: Traditional mechanical airspeed indicator with stall and structural speeds painted on.....	74
Figure 46: Stall and Structural Speeds on an electronic airspeed tape.	74
Figure 47: Dynamic Stall and V-Speed System Design	75
Figure 48: Increased stall speeds during a steep turn. Stall speed for landing configuration, V_{so} , is shown at the top of the red arc, and stall speed in clean configuration, V_s , is shown at the bottom of the green arc.....	76
Figure 49: 1) Best Rate of Climb Speed, V_Y , and Best Angle of Climb Speed, V_X 2) Best Glide Speed, V_G	77
Figure 50: Airspeed and Stall Speeds in Slow Flight for Subject 4. Airspeed is the dotted line, flaps-up stall speed is the upper line based on 70 KCAS, and the flaps-down stall speed is the lower line based on 59 KCAS.	79
Figure 51: Airspeed and Stall Speeds during slow flight for Subject 5.....	81
Figure 52: Airspeed and Stall Speeds during slow flight for Subject 6.....	81
Figure 53: Two steep turns with fixed stall speeds displayed only, no dynamic stall speeds.....	82
Figure 54: Two steep turns with dynamic stall speeds displayed.....	83
Figure 55: Steep turn in slow flight, static stall speeds displayed only, Subject 5.....	84
Figure 56: Steep turn in slow flight, dynamic stall speeds displayed, Subject 5.....	84
Figure 57: Two steep turns, both with dynamic stall speed displayed, Subject 6.....	85
Figure 58: Two chandelles performed by Subject 4, the first with only static stall speeds, the second with the dynamic stall speed displays.....	86
Figure 59: Chandelles with only static stall speed and with dynamic stall speeds for subject 5.....	87
Figure 60: Speed During Takeoff and Climbout for Subject 6.....	88
Figure 61: Airspeed and Best Glide Speed during simulated engine-out, Subject 5.....	89
Figure 62: Airspeed and Best Glide Speed during simulated engine-out, Subject 4.....	90

Figure 63: Lift Coefficient vs. Angle of Attack and the critical angle of attack where stall occurs	94
Figure 64: The Lift method estimates the angle of attack by determining how much lift is required	96
Figure 65: The Angle AOA method finds the geometric difference between the direction the aircraft is pointed and the direction the aircraft is moving	97
Figure 66: 1) Traditional-design angle of attack indicator 2) Pitch Limit Indicator	99
Figure 67: Adjusted vane and estimator outputs at constant altitude, constant speeds ..	102
Figure 68: Constant altitude acceleration from slow flight to maximum level cruise, followed by deceleration until power-off stall.....	103
Figure 69: Power-off stall, flaps up.	104
Figure 70: Slow flight and two power-off stalls with flaps up	105
Figure 71: Close-up of two power-off stalls after slow flight with flaps up.....	106
Figure 72: Slow Flight, Flaps Down.....	107
Figure 73: Power-off Stall in slow flight, full flaps down.....	107
Figure 74: Two pull up/push down maneuvers, flaps up.....	108
Figure 75: Two steep turns, flaps up.....	109
Figure 76: Chandelle, flaps up.....	110
Figure 77: Lazy-8, flaps up.....	111
Figure 78: Unusual Attitude Alerter System Design	116
Figure 79: 1) Informing alert 2) Commanding alert	117
Figure 80: Default Unusual Attitude Alert, Subject 4	118
Figure 81: Command Unusual Attitude Alert, Subject 4.....	119
Figure 82: Inform Unusual Attitude Alert, Subject 4	120
Figure 83: An analog Go/No Go acceleration-based indicator, reproduced in [12].....	125
Figure 84: Khatwa's TOPM display, reproduced in [12].....	125
Figure 85: NASA Langley's TOPM to be displayed on the HSI. Left side is what is displayed while accelerating, right side is displayed if braking [29].....	126

List of Tables

Table 1: Tests pilots involved in study 30
Table 2: Flight Test Protocols..... 31
Table 3: Takeoff Performance Monitor Flight Test Power Settings..... 51
Table 4: V-Speeds Flight Test Maneuvers..... 78
Table 5: Angle of Attack Flight Test Maneuvers 100

List of Acronyms

ADAHRS	Air Data and Attitude Heading Reference System
ADI	Attitude Direction Indicator
AHRS	Attitude Heading Reference System
AOA	Angle of Attack
AOPA	Aircraft Owners and Pilots Association
ASI	Airspeed Indicator
FTE	Flight Test Engineer
GPS	Global Positioning System
HSI	Horizontal Situation Indicator
IFR	Instrument Flight Rules
IMC	Instrument Meteorological Conditions
KCAS	Knots Calibrated Airspeed
KIAS	Knots Indicated Airspeed
KMLB	Melbourne International Airport
MFD	Multi-Function Display
NASA	National Aeronautics and Space Administration
PFD	Primary Flight Display
PIC	Pilot-In-Command
PLI	Pitch Limit Indicator
POH	Pilot's Operating Handbook
RMS	Root Mean Square
SAE	Society of Automotive Engineers
TOPM	Takeoff Performance Monitor
USB	Universal Serial Bus
V_{FE}	Maximum Flaps Extended Speed
V_G	Best Glide Speed
V_{NE}	Never Exceed Speed
V_{NO}	Maximum Structural Cruising Speed
V_{S0}	Flaps-down Stall Speed
V_{S1}	Flaps-up Stall Speed

V _X	Best Angle of Climb Speed
V _Y	Best Rate of Climb Speed
VFR	Visual Flight Rules
VMC	Visual Meteorological Conditions
VSI	Vertical Speed Indicator
WAAS	Wide Area Augmentation System

Chapter 1 Introduction

The information architecture of general aviation cockpits is evolving toward centralized databuses and liquid crystal displays, presenting an opportunity to utilize the information, processing power, and display capability of the Primary Flight Display (PFD) to improve general aviation safety. Accident data for general aviation showed *Stall, Takeoff and Climbout*, and *Spatial Disorientation* are accident causes that can be addressed by several prototype primary flight display enhancements.

1.1 Evolution of the Cockpit Information Architecture

Since the 1990's, advances in information technology have been changing the information architecture of general aviation aircraft [1]. Historically, aircraft relied on independent mechanical and electrical instruments for monitoring systems, navigating, and communicating. Vacuum pumps drove mechanical gyroscopes for determining orientation. Mechanical pressure sensors fed directly by the pitot-static system measured speed and altitude and were displayed independently on "steam gauge" dials. Tuning to radio navigation aids helped the pilot triangulate position on a paper chart. In an abstract sense, the flight data were all sensed, interpreted, and displayed independently, as shown in Figure 1, leaving the integration to the mind of the pilot.

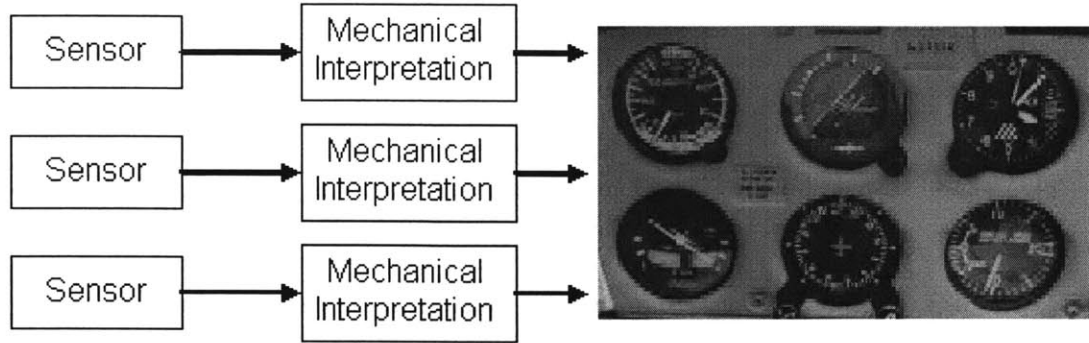


Figure 1: Cockpit information architecture of the “Steam Gauge Era”¹

Starting in the 1970’s, electronic flight information systems in the cockpit began displacing the independent mechanical model, first in commercial aviation and more recently in general aviation, as the cost and weight of microprocessors, liquid crystal displays, electronic sensors have dramatically fallen. Standardized databuses were developed that facilitated the sharing of flight information across the instruments. Figure 2 shows how these databuses led to a new information architecture, where all of the sensor data are accumulated into a single flight information databus. The display systems then retrieve their data and display it to the pilot.

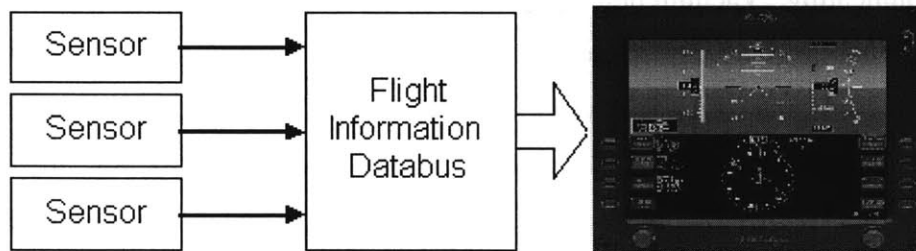


Figure 2: Early generation integrated cockpit architecture²

Figure 3 shows the typical architecture of a current generation integrated flight information system for general aviation. In this architecture, air data as well as attitude angles, rates, and accelerations are available from on-board solid-state sensors. GPS, navigation, and communication are accessible through external instruments. Engine data, such as power, speed, and temperatures, are available from sensors in the power plant. Finally, satellite datalink opens a new opportunity to find information previously

¹ Instrument image from [6]

² PFD image from www.avidyne.com

inaccessible, such as weather conditions, forecasts, uploaded flight plans, and two-way communication.

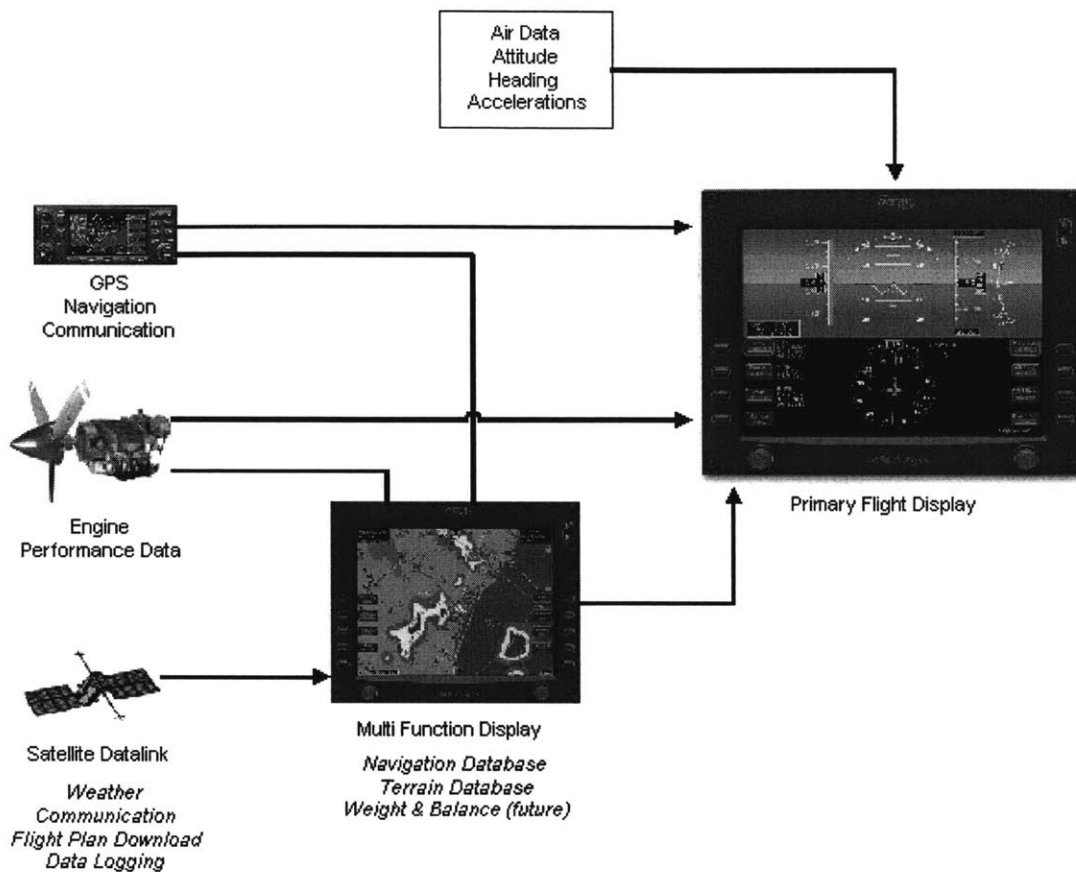


Figure 3: Data architecture in an integrated glass cockpit³

While the displays used for maintaining flight control in “glass cockpits” have remained fairly consistent with their mechanical predecessors and commercial aircraft conventions, integrated electronic cockpits have already set precedents for the type of innovation that can occur by accumulating, processing, and displaying various data. Airborne navigation has seen substantial advances with moving maps, plotted flight plans, and other information specifically tailored to the pilot’s immediate needs. This information is accumulated from various flight data and navigation databases and

³ GPS image from <http://www.garmin.com/products/gns430/>, Engine image from <http://www.professionalpilot.ca/aerodynamics/performance/power.htm>, Satellite image from <http://www.dnr.state.wi.us/org/water/fhp/lakes/selfhelp/forvolunteers.htm>, PFD and MFD images from www.avidyne.com

displayed electronically. The primary displays for maintaining flight control and safety, however, have not seen the same level of innovation. Most of the flight control and safety research has been focused on head-up-displays and synthetic vision systems such as “highway in the sky” and not as much on enhancements of the traditional primary head-down instruments.

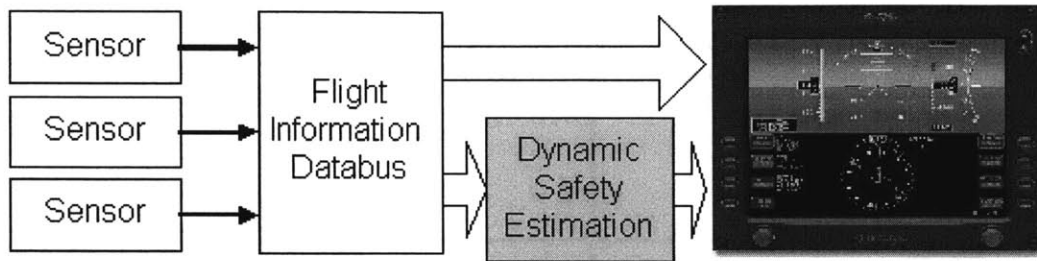


Figure 4: Next generation integrated cockpit architecture⁴

An opportunity now exists to take additional advantage of the current information, processing power, and display capability available in the modern integrated cockpit to improve general aviation safety with enhancements to the primary flight display. Without adding the cost of additional sensors, it is possible to enhance the current integrated system with additional safety features targeted to general aviation safety issues.

1.2 Flight Accident Trends and Opportunities for Improvement

In order to identify key opportunities for improving general aviation safety, historical accident data was studied to identify accident causes that might be addressed on a PFD. It was determined that *Stall, Takeoff and Climbout*, and *Spatial Disorientation* were potential candidates for cockpit information safety systems.

All three are critical aspects of flight that produce the bulk of accidents, both fatal and non-fatal. They are also good candidates for new features of the Primary Flight Display, to which the scope of research was narrowed. Furthermore, while efforts have been made to bring improved weather and navigation information into the cockpit, relatively few primary safety enhancements addressing these accident causes have made

⁴ PFD image from www.avidyne.com

their way to commercial implementation. Although landing accidents were not pursued explicitly, stalls in the traffic pattern and on approach account for a large portion of landing accidents, so addressing stall accidents indirectly addresses many landing accidents as well.

1.2.1 Stall Accidents

In a study of general aviation accidents from 1993-2001, approximately 10% of all accidents involve stall [2]. Stall accidents, however, tend to result in fatalities more often than other types of accidents, accounting for 13.7% of all fatal accidents. Twenty-eight percent of all stall accidents are fatal, compared to just 20% of all general aviation accidents.

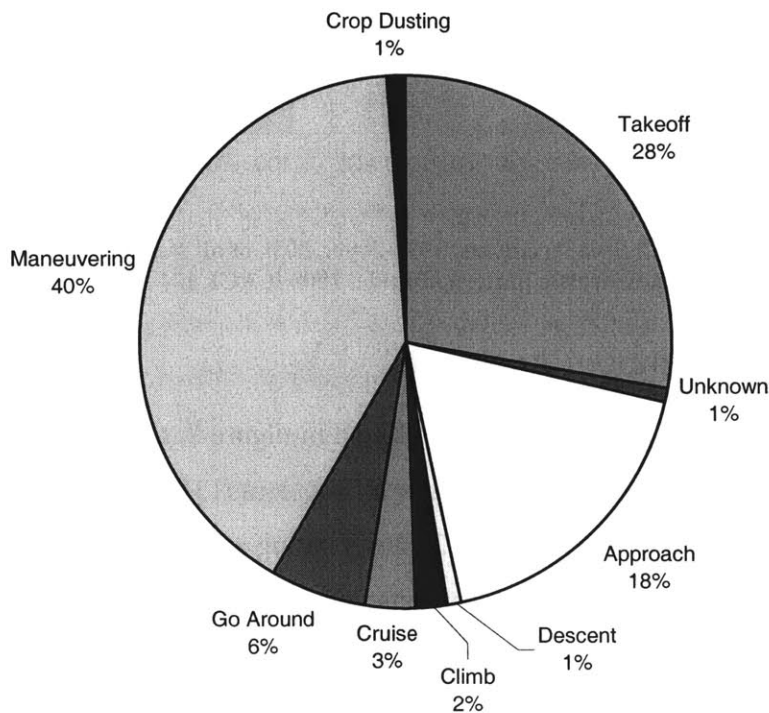


Figure 5: Fatal Stall/Spin Accident Phases of Flight, 1991-2000 [2]

As shown in Figure 5, stall accidents occur in all phases of flight, but primarily in maneuvering flight, takeoff, and approach. Clearly, the takeoff and approach phases tend to be lower in altitude, thus leaving the pilot with less margin for recovery. In fact, as

seen in Figure 6, almost all stall accidents, between 80-90%, occur at or below 1,000 feet above ground level.

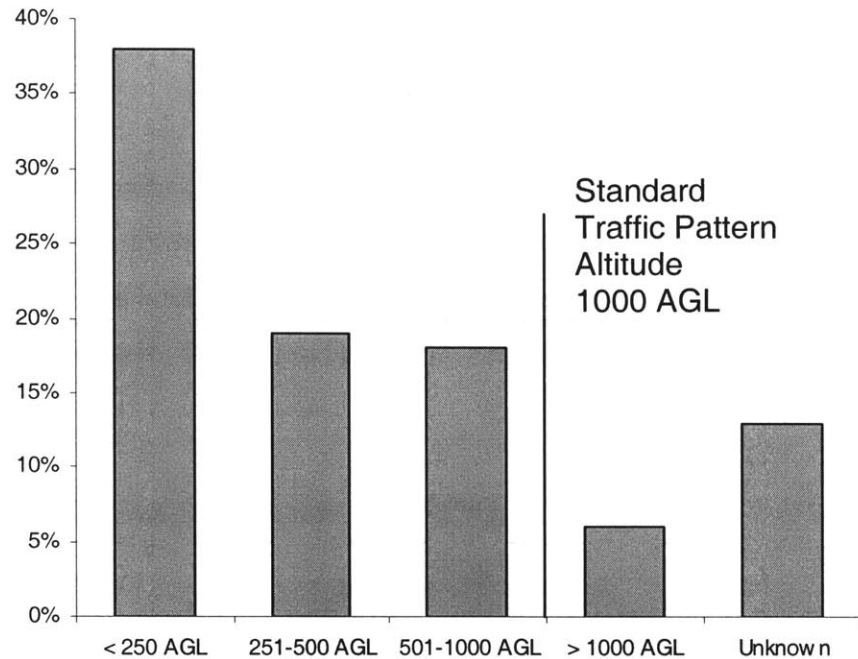


Figure 6: Altitudes of Fatal Stall Spin Accidents, 1991-2000. 80% of all stall/spin accidents occur at or below traffic pattern altitude, 1000 ft AGL [2]

1.2.2 Takeoff and Climbout Accidents

For general aviation accidents in 2002 plotted in Figure 7, takeoff, landing, and maneuvering flight made up nearly two thirds of all accidents [3]. While landing accounted for most of the total accidents, at 38.8%, landing accidents were relatively forgiving, causing only 3.3% of all fatal accidents. During takeoff, on the other hand, fatal and non-fatal accidents occurred at similar rates, at 17.9% of fatal accidents and 18.1% of all accidents. Accident data for the previous two years show the rate of fatal and non-fatal accidents have remained steady [3,4,5].

As previously noted, at least 80% of all stalls and spins occur at or below 1,000 feet above ground level, the standard pattern altitude. This indicates that a significant portion of these stall accidents are related to takeoffs and landings [2]. In fact, 28% of all fatal stall/spin accidents in that study occurred during takeoff.

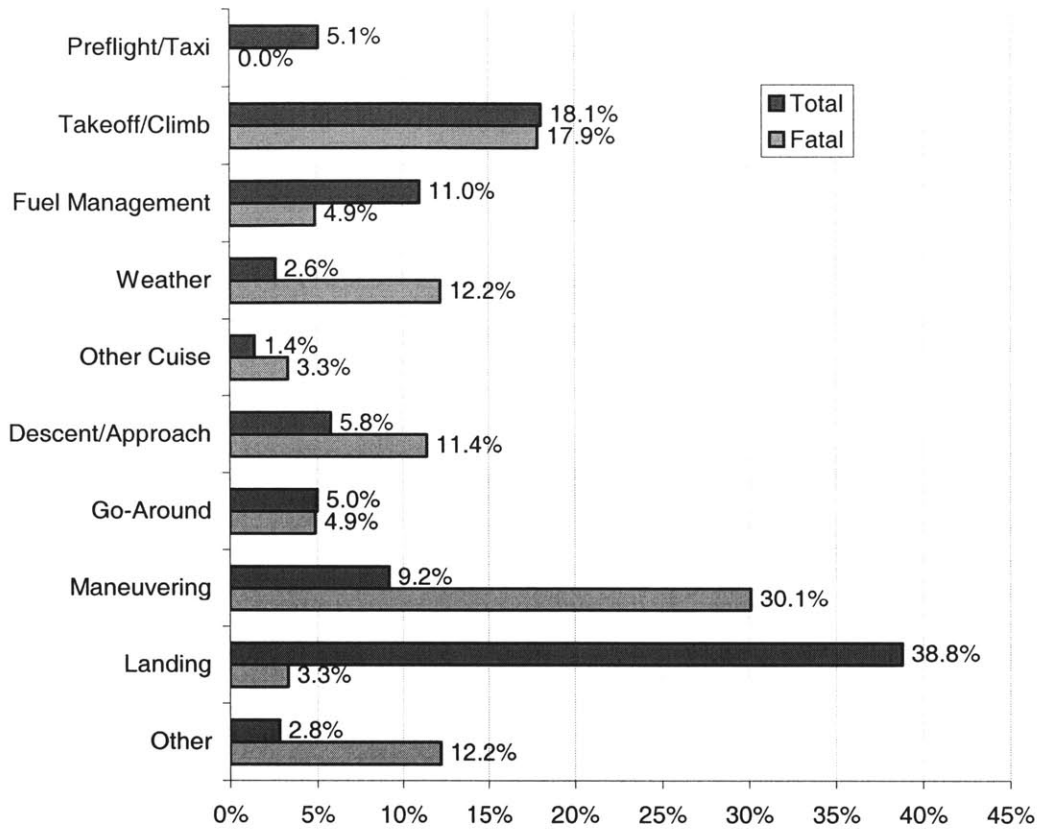


Figure 7: Accident causes for single-engine fixed-gear in 2002 [3]

1.2.3 Spatial Disorientation

Spatial disorientation is very rare, but when it does occur, it almost always results in a fatal crash. From 1994-2003, 184 of 202 spatial disorientation accidents (91%) were fatal [6].

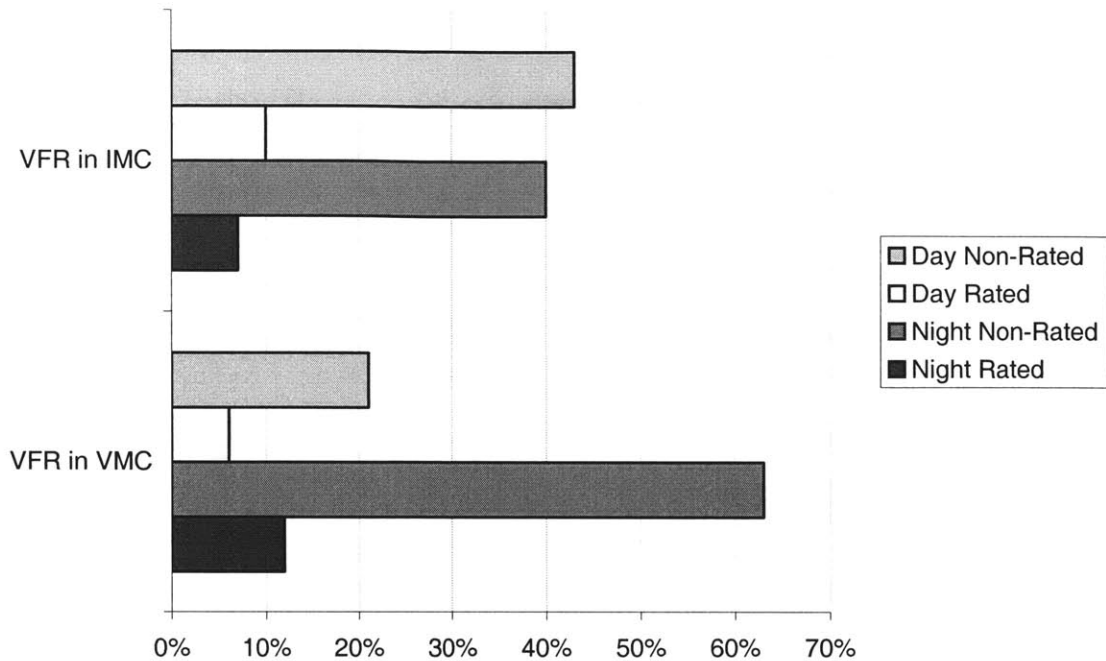


Figure 8: VFR Spatial Disorientation Accidents from 1994-2003, sorted by Meteorological Conditions, Day/Night, and Pilot's Instrument Rating [6]

The two primary causes of spatial disorientation are continued flying under visual flight rules (VFR) into instrument meteorological conditions (IMC), the leading cause of spatial disorientation at 41% of all spatial disorientation accidents, followed by disorientation in visual meteorological conditions (VMC) at 33% [6]. Figure 8 breaks down the VFR in IMC and VFR in VMC accidents by day and night as well as whether the pilot was instrument rated or not. About 75% of those VFR in VMC disorientation accidents occurred at night, when it is more difficult to see the horizon and pilots are more susceptible to optical and vestibular illusions.

Chapter 2 Thesis Overview

In order to address the accident causes discussed in Section 1.2, four new features were designed, implemented, and flight-tested on a baseline electronic Primary Flight Display (PFD), described in Section 2.1. The four features are a *Takeoff Performance Monitor*, *Dynamic Stall and V-Speeds*, an *Angle of Attack Estimator*, and *Unusual Attitude Alerting*. The design and evaluation of each of these features are summarized in Section 2.2 and more extensively treated in subsequent chapters.

To evaluate the new features implemented on the PFD, a test system was constructed to receive and record data from flight tests in an experimental Cirrus SR22. A laptop computer received and sent data to the PFD, and received GPS position from a handheld unit and angle of attack data from a reference vane added to the aircraft.

Flights using this test system were conducted to evaluate the safety features. Takeoffs under full and reduced power were performed to compare predicted takeoff distances to the actual takeoff distances. Pilots flew maneuvers in slow flight while avoiding stall to evaluate the usability of the dynamic stall speeds and the angle of attack displays. The angle of attack estimates in flight were compared to a reference vane. Finally, pilots performed simulated instrument unusual attitude recoveries using the unusual attitude alerting system.

2.1 Baseline System

The new safety features were integrated into a state of the art general aviation Primary Flight Display (PFD) shown in Figure 9. The PFD consists of the basic “T” of primary flight instruments:

- Artificial horizon, or Attitude Direction Indicator (ADI) stretching across the entire top of the screen
- Airspeed Indicator (ASI) tape to the left side of the ADI
- Altimeter tape to the right of the ADI

- Vertical Speed Indicator (VSI) to the right of the altimeter on the upper right hand side.
- Horizontal Situation Indicator (HSI) on the bottom center with the standard compass card as well as a moving map for overlaying flight plans.

Although a purely digital system, the PFD portrays the same information found in a purely mechanical system, with the exception of the moving map on the HSI.

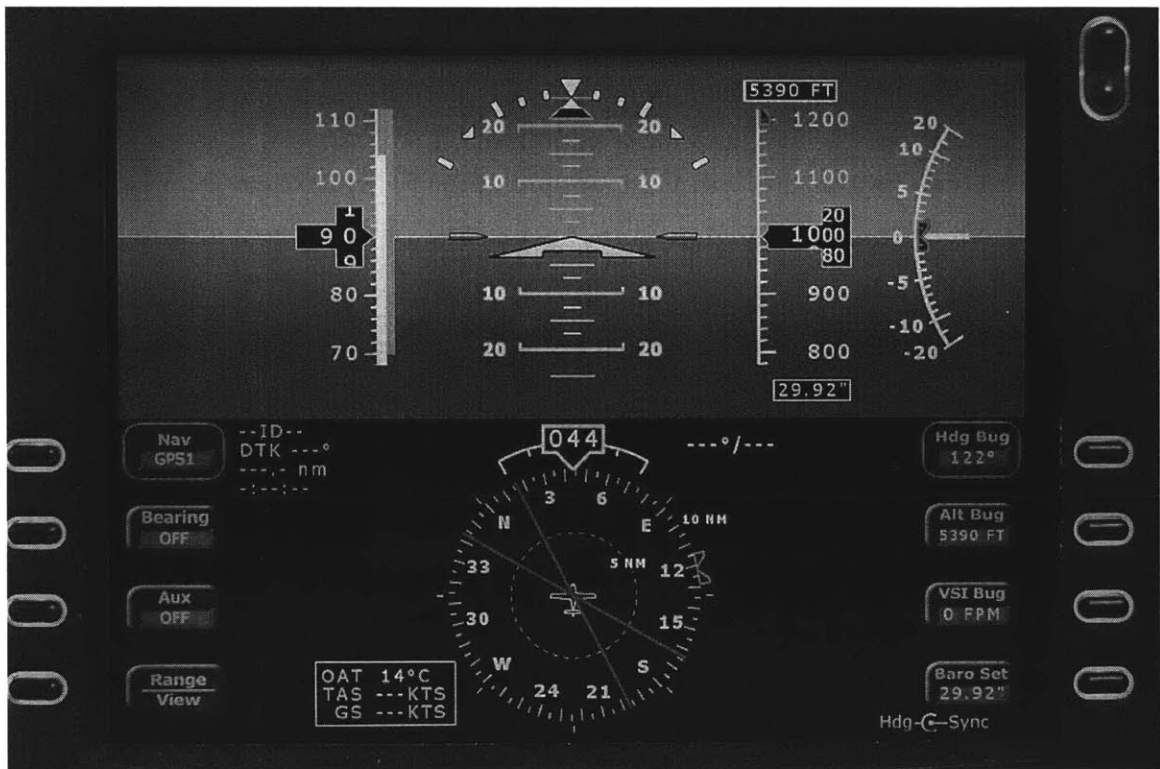


Figure 9: Baseline Avidyne Primary Flight Display

The PFD can access additional data from onboard databases as well as information from the databus. The system architecture of the PFD was designed to be amenable to adding new functionality.

At the core of the PFD is the Air Data and Attitude Heading Reference System (ADAHRS). The ADAHRS provides all the inertial and air data to the system. The inertial data (AHRS), is composed of the attitude angles, angular rates in all three directions of rotation, and accelerations in all three of the body axes. The AHRS updates

at 33 Hz. The air data updates slightly slower, at 8 Hz, and provides true and calibrated airspeeds, vertical speed, barometric altitude, and temperature.

The PFD also receives information from external devices. GPS data comes over an ARINC 429 databus from a Garmin GNS-430. The PFD thus has access to GPS position, in latitude and longitude, as well as GPS altitude and ground speed. The GPS updates approximately once per second, and is capable of using the enhanced accuracy of the Wide Area Augmentation System (WAAS).

Other data sources are being considered for future implementation in the PFD or were otherwise unavailable for use, so they were simulated in this prototype. For example, engine data functionality exists but was unavailable on the system used in this prototype, so the engine data system was used to simulate and control aspects of the prototype displays.

Currently, the PFD is not integrated with the Multi-Function Display's (MFD's) satellite datalink system. However, as the electronic cockpit becomes more closely integrated, that capability will become available. It is assumed for these prototypes that the MFD is accessible, and that existing data, like weather information and navigation databases, can be sent to the PFD, as well as future-planned data, like weight and balance. For these prototypes, the data are either hard-coded into the PFD or input manually through an external laptop connected to the PFD.

2.2 Prototype Features

Integrated into the baseline PFD displays are four prototype features whose visual displays are shown in Figure 10.

A *Takeoff Performance Monitor* looks up published takeoff distances, observes acceleration performance during takeoff, and predicts future performance based on achieved results. The TOPM is situated to the immediate left of the airspeed indicator. The design of the *Takeoff Performance Monitor* is detailed in Chapter 3.

A *Dynamic Stall and V-Speeds* feature calculates stall speeds, climb speeds, and best glide speed given the current flight conditions and marks them on the airspeed indicator. The *Dynamic Stall and V-Speeds* design is described in Chapter 4.

An *Angle of Attack Estimator* uses one of two different methods to compute the angle of attack that require only the data available of the PFD without additional sensors. These angle of attack estimates can then be shown in two ways; either on a traditional angle of attack gauge, situated to the lower right of the airspeed indicator, or on a Pitch Limit Indicator on the ADI. The *Angle of Attack Estimator* design can be found in Chapter 5.

Finally, *Unusual Attitude Alerting* provides specific verbal cues to aid a pilot in recovery from unusual attitudes. Alert messages are played over the intercom when pitch or roll limits are exceeded. *Unusual Attitude Alerting* is described in Chapter 6.

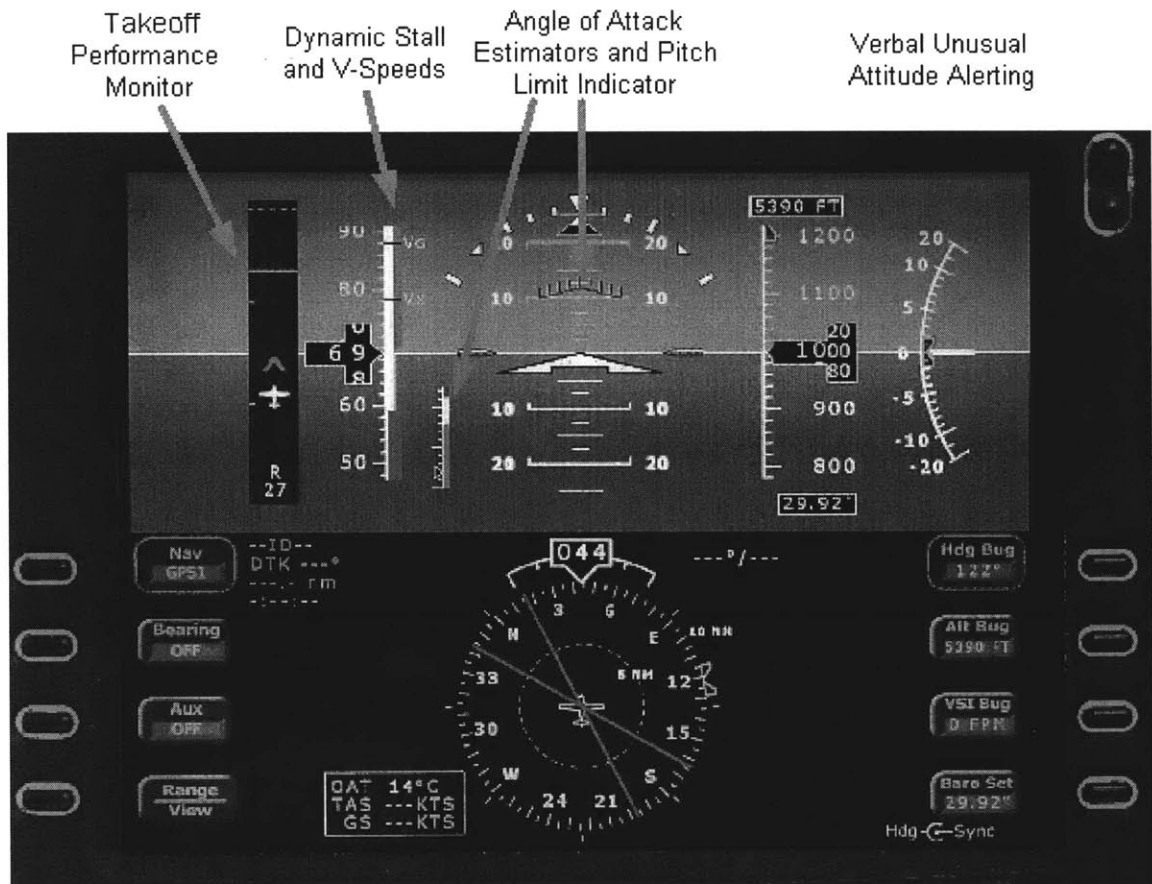


Figure 10: Prototype Display Components

2.3 Flight Test Implementation

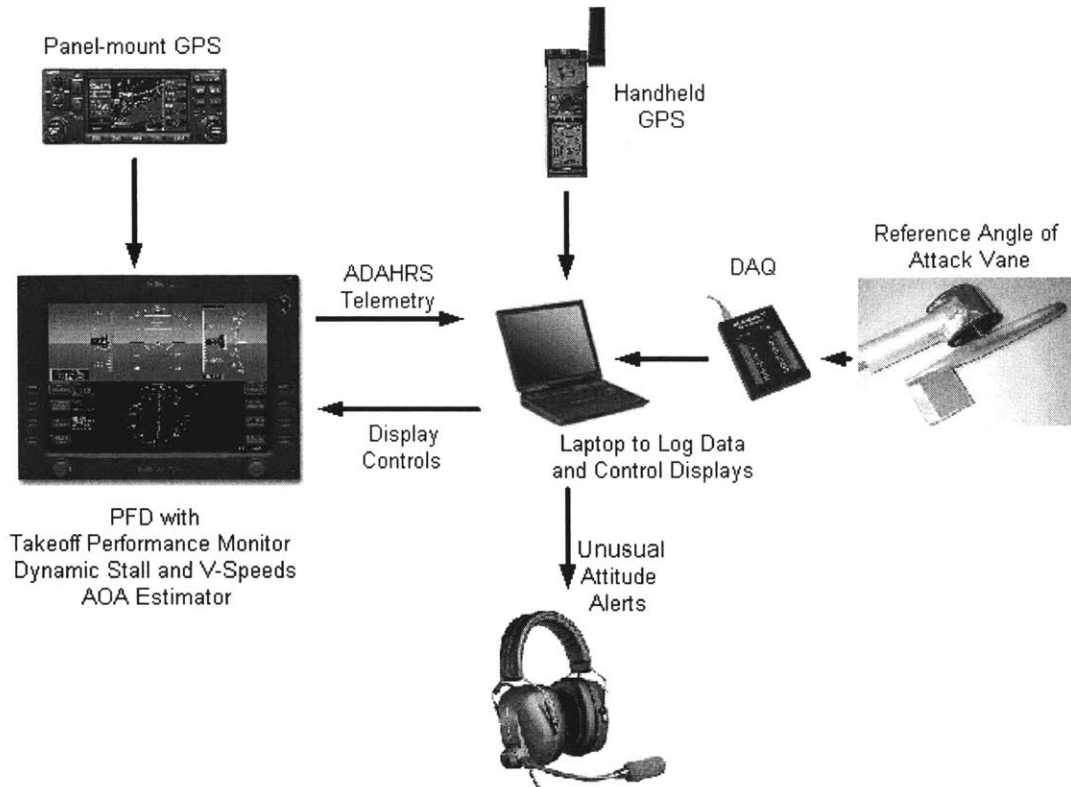


Figure 11: Flight Test System Setup⁵

In order to evaluate the prototype features incorporated in the PFD, a flight test control and data recording system was developed, as depicted in Figure 11. A laptop computer served as the central hub of the system, receiving and logging data from the PFD and other sensors, sending data to the PFD to simulate unavailable data and to control which displays are shown, and producing the unusual attitude alerts. The laptop software also served as an event logger to record time-tagged events during the test flights. A screenshot of the laptop software is shown in Figure 12.

⁵ Panel-mount GPS image from <http://www.garmin.com/products/gns430/>, Handheld GPS image from <http://www.garmin.com/products/gpsmap196/#>, Laptop image from <http://www.pcconnection.com/ProductDetail?sku=453081>, DAQ image from http://www.labjack.com/labjack_u12.html, Headphones image from http://www.aircraftspruce.com/menus/av/headsets_sennheiser.html, PFD image from www.avidyne.com

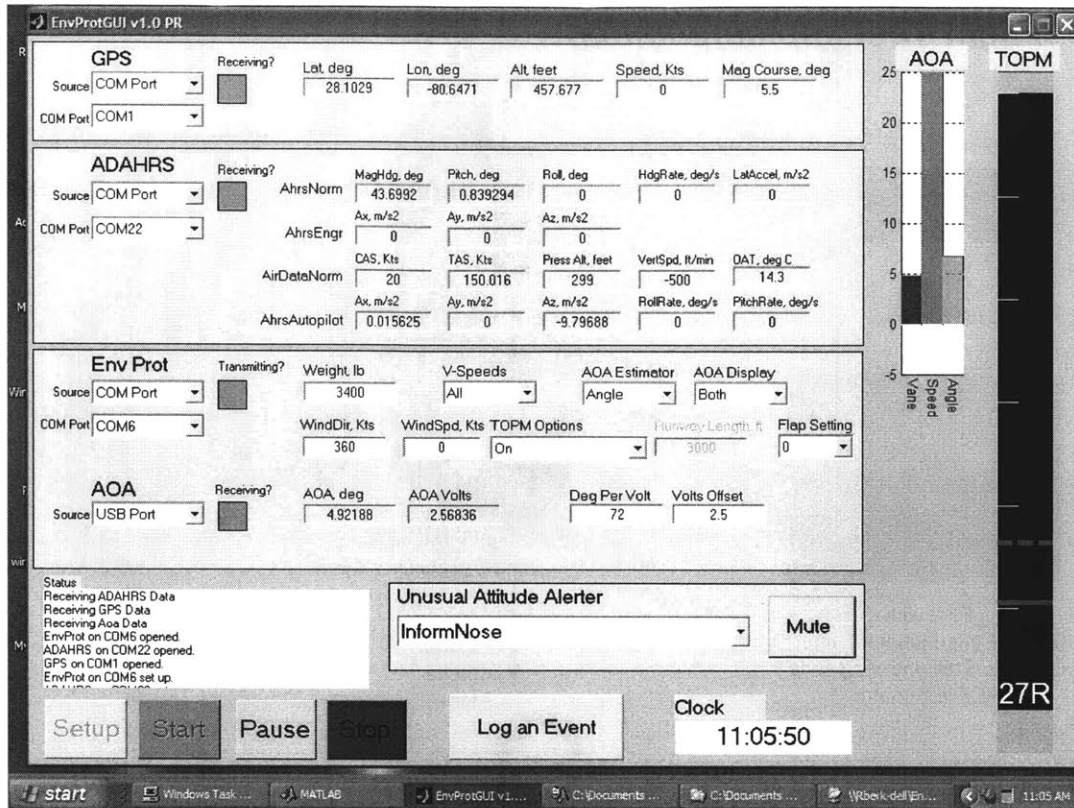


Figure 12: Screenshot of the flight test telemetry software

The PFD receives ADAHRS data from its self-contained sensors, obtains GPS from the panel-mounted Garmin GNS-430 over the ARINC 429 databus, and receives engine data over an RS-232 serial port. The engine data port on the PFD was used to input unavailable data, such as weight and wind, as well as to control which displays were shown on the screen.

The PFD outputs only the ADAHRS data over a serial port, which was captured on the laptop computer. Since the laptop was not equipped with ARINC 429 hardware to capture the GNS-430 GPS data, a secondary handheld GPS unit sent data to the laptop to be recorded.

Since the PFD did not have the capability to output other data such as the outputs of the prototype features, the laptop also duplicated all the calculations of the prototype features using the ADAHRS data from the PFD and the GPS data from the handheld unit. Similarly, because the PFD had no audio interface, the unusual attitude alerts were

produced on the laptop using ADAHRS telemetry and output to the intercom via the headphone jack.

In order to evaluate the accuracy of the angle of attack estimators, a reference angle of attack vane was constructed and mounted on a carbon fiber boom extending from the leading edge of a modified wingtip. The vane data was digitized with a resolution of 0.7° by a LabJack U12 data acquisition board and sent to the laptop through a USB port.

2.4 Flight Test Evaluations

In order to evaluate the safety features, two sets of flight tests were conducted to explore technical and usability issues. All flights were made from Melbourne International Airport (KMLB), in Melbourne, Florida in experimental Cirrus SR22 N754CD, shown in Figure 13. This section provides an overview of the flight test methodology and process. The specific tests and results from the flight tests are reported in the individual chapter for each feature.



Figure 13: Experimental Cirrus SR22 N753CD used for test flights, with angle of attack vane mounted on the boom of a modified wingtip

N753CD is a standard Cirrus SR22 operating under an experimental ticket for use in developing and demonstrating new avionics systems. For these flight tests, a stock PFD with a special software build was installed in the aircraft. In addition to the PFD,

the right wingtip was replaced with a wingtip modified with a carbon fiber boom that extended three feet forward from the leading edge to hold the angle of attack vane.

In all, six pilots with varying flying experience and exposure to the new features flew test flights. The pilots ranged from former military pilots and Certified Flight Instructors to recent private pilots. All the pilots and their experience level are listed below in Table 1.

Table 1: Tests pilots involved in study

Pilot	Hours	Rating	Experience
1	1600	Commercial Multi-engine	Test Pilot
2	3000	CFI ATP Multi-engine	Test pilot Flight Instructor
3	3000	Commercial Multi-engine	Former A-10 pilot PFD System Engineering Manager
4	200	Private Pilot	Engineer Some instrument training No exposure to prototype features before flight
5	400	Instrument Rating	Engineer No exposure to prototype features before flight
6	85	Private Pilot	Designed and implemented the prototype features

Two types of flights were conducted that determined the crew configuration. For technical demonstrations and evaluations, the flight test crew consisted of two people: a Pilot-In-Command (PIC) and a Flight Test Engineer (FTE) to operate the laptop. For flights involving usability tests, a Subject Pilot flew from the left seat while final authority and responsibility for safety remained with the PIC sitting right seat.

The first set of flights, an initial look and shakedown of the system, took place on January 25-26, 200. The actual data gathering flights took place on April 6-8, 2005. Three different test protocols were used during six flights, as described in Table 2.

Table 2: Flight Test Protocols

Protocol	Crew	Objective
1	PIC FTE	Demonstrate AOA Estimators and compare them to the reference vane
2	PIC FTE	Demonstrate Takeoff Performance Monitor under full and partial power
3	PIC Subject FTE	Acquire subjective feedback on Dynamic V-Speeds, AOA Estimators, and Unusual Attitude Alerting

Test Protocol 1 demonstrated the Angle of Attack Estimators. The results and conclusions regarding the Angle of Attack Estimators are detailed in Section 5.6.

Test Protocol 2 demonstrated the Takeoff Performance Monitor under full power, partial power, and a sudden loss of power. The Takeoff Performance Monitor results and conclusions can be found in Section 3.6.

Test Protocol 3 was repeated three times, allowing several pilots to fly the system through maneuvers in slow flight attempting to avoid stall and also recovering from unusual attitudes induced by disorientation under simulated instrument conditions. Results pertaining to the Dynamic Stall and V-Speeds can be found in Section 4.5, while Unusual Attitude Alerting can be found in Section 6.5.

Chapter 3 Takeoff Performance Monitor

A *Takeoff Performance Monitor* was designed and implemented on a PFD to address two fundamental causes of takeoff accidents: exceeding the performance limits of the aircraft and performance deficiencies. The takeoff monitor addresses exceeding performance limits by automating the published performance calculations normally required to be performed by the pilot before each takeoff. Performance deficiencies are addressed by the real-time liftoff distance predictor that uses achieved performance at the beginning of the takeoff to predict the performance of the remainder.

In order to explain the takeoff monitor, the physics of a takeoff must be understood. Historical takeoff accident data was investigated to identify key causes. From those causes, the strategy for monitoring takeoff performance was developed. That strategy was then implemented on a PFD and flight tested.

It was shown that automating the published performance calculations was a simple and useful safety enhancement. It was also shown that performance deficiencies can be observed within the first few seconds of takeoff. Furthermore, a real-time takeoff distance predictor was able to predict the liftoff point within 200 feet by 55 knots using a simple constant average acceleration approximation.

3.1 Anatomy of a Takeoff

For every airplane, large or small, the same fundamental forces are at work, as shown in Figure 14. In the longitudinal direction, thrust propels the plane forward while drag and ground friction push backward. Vertically, lift pushes the plane up and the weight pulls it back down. Understanding how these five forces behave during the different phases of a takeoff allows one to understand, measure, and predict takeoff performance.

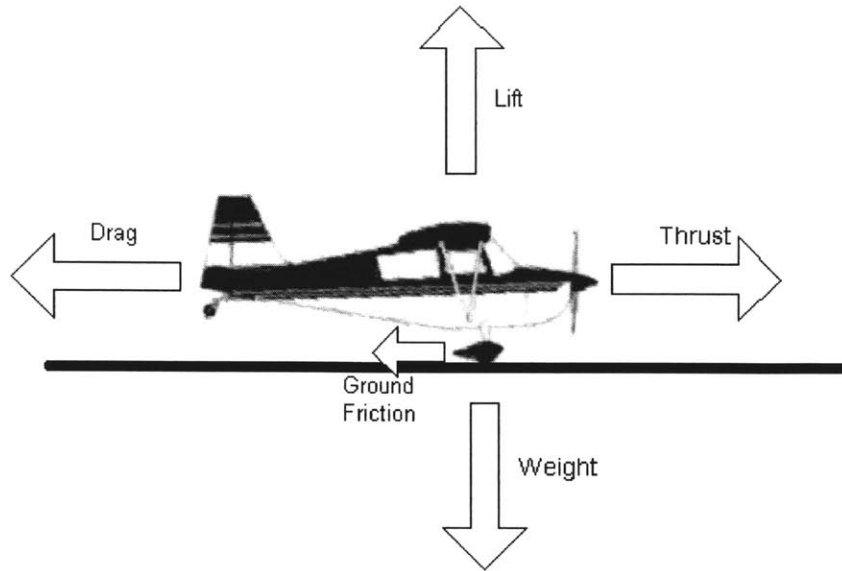


Figure 14: The five forces acting on an airplane during takeoff⁶

3.1.1 Phases of a Takeoff

A simple takeoff can be divided into five phases, as depicted in Figure 15. These phases are throttle-up, ground run, rotation, flight in ground effect, and finally, climbout. When the pilot opens the throttle, the engine goes from idle to maximum power. The propeller is stalled initially, but generates enough thrust to overcome the static friction between the wheels and the ground and the airplane begins to roll forward. As it starts to move, the propeller can take bigger bites out of the air and generate more thrust, while aerodynamic drag remains negligible because the airplane has not picked up much speed. Once the throttle is full open and the propeller is no longer stalled, the maximum amount of thrust possible is achieved at the same time that drag is still negligible. This results in a peak in the acceleration at the beginning of the ground run.

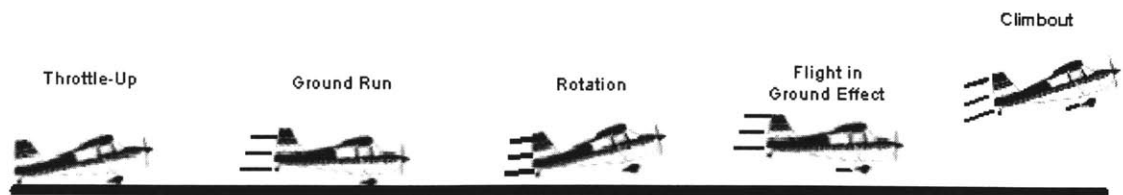


Figure 15: The five phases of a takeoff⁶

⁶ Aircraft modified image from <http://www.pilotfriend.com/aircraft%20performance/champion/gallery.htm>

With more thrust than drag, this net force pushes the airplane forward and accelerates it down the runway. As the airplane gains speed, the aerodynamic drag increases, reducing the net force and slowing the acceleration of the airplane. At the same time, a slight reduction in the ground friction results from the fact that the lift is beginning to support some of the aircraft's weight, relieving some of the weight supported by the landing gear.

The aircraft continues to accelerate to the rotation speed, at which the pilot applies back pressure and the aircraft lifts off the runway. While the aircraft is within one wingspan of the ground, it is considered in ground effect, accelerating in the absence of ground friction. Finally, with more back pressure, the pilot pitches the airplane up for a constant speed climbout. The angle of climbout is determined by the amount of excess thrust, or the difference between the thrust and the drag. The more excess thrust available, the more energy can be put into gaining altitude.

3.1.2 Acceleration and Speed in the Ground Roll

During the throttle-up and ground roll phases of a takeoff, the longitudinal acceleration peaks very early, then tapers off with the square of the speed as the drag reduces the net force on the airplane. Once the airplane is established on a constant speed climb, the longitudinal acceleration drops to zero. Figure 16 depicts how the acceleration changes as the speed increases during a takeoff. The peak acceleration and the consistent manner in which acceleration reduces during takeoff will be very useful in measuring takeoff performance and predicting liftoff distances in real-time.

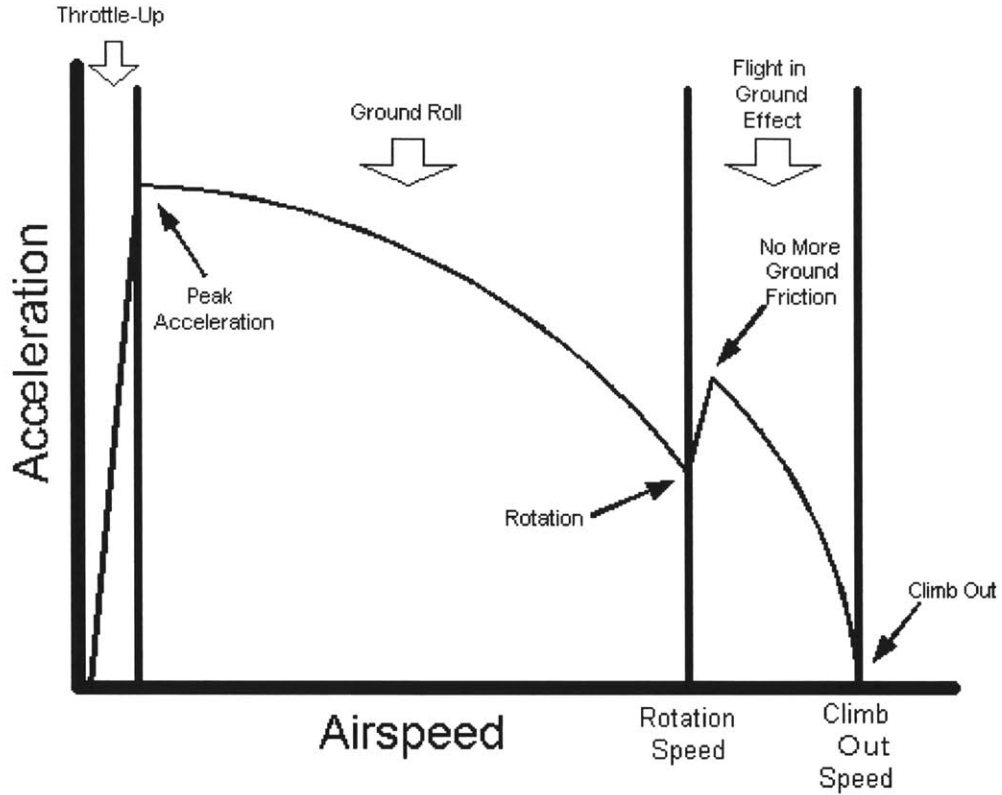


Figure 16: Acceleration as speed increases during the phases of takeoff

From peak acceleration until rotation, the acceleration during a takeoff can be modeled as a quadratic function of the airspeed. The constants of that acceleration equation are composed of performance constants; thrust, drag, ground friction, runway slope, and weight, as shown in Equation 1.

$$a(V_{air}) = \frac{g}{W} \left(T + W(\sin \phi - \mu) + (\mu C_L - C_D) \frac{1}{2} \rho_{\infty} S V_{air}^2 \right) \quad (1)$$

Equation 1 shows that if all of the performance constants are known, then the acceleration behavior of the aircraft is known and the takeoff distance can be predicted. Earlier takeoff monitors attempted to estimate each of those parameters individually, but Pinder, Crowe, and Nikiforuk showed how the parameters can be combined into a “lumped parameter model” as shown in Equation 2 [7].

$$a(V_{air}) = P_1 + P_2 V_{air} + P_3 V_{air}^2 \quad (2)$$

The lumped parameter model is useful because it eliminates the need to isolate thrust, drag, weight, and the other parameters. A real-time takeoff distance predictor need not determine what the thrust is. Instead, it must only determine the net affect all the parameters have on the acceleration equation as a whole.

A further simplification can be made by approximating a constant average acceleration during the course of a ground run, composed of the maximum acceleration at the end of the throttle-up and the acceleration at liftoff [8]. If this average acceleration during the takeoff is known, then the takeoff distance can be estimated.

3.2 Takeoff Accident Causes

A study by the AOPA Air Safety Foundation showed that 30.2% of all takeoff accidents from the years 1991-2000 resulted from loss of control, induced by failure to establish positive rate of climb, stalling, wind conditions, power loss, and other factors.

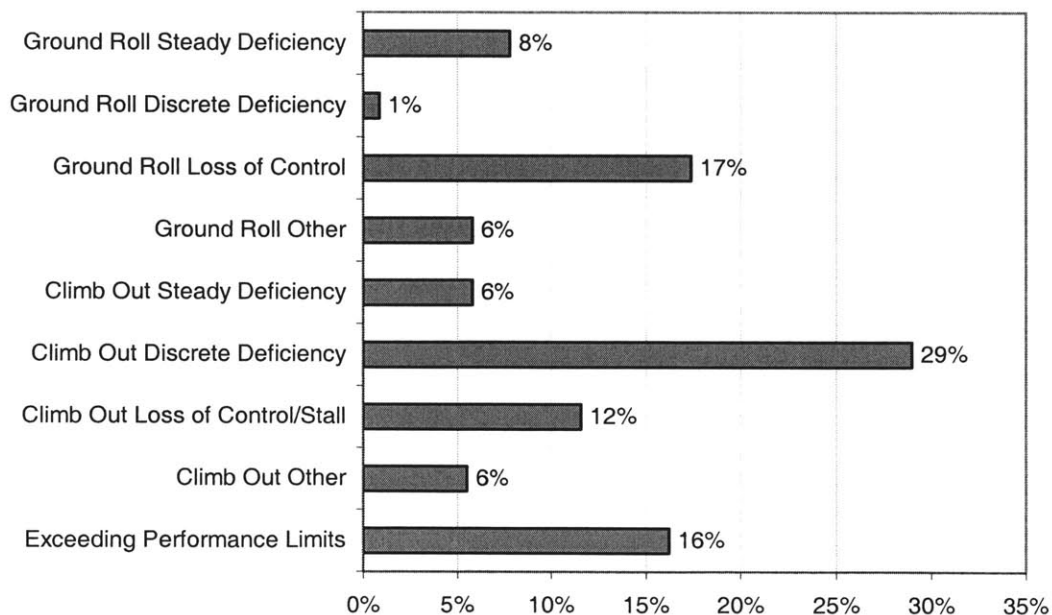


Figure 17: Takeoff Accident Causes, 2000 [9]

The takeoff accident data shown in Figure 17 demonstrates that, aside from loss of control by the pilot, the main accident causes are *exceeding the performance limits of the aircraft*, and *performance deficiencies*. Performance deficiencies can be broken

down into *steady deficiencies*, where performance is degraded steadily over the entire takeoff, and *discrete deficiencies*, where a discrete event during the takeoff degrades performance. Understanding these types of performance problems is crucial to design an effective takeoff performance monitor.

3.2.1 Exceeding Performance Limits

By exceeding the performance limits of the airplane, the pilot is attempting a takeoff that is impossible, even if the airplane performs like new and the pilot's technique is flawless. Essentially these accidents result from a lack of planning for the effect of varying conditions on takeoff performance. A pilot may neglect to check the density altitude, overload the aircraft beyond the maximum gross weight, attempt the takeoff with a tail wind, or not account for a sloped runway. In all these cases, the common failure is attempting to takeoff with insufficient runway and/or insufficient clearance from obstacles on climbout.

Exceeding the performance limits of an aircraft is easily preventable. In fact, before each flight, a pilot is supposed to perform a takeoff distance calculation using published performance tables in the Pilot's Operating Handbook, such as the one shown in Figure 18. Calculating takeoff performance before flight, taking into account all relevant factors, such as weight, density altitude, wind, slope, and surface type, and comparing it to available runway distance can and does aid pilots in making safe takeoff decisions.

Takeoff Distance

PRESS ALT FT	DISTANCE FT	TEMPERATURE - °C					ISA
		0	10	20	30	40	
SL	Grnd Roll	910	982	1058	1137	1219	1020
	50 ft	1414	1520	1629	1742	1860	1574
1000	Grnd Roll	1003	1084	1167	1254	1344	1108
	50 ft	1554	1670	1790	1915	2044	1706
2000	Grnd Roll	1108	1196	1289	1385	1484	1206
	50 ft	1710	1837	1970	2107	2248	1851
3000	Grnd Roll	1224	1322	1424	1530	1640	1312
	50 ft	1883	2024	2169	2320	2476	2010
4000	Grnd Roll	1354	1463	1575	1693	1814	1430
	50 ft	2076	2231	2392	2558	2730	2185
5000	Grnd Roll	1500	1620	1746	1875	2009	1560
	50 ft	2291	2462	2640	2823	3013	2377
6000	Grnd Roll	1663	1796	1935	2078	2228	1704
	50 ft	2532	2721	2917	3120	3330	2590
7000	Grnd Roll	1846	1994	2147	2307	2473	1862
	50 ft	2801	3010	3227	3452	3684	2824
8000	Grnd Roll	2052	2216	2387	2564	2748	2038
	50 ft	3103	3335	3575	3823	4080	3083
9000	Grnd Roll	2284	2466	2656	2853	3058	2233
	50 ft	3442	3698	3965	4240	4526	3370
10000	Grnd Roll	2544	2748	2959	3179	3407	2449
	50 ft	3822	4107	4403	4709	5026	3687

Figure 5-9
Sheet 1 of 2

Figure 18: Pilot's Operating Handbook takeoff distance table for a Cirrus SR22 at 3400 pounds gross weight

3.2.2 Deficient Performance Takeoff

In contrast to accidents where better planning could have prevented an accident, performance deficiencies can result in accidents, even if the pilot takes all the proper planning measures. A performance deficiency is anything that has an adverse affect on the acceleration of the aircraft. These performance deficiencies primarily occur in the engine, but may also be due to other factors resulting in extra drag. Performance deficiencies can be broken down into two categories, steady deficiencies and discrete deficiencies.

3.2.2.1 Steady Deficiencies

When a steady deficiency occurs, the engine produces much less thrust than normal, but there was no discrete failure event during the takeoff. The cause may be fuel contamination, a bad spark plug, corroded exhaust port, or some other problem that reduces engine performance but still allows it to run. The aircraft can still reach rotation speed, though much farther down the runway than normal. Despite reaching rotation speed, it may or may not have enough excess thrust to climb out and if it does, the climb angle will be much shallower than normal. A cartoon of the acceleration-airspeed curve for a reduced engine power takeoff is shown in Figure 19.

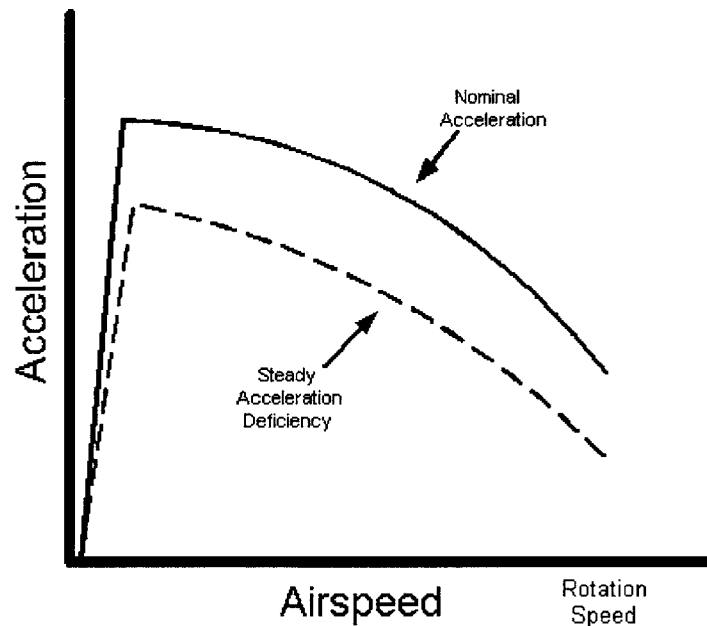


Figure 19: Consistent loss of acceleration during a takeoff ground roll

In the continuous case, the acceleration curve is consistently below that of a typical takeoff. Such an acceleration gap would be observable at the peak acceleration, measured very early in the takeoff.

3.2.2.2 Discrete Deficiencies

A discrete deficiency is an event affecting the takeoff that occurs at a specific instance. An engine failure would certainly be the most drastic discrete event, but it

could also be a sudden loss of one or more of the cylinders in the engine, or even a gust of wind. A cartoon of the acceleration-airspeed curve with a discrete deficiency is shown in Figure 20. In this example, the takeoff begins as a normal takeoff. When the event occurs, it causes a sudden drop in the observed acceleration.

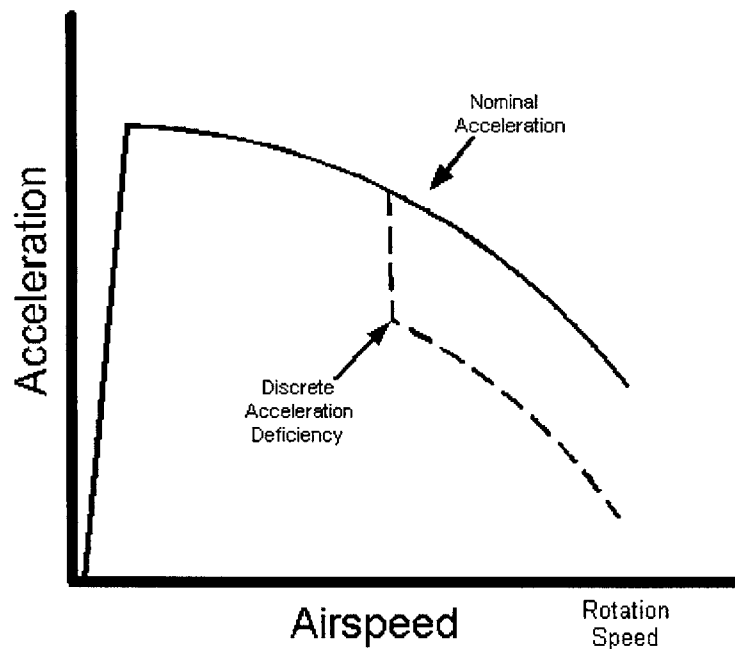


Figure 20: Discrete loss in acceleration during a takeoff ground roll

3.3 Previous Takeoff Safety Methods

In order to ensure takeoff safety, many methods of predicting and observing takeoff performance have been developed over the years. The most basic prediction method is the takeoff performance chart. Found in the Pilot's Operating Handbook of every airplane, takeoff performance charts provide the pilot with the information to predict the distance to rotation and the distance to clear a 50 feet tall obstacle. An example table from the Cirrus SR22 was shown above in Figure 18. The pilot must obtain the pressure altitude, temperature, weight, headwind, runway slope, and runway surface type. With that information, the pilot simply looks up the distances. Looking up takeoff distances is supposed to be part of every pre-flight planning procedure, but pilots often skip those steps.

If used correctly, the takeoff distance look-up tables can be very effective at predicting performance and preventing accidents. The tables do not, however, have any way to account for performance deficiencies. This lack of real-time monitoring led to two low-tech solutions: *runway distance markers* and *decision speed* [10].

Used more by military pilots than in civil aviation, distance markers are placed along the runway allowing the pilot to use a stop watch to perform time-to-speed checks during the takeoff ground roll. Effectively, this use of distance markers is checking the acceleration of the airplane relative to the ground. What it is not able to observe, though, is acceleration relative to the air, which is what matters for becoming airborne.

The decision speed is another method for monitoring the safety of takeoff. Typically used by larger transport-sized aircraft, it works better for discrete deficiencies. The decision speed is defined as the speed at which the pilot must decide whether to continue or abort. It is based on the stopping distance required, such that, after the decision speed has been reached, the airplane cannot stop on the remaining runway, and must takeoff even if a failure event occurs. If a failure event occurs before the decision speed, the takeoff can be safely aborted.

The decision speed does not, however, help in the case of continuous deficiency that has gone unnoticed by the pilot, as the crash of Air Florida Flight 90 in 1982 demonstrated [11]. As the Boeing 737 took off on a snowy January 13th at Washington National Airport, the pilots mistakenly set the engines to less than maximum thrust due to ice contamination of the inlet pressure probes that drove the engine instruments. The aircraft did reach the decision speed and the pilots elected to continue the takeoff, even though reaching rotation speed took an extra 2,000 feet and 15 seconds longer than normal. The aircraft failed to climb, struck a bridge, and plunged into the frozen Potomac River, killing 78 of the 87 people on board.

3.3.1 Previous Takeoff Performance Monitor Research

The investigations of the 1982 Air Florida accident resulted in renewed efforts to develop a Takeoff Performance Monitor, or TOPM. Such instruments had been in development since the 1950's and several examples are shown in Appendix A [12].

Many used simple accelerometers and measured only achieved performance for comparison with some record of nominal performance. After the Air Florida crash, the emphasis shifted to predictive takeoff monitoring.

The Society of Automotive Engineers produced a standard for three types of takeoff performance monitors [13]. Type I monitors are non-predictive and only compare achieved performance with nominal performance. A Type II monitor adds the capability to predict takeoff distance, while a Type III predicts not only takeoff distance but also stopping distance in the case of an abort. Human factors experiments indicated that Type III TOPM's provided the best improvement of safety, followed by Type II, and then Type I [14].

Several attempts at predictive takeoff monitors were made in the 1980's and early 1990's [15, 16]. The most advanced takeoff monitor was developed at NASA and tested in NASA Langley's 737 research test-bed. It was considered for inclusion in Boeing's 777, but was rejected because of worries that nuisance alerts resulting from the tight tolerances required to avoid missed alerts would lead pilots to ignore the device [17]. Another problem with the takeoff monitors was the inability to accurately predict the stopping distance when the runway has any contamination, such as ice or rubber [18].

These earlier systems used expensive instrumentation available only on large transport aircraft, making their use in general aviation problematic. In particular, before GPS became available, ground speed and position were difficult to obtain, requiring specialized sensors. However, general aviation takeoff monitors have been studied using inexpensive accelerometer systems [19], as well as GPS [20], that have shown promise. Even so, these systems were developed as free-standing instruments and not integrated into an electronic flight information system. For example, neither system took airspeed into account, which is crucial for determining liftoff distances in windy conditions. As the information architecture in the general aviation cockpit moves to fully integrated databases and displays, the opportunity exists to create a takeoff monitor that can account for position, ground speed, and airspeed without requiring any additional sensors.

3.4 Prototype Takeoff Performance Monitor Design

This prototype takeoff performance monitor for a general aviation integrated flight deck is based on three propositions. First, published takeoff performance data provide can provide accurate takeoff distance predictions for aircraft not experiencing performance deficiencies. Second, performance deficiencies can be detected though measurements of the aircraft's acceleration. Third and lastly, these acceleration measurements can be used to predict the actual takeoff distance with or without performance deficiencies.

The design utilizes a two-pronged strategy for detecting and preventing accidents that result from the exceeding performance limits and from performance deficiencies. Exceeding performance limits is addressed by automating the published takeoff distance look-up tables, receiving as many of the inputs as possible from on-board sensors and data transmitted via satellite datalink. The liftoff and obstacle clearance distances can then be compared to the length of the current runway, as determined from a runway database.

A real-time liftoff distance predictor addresses performance deficiencies. Using the on-board accelerometers, air data computer, and GPS, the distance to rotation speed is predicted in real-time, based on achieved performance.

The system qualifies as an SAE Type II takeoff monitor, as it contains nominal performance data, in the form of the published performance tables, as well as predictive rotation distance capability. The system does not predict braking distance, partly because of the high difficulty in accurately estimating ground friction, but also because steady deficiencies can be detected very early in the takeoff, before stopping distance becomes an issue. As for discrete deficiencies late in the takeoff, such as an engine failure, a single-engine airplane does not have the option to continue the takeoff if it cannot stop within the length of the runway. It is the takeoff distances, both nominal and real-time predicted, that matter most to the general aviation pilot.

3.4.1 Prototype Takeoff Performance Monitor Architecture

The information architecture of the takeoff performance monitor is shown below in Figure 21. The only pieces of information that are not obtainable from automation are

the aircraft weight and headwind, both of which require pilot input. Position and ground speed are determined by the GPS, while airspeed, acceleration, and heading are measured by the on-board ADAHRS. Once the input data are obtained, the takeoff monitor performs three routines. First, the *Runway Selector* chooses the most likely runway for the takeoff, then the *Published Takeoff Distances* are looked up, and finally the *Real-time Takeoff Prediction* is made.

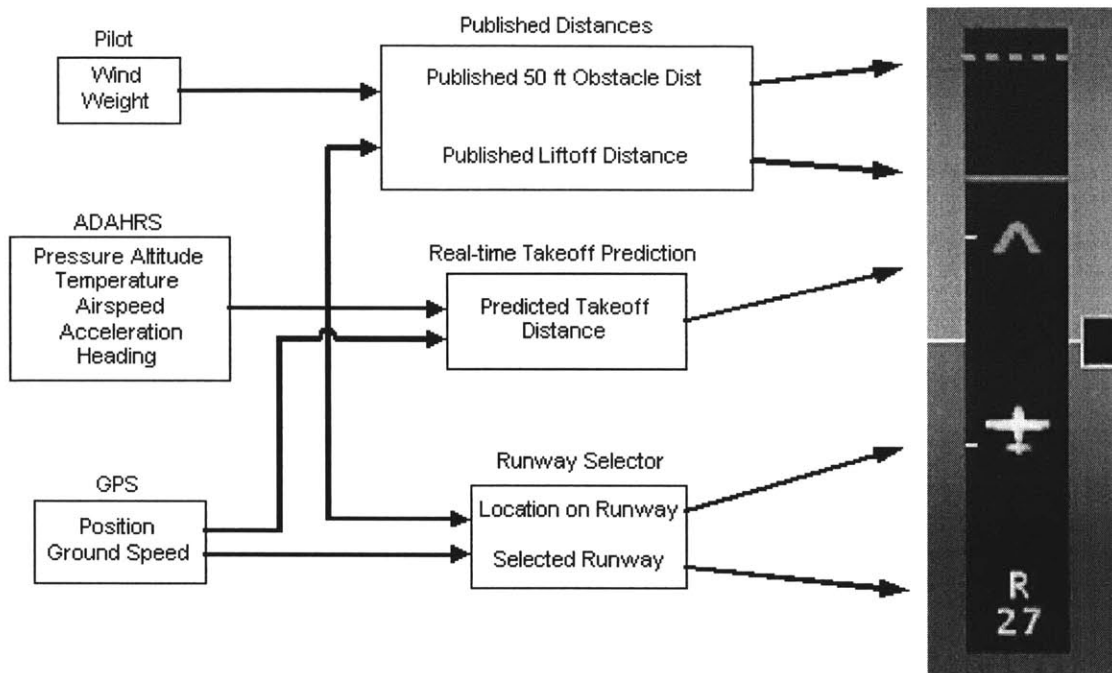


Figure 21: Real-time Takeoff Performance Monitor Architecture

The Runway Selector determines the most likely runway to be used and, if the airplane is on that runway, the airplane’s location on it. The runway and aircraft are then depicted on the display, with the runway number shown at the bottom, thousand foot markers shown along the left side to indicate length, and an aircraft symbol indicating present position on the runway.

Having selected the current runway, the Published Takeoff Distances routine looks up the published takeoff and obstacle clearance distances. The distances are then shown on the runway depiction with a solid magenta line and a dashed magenta line, respectively.

Finally, once the aircraft has begun the takeoff, the Real-time Takeoff Prediction routine predicts the remaining distance required to reach rotation speed, which is shown

with an inverted “V” pointing to the predicted rotation location. If the climbout distance from the real-time predicted liftoff point is longer than the runway, the runway depiction flashes yellow indicating “caution” and that care must be taken if there are obstacles near the end of the runway. If the real-time predicted rotation point is beyond the end of the runway, the runway depiction flashes red, warning the pilot that the takeoff should be aborted immediately.

3.4.2 Runway Selector

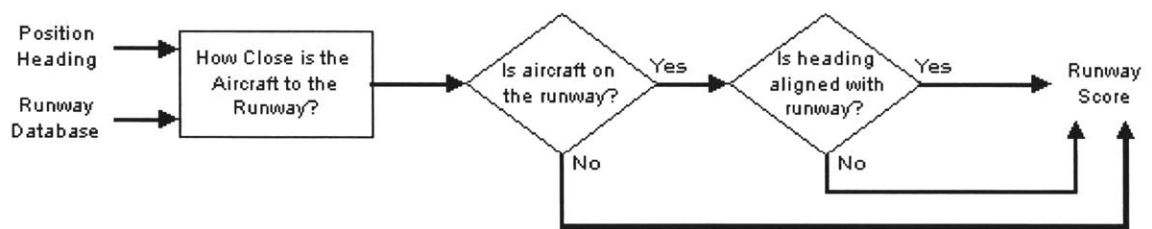


Figure 22: Runway Selector scoring algorithm

The runway selector contains a database of runways, storing not only their positions and lengths, but also their slopes and surface types. In this version of the takeoff monitor, a crude selection algorithm, shown in Figure 22, was used along with a limited database of two airports. The system first detects which airport is nearest, and then uses a scoring algorithm that takes into account position and heading to rate the likelihood that a runway will be used or is being used for the takeoff. The runway with the highest score is selected.

3.4.3 Published Takeoff Distance

Once the current runway and conditions are known, the system then looks up the liftoff and obstacle clearance distances from the published performance tables. Density altitude is computed from the temperature and pressure altitude provided by the ADAHRS, while the headwind is determined from the wind input and the current runway heading. The slope and surface information in the database, along with the manual weight input, provide all the necessary information to lookup the correct liftoff and obstacle clearance distances.

3.4.4 Real-time Takeoff Prediction

Predicting the real-time takeoff distance is accomplished first by estimating the lumped parameter coefficients and using them to calculate the average acceleration during the ground roll. The acceleration and the current airspeed are then used to calculate the time-to-rotation, over which the acceleration, ground speed, and position are integrated to find predicted rotation point. The process is depicted in Figure 23.

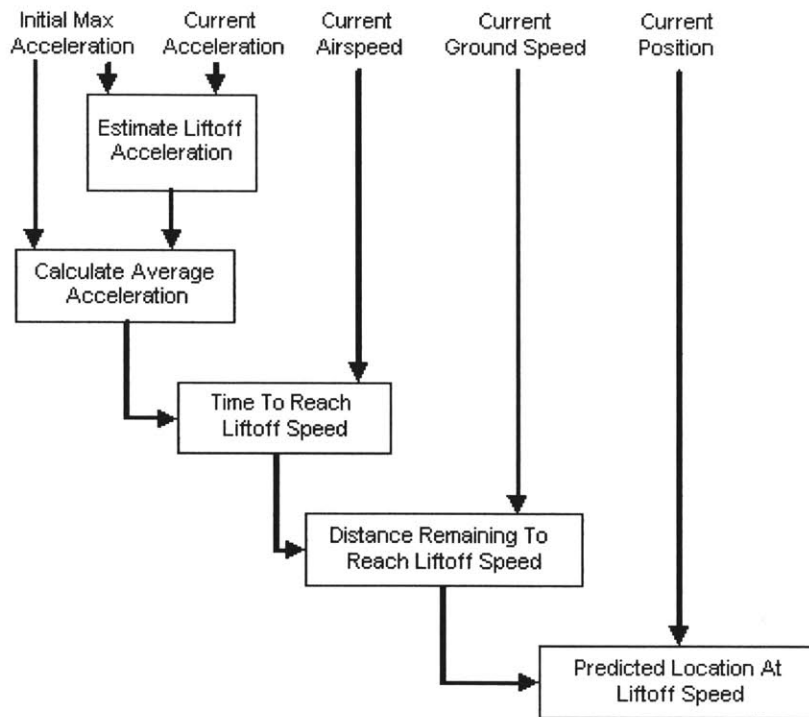


Figure 23: Real-time takeoff distance prediction method

Estimating the liftoff acceleration is accomplished by using pre-defined estimates of the first and second order lumped parameter coefficients, which consist of the drag and friction coefficients as well as any thrust behavior with airspeed. Knowing the current airspeed and acceleration, along with the lumped parameter coefficients, the acceleration at rotation speed is then solved for, as depicted in Figure 24.

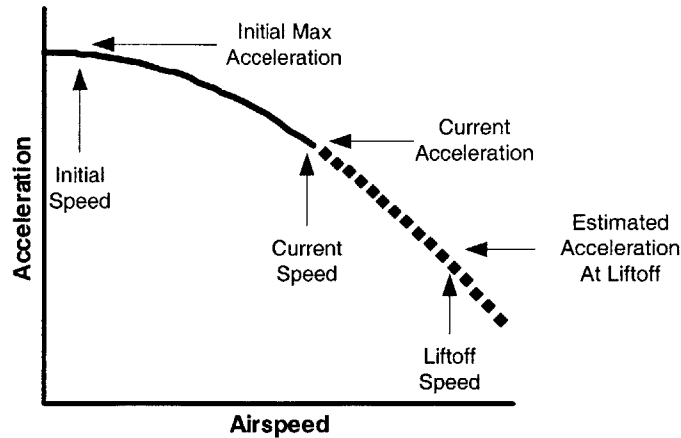


Figure 24: Predicting the acceleration at rotation based on current speed and acceleration

Using the constant average acceleration approximation, the predicted acceleration at liftoff is averaged with the current acceleration. Once the average remaining acceleration is estimated, the time-to-rotation can be solved for, given the current airspeed.

To find the rotation distance, it is assumed that the airplane’s acceleration with respect to the ground and acceleration with respect to the airmass are equal. This is essentially assuming that the wind speed is constant during the course of the takeoff. While the wind certainly can gust, it is a reasonable approximation because the wind rarely shifts too much during the 20 seconds of takeoff.

Assuming the airspeed acceleration is equal to the ground speed acceleration, and knowing the time-to-rotation, the acceleration and ground speed is integrated over the time-to-rotation to find the distance-to-rotation. Finally, adding the distance-to-rotation to the current position on the runway produces the predicted rotation point on the runway.

3.4.5 Takeoff Monitor Display Design

With the takeoff performance data calculated, it must be displayed in a usable way to the pilot. The display issue is not trivial, as many of the complaints against previous takeoff monitors were due to clutter and distraction.

While the pre-takeoff published distance calculations and display do not necessarily need to be in the primary field of view, the real-time predictions must be, to allow the pilot to quickly glance at and interpret the display. As such, the takeoff monitor display, depicted earlier in Figure 21, was placed to the immediate left of the airspeed indicator, the primary instrument used during takeoff.

Takeoff data is displayed with a representation of the runway. This was chosen because of its simple translation to reality and because a small study showed that pilots made better decisions with and preferred a distance-based runway depiction over an acceleration-based display [21].

The published liftoff and obstacle distances are displayed as soon as they are first calculated and remain displayed during the actual takeoff. This maximizes the number of opportunities for the pilot to make a decision based on the published numbers, as well as allows the pilot to compare the published distance to the real-time predicted distance, which is displayed as soon as it is available. In the event of a partial steady deficiency, the airplane may be able to reach liftoff speed while on the runway, but it will be readily apparent that the aircraft is performing poorly, giving the pilot the option to abort and explore the problem.

In order to help the pilot make the “Go or No Go” decision, the display has two caution and warning modes. The “Caution” and “Warning” displays, along with the “Normal” and “No Prediction” modes, are shown below in Figure 25.

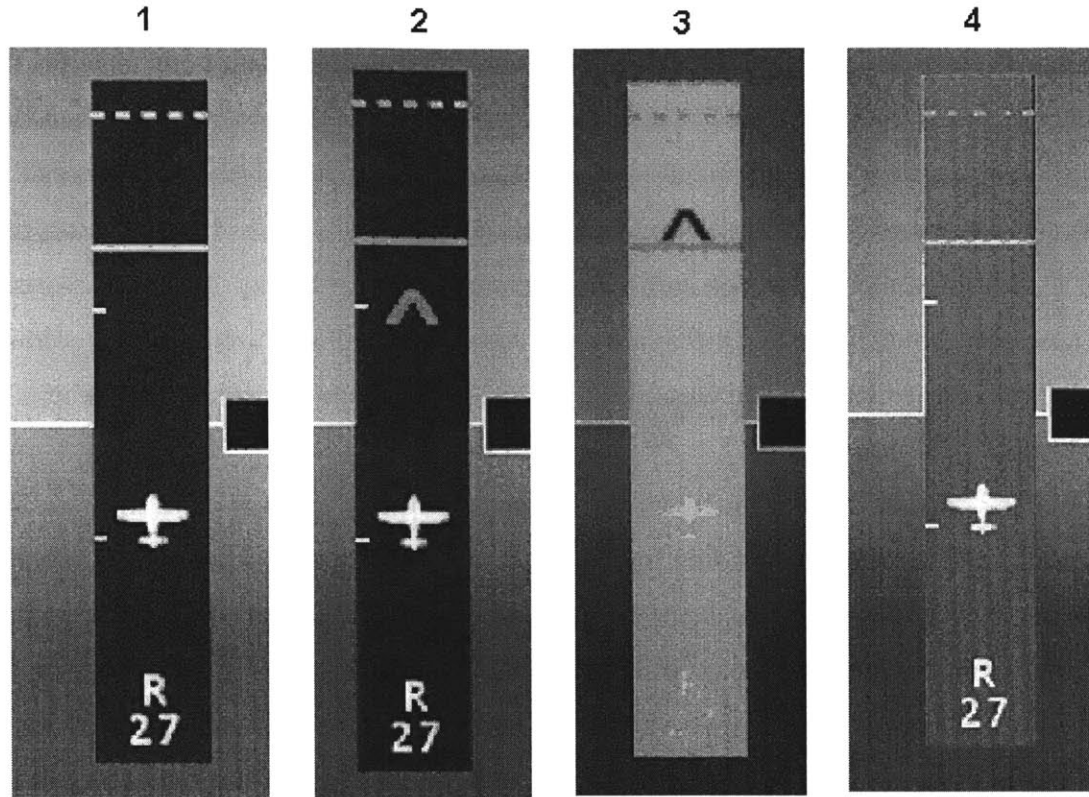


Figure 25: Takeoff Monitor in four situations. 1) POH values displayed, but no real-time prediction yet 2) Real-time prediction marked by inverted "V" 3) Runway flashes yellow for Caution 4) Runway flashes red for Warning

A “Caution” is indicated when it is suspected that the airplane will not clear a foot obstacle at the end of the runway, even though it will liftoff before the end of the runway. In this case, the pilot need not automatically abort, but should exercise caution if there are any obstacles to clear. On the other hand, a “Warning” is indicated when the real-time liftoff distance plus a 200 feet safety buffer exceeds the length of the runway. In this case, the airplane will likely not liftoff on the length of the runway, and the pilot should abort as soon as possible.

3.5 Takeoff Performance Monitor Flight Tests

In order to evaluate the takeoff performance monitor, the published and predicted takeoff distances were compared with the actual takeoff distances of a series of takeoffs with full and partial power. A list of the power settings used in the flight tests is shown in Table 3.

Table 3: Takeoff Performance Monitor Flight Test Power Settings

Power Setting
100% Steady
90% Steady
80% Steady
70% Steady
60% Steady
100% until 60 KIAS, then 70%
100% until 50 KIAS, then 70%
100% until 40 KIAS, then 70%
100% until 30 KIAS, then 70%

Two types of power application were performed. First, steady performance deficiencies were simulated by performing takeoff runs at power settings between 100% and 60%. Discrete performance deficiencies were simulated by beginning a takeoff run at 100% until reaching a certain speed, in Knots Indicated Airspeed (KIAS, sometimes also referred interchangeably as *calibrated* airspeed, or KCAS), then suddenly reducing power to 70%. At the start of each run, the brakes were set until the power was set. The steady power setting takeoff runs were each performed twice while the discrete power drop runs were performed only once. The order of the takeoffs was randomized to help reduce any hysteresis or learning effects.

Since the takeoff performance monitor predicted ground roll distances only and Melbourne’s long runway extends 10,000 feet, some takeoff runs were actually high-speed taxis, where the aircraft was accelerated to the rotation speed, then brought to a stop on the runway. The next takeoff run was then performed, this time becoming airborne and flying around the pattern before returning to land and perform the next takeoff.

3.6 Flight Test Results

The takeoff performance monitor flight tests evaluated the three propositions that the design was based on. First, for each takeoff, the takeoff monitor computed the published takeoff distances. The acceleration during the takeoffs was recorded and demonstrated that it was possible to observe performance deficiencies from that data. Lastly, GPS position errors prevented the real-time predictor from functioning properly in

flight, but a reconstructed real-time predictor running the recorded data was able to predict the takeoff distance within 200 feet by reaching 55 KCAS.

3.6.1 Examples of Data Plots

To aid in interpreting the flight test data, examples of four types of data plots that were useful will be given. These data plots are *Distance vs. Time*, *Speed vs. Time*, *Acceleration vs. Airspeed* and *Acceleration vs. Time*.

3.6.1.1 Distance vs. Time

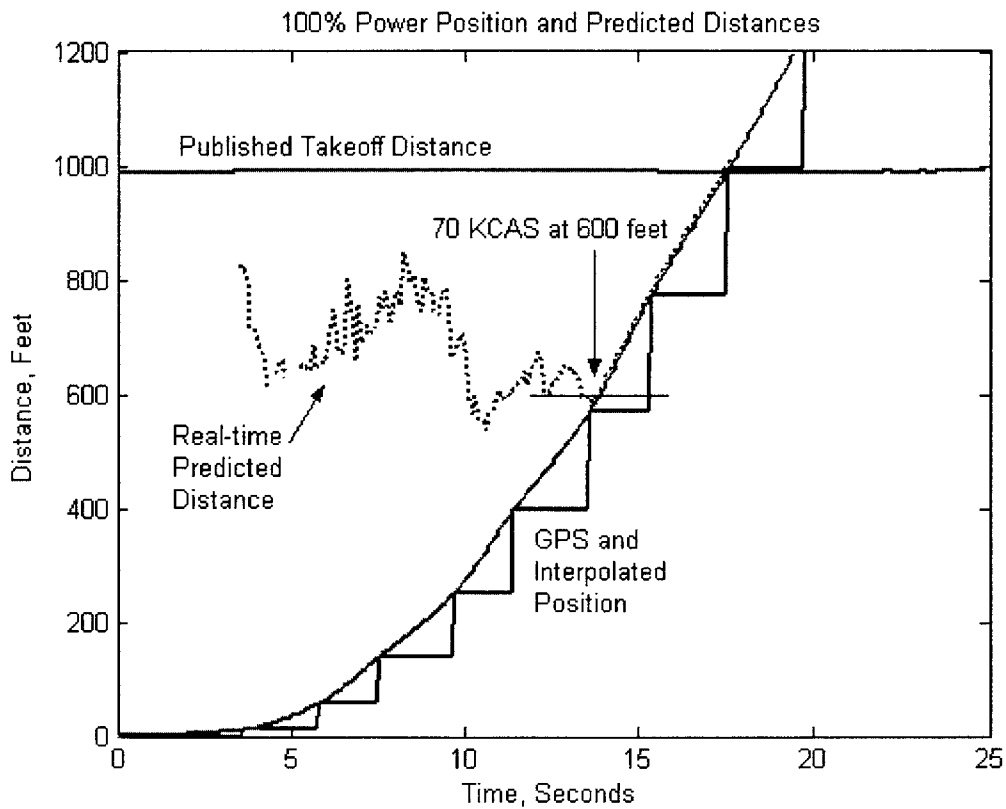


Figure 26: Takeoff 1, Distance vs. Time Plot

Figure 26 plots position, real-time predicted takeoff distance, and published takeoff distance from the beginning of the takeoff as time elapses. Time, on the horizontal axis, is measured from the beginning of the takeoff data, while distance, on the vertical axis, is measured from the location of the aircraft when time is zero. Since GPS

only updates once every two seconds, the position between updates is interpolated, as shown by the smooth line connecting each of the steps of GPS position.

The distance of the real-time predicted liftoff point relative to the start of the takeoff is shown in the dotted line above the position. Clearly, the real-time predicted distance initially over-predicts the actual point where liftoff speed of 70 KCAS was reached, shown at 600 feet, before converging on the actual distance. For reference, the published liftoff distance is drawn across the top of the plot, representing the conservative performance estimated in the Pilot's Operating Handbook.

3.6.1.2 Speed vs. Time

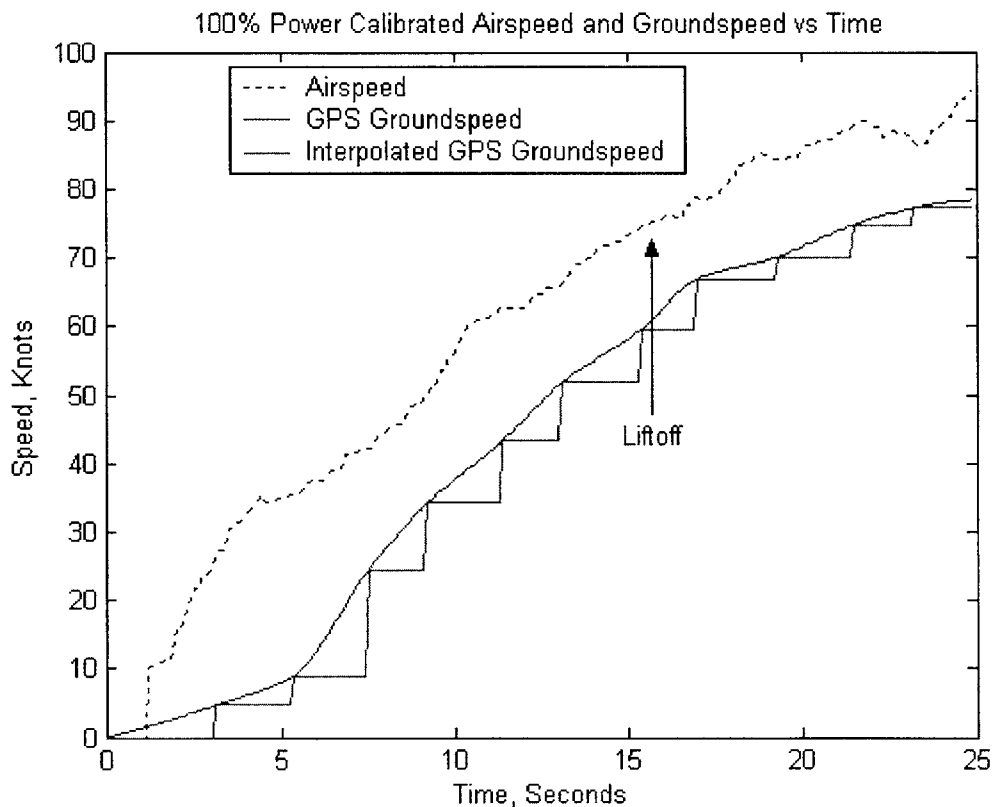


Figure 27: Takeoff 1, Airspeed and Ground Speed vs. Time Plot

Figure 27 shows the airspeed and ground speed during the same takeoff. The airspeed is much higher than the ground speed, reflecting the strong head wind prevalent on the test day. Like the position, the GPS ground speed updated only once every two seconds, so the speed was interpolated between data points.

3.6.1.3 Acceleration vs. Airspeed

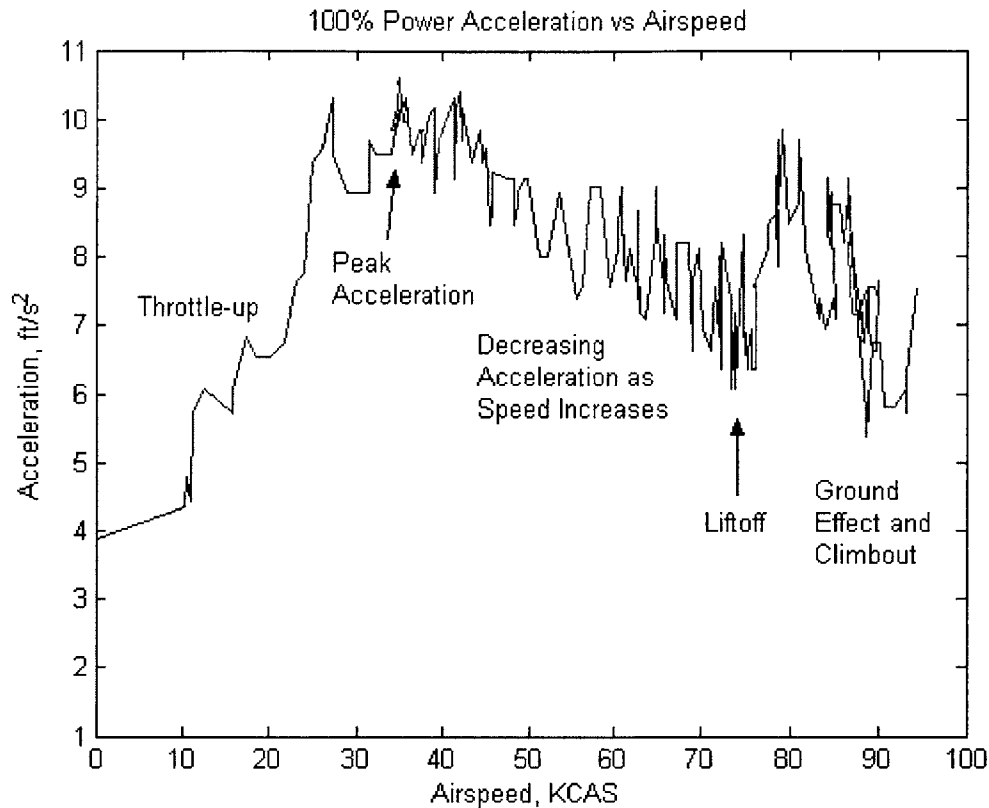


Figure 28: Takeoff 1, Acceleration vs. Airspeed Plot

Figure 28 shows the acceleration versus the airspeed, demonstrating the validity of the theoretical model of takeoff described in Section 3.1.2. At low airspeeds, when the aircraft is moving slowly or at rest relative to the ground, the acceleration fluctuates above and below zero as the aircraft moves into position for takeoff. After throttle-up and brake release, the acceleration quickly rises to a peak of approximately 10 ft/s^2 . Then as airspeed increases, the acceleration tapers off in what appears an almost linear, but slightly curved function of airspeed. Such acceleration behavior serves to validate the lumped parameter model.

The aircraft lifts off shortly after reaching 70 KCAS, and the acceleration increases due to the sudden lack of ground friction. As the aircraft climbs out, the acceleration begins dropping as the aircraft settles into a constant speed climb. The acceleration does not drop to zero in this case because the aircraft is pitched up, and thus the longitudinal accelerometer will detect a component of gravity.

3.6.1.4 Acceleration vs. Time

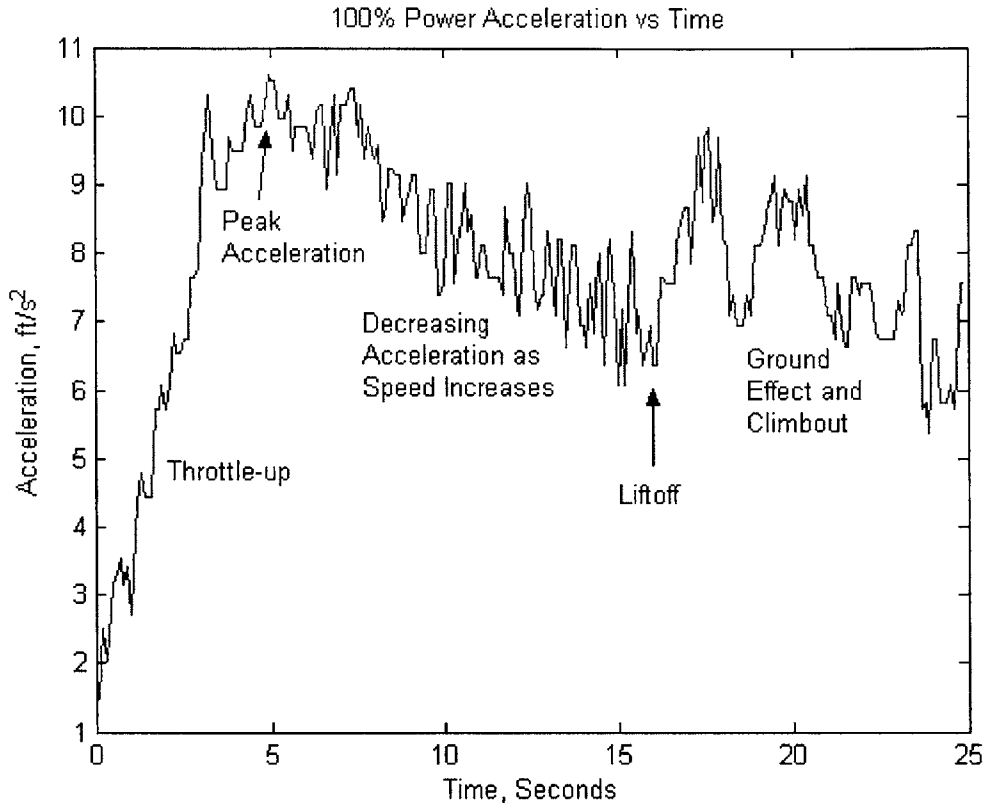


Figure 29: Takeoff 1, Acceleration vs. Time Plot

Figure 29 shows the acceleration versus time elapsed during the takeoff. As shown in the position, speed, and previous acceleration plots, the aircraft throttles up and quickly accelerates quickly to the peak. As the aircraft picks up speed during the takeoff, the acceleration decays. The acceleration change appears linear, possibly slightly curved, but linear enough to support the constant average acceleration assumption.

Liftoff occurs at approximately 16 seconds into the takeoff, and is marked by the increase in acceleration due to the lack of ground friction. The aircraft then pitches up and begins the climbout, causing the acceleration to again drop.

3.6.2 Published Takeoff Distances

The published takeoff distance was calculated on the takeoff monitor using the weight and wind, as reported by the control tower, input to the laptop by the FTE. The liftoff and climbout distances were then displayed on the runway depiction. Figure 30

plots the actual takeoff distance for each steady power takeoff run along with the published takeoff distances calculated from the reported wind.

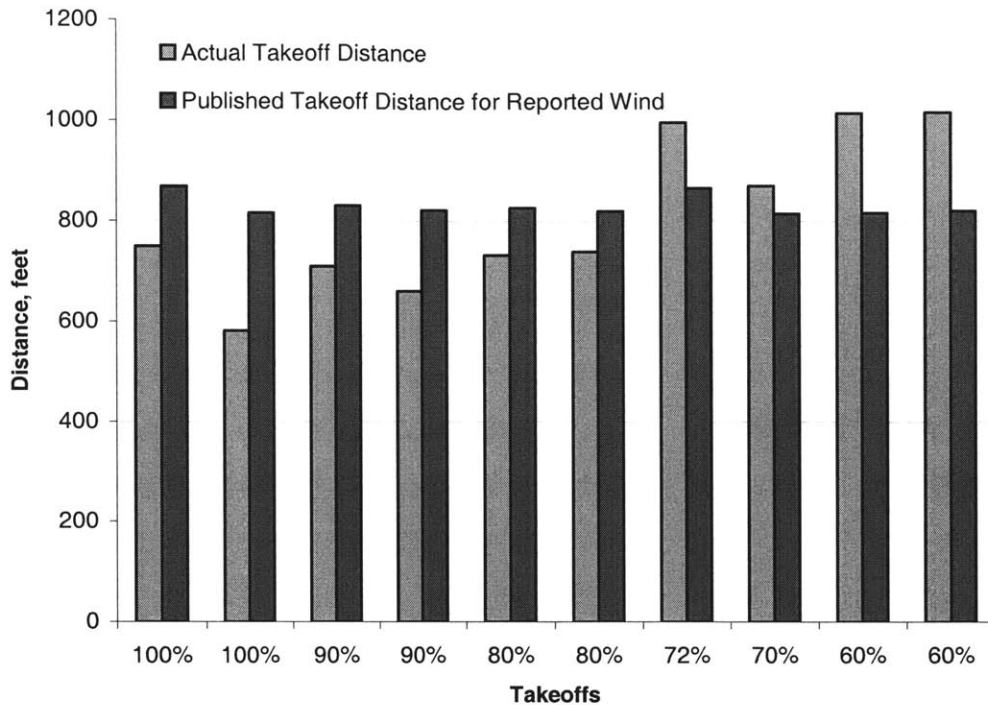


Figure 30: Actual takeoff distances for each steady power takeoff with the published takeoff distance for the wind reported before the takeoff

Figure 30 shows that the published takeoff distances are somewhat conservative. Down to 80% power, the published distances are longer or equal to the actual takeoff distances.

Displaying the published distances won approval by the pilots involved. None of them paid attention to the distances during the takeoff, but all of them said that seeing the distance calculations before the takeoff would be helpful to the pilot.

3.6.3 Observing Steady Deficiencies Through Acceleration

As described in Section 3.1.2, the longitudinal acceleration is the sum of the thrust and drag. At the beginning of the takeoff, as airspeed is low, the acceleration is mostly composed of thrust. Thus, it should be possible to observe performance deficiencies through acceleration. In particular, steady deficiencies should be observable at the peak acceleration in the beginning of the takeoff.

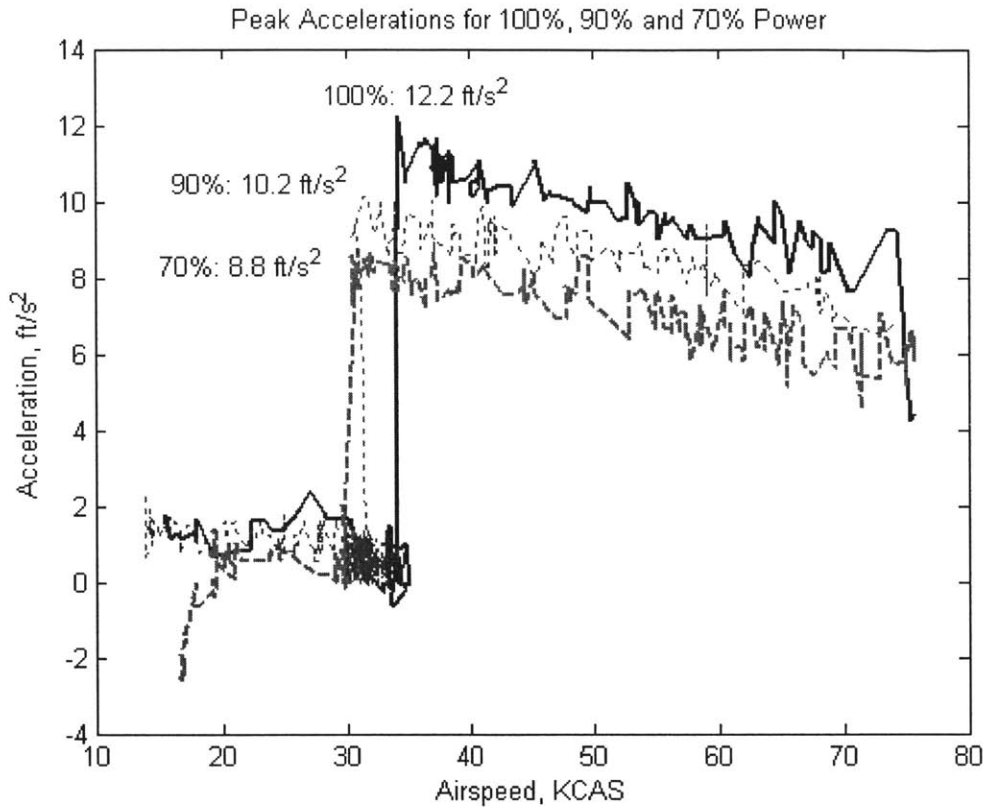


Figure 31: Acceleration plots for 100%, 90%, and 70% power settings

Figure 31 shows that it was indeed possible to observe the steady deficiencies of power reduction. The plot depicts the acceleration versus airspeed for three of the steady power takeoffs as well as the peak accelerations for each power setting. Following the peak acceleration, they all decay at the same rate, which was expected because the drag coefficient of the aircraft did not change between takeoffs. The offset in acceleration, however, is quite observable.

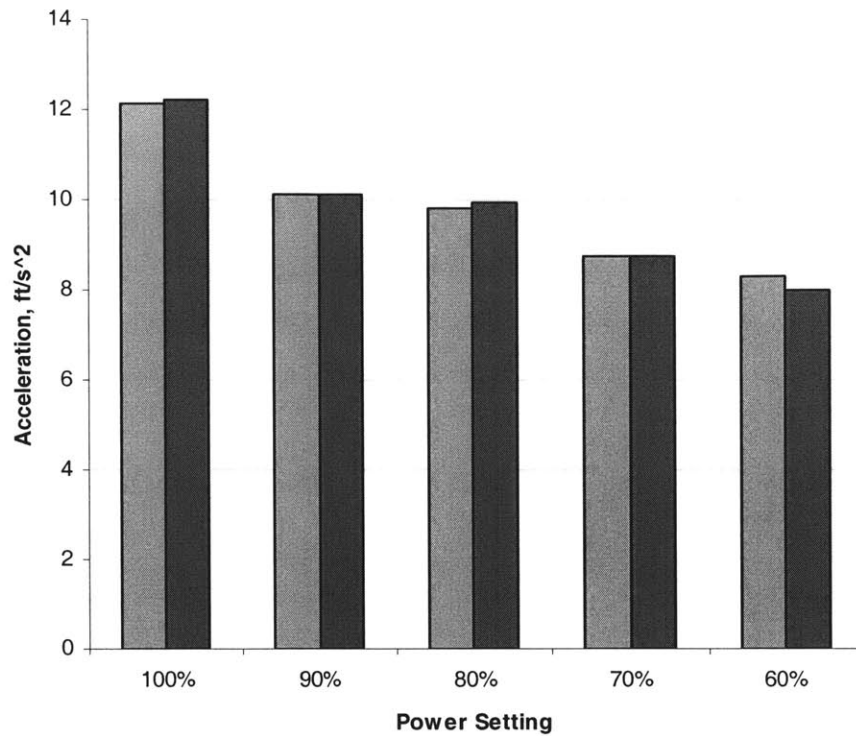


Figure 32: Peak accelerations for steady power takeoffs, two for each power setting

Figure 32 shows the peak accelerations for all the steady power takeoffs performed in this study. Each power setting was repeated twice. There is a clear relationship between power setting and peak acceleration, though it is difficult to distinguish between the 90% and 80% power takeoffs.

3.6.4 Observing Discrete Deficiencies Through Acceleration

Just as the acceleration can be used to observe steady power reductions, the acceleration also shows discrete deficiencies. Figure 33 shows the acceleration plotted against airspeed for the takeoff in which the power was reduced from 100% to 70% when the airspeed reached 50 KCAS. Just after 50 KCAS, the acceleration drops suddenly from its previous trend as the pilot reduces power.

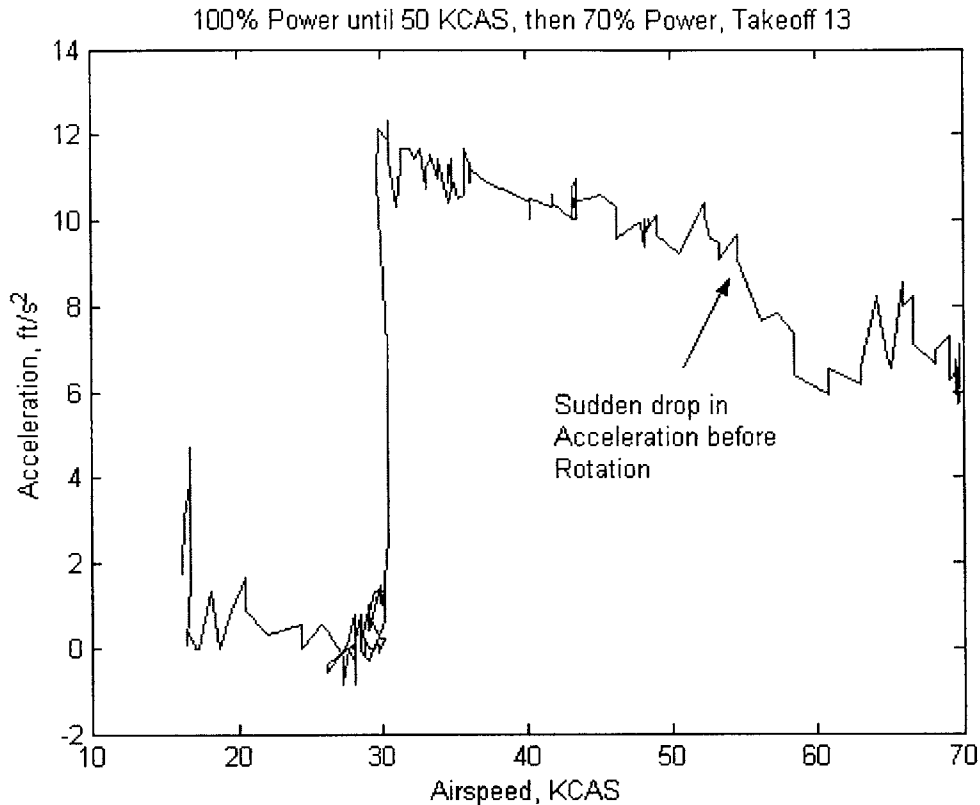


Figure 33: Discrete drop in power at 50 KCAS

3.6.5 Real-time Takeoff Distance Prediction

During the flight test, the prototype takeoff performance monitor functioned erratically, occasionally predicting takeoff distance while other times not even selecting the correct runway. The root cause of these problems was determined to be inaccuracy in either the GPS position or the airport database. Both the handheld and panel-mount GPS units are specified to be accurate within ± 49 feet RMS [22, 23], but appeared to be far less accurate.

At the hold short line before takeoff on a later flight, the handheld and panel-mount positions were both recorded and these are plotted in Figure 34. The handheld GPS reported a position 1866 feet from the runway endpoint, while the panel-mount GPS reported a position 2321 feet from the endpoint. The actual position was less than 200 feet from the endpoint.

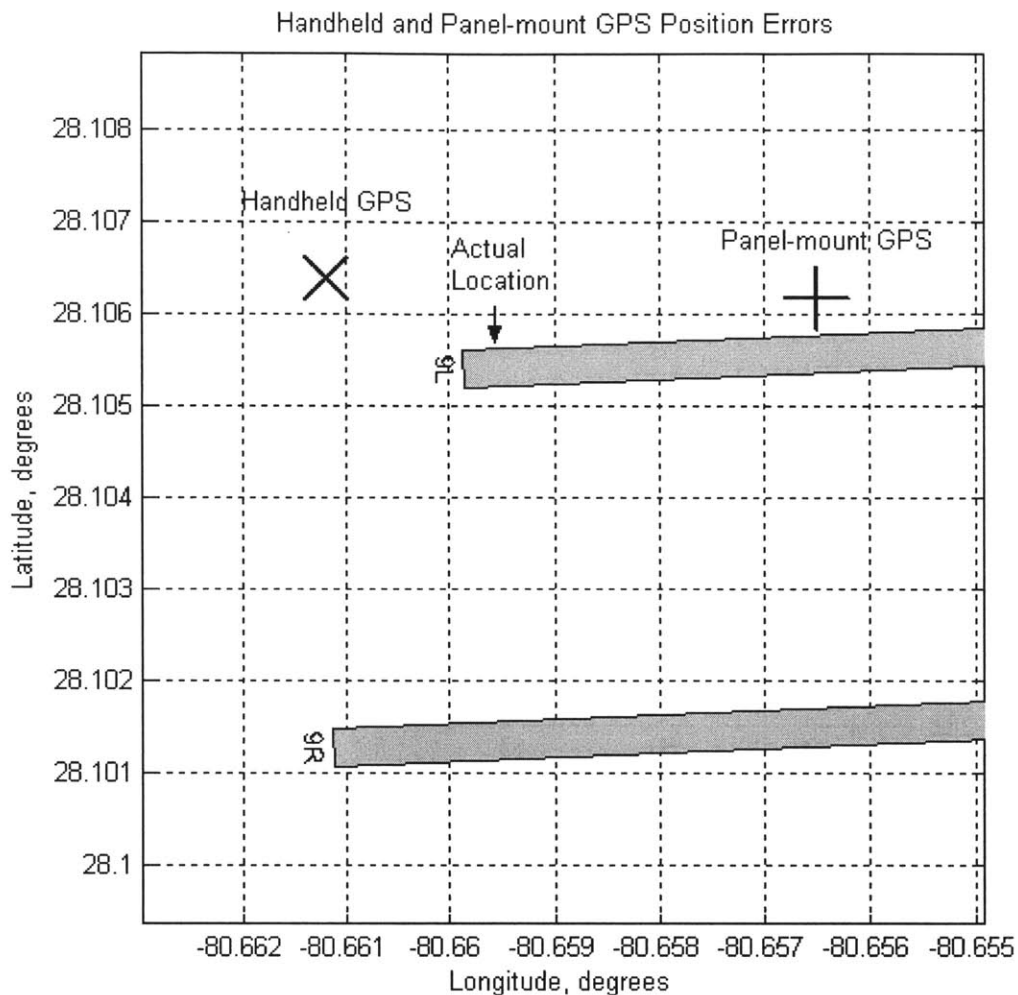


Figure 34: GPS positions recorded when the aircraft was at the hold short line for runway 9L

Such large position errors contributed to the erratic behavior of the takeoff performance monitor because the Real-time Takeoff Prediction algorithm depended on the Runway Selector telling it when the aircraft is on the runway. Only when the aircraft was on the runway and had passed the point of peak acceleration did the takeoff monitor begin predicting the real-time takeoff distance.

It is unclear why the GPS position errors were so high. In any case, for a takeoff monitor of this design to function properly, it must have a more accurate GPS. Assuming the relative GPS position and speed measurements were more accurate, the takeoff monitor was reconstructed to determine what it *would* have predicted with correct position. The “starting point” of the takeoff was chosen by hand, then the relative

distances from that point were determined from the GPS data. From this starting point until reaching liftoff speed, the aircraft was considered “on the runway” and the prediction algorithms worked as designed. The reconstructed takeoff data is then shown in four different plots, which will be explained.

3.6.6 Reconstructed Takeoff Distance Predictor

In addition to the GPS position errors, another error was observed that caused trouble for the real-time predictor. In the simple implementation of this prototype, the time-to-rotation estimator computes the difference between the current airspeed and the airspeed at rotation. The predicted average acceleration between the current point and the rotation point is then used to find the time remaining to reach rotation speed. For every takeoff performed, the time-to-rotation was consistently low, in that it predicted the aircraft would takeoff sooner than it actually did, which in turn caused the distance predictor to under-predict the takeoff distance.

The apparent cause of this was a bias in the difference between the airspeed and the ground speed, which should essentially be the headwind. At low speeds, the difference between the airspeed and the ground speed was nearly twice the difference at rotation speed, which was generally much closer to the reported headwind. It seems plausible that the GPS ground speed measurement has latency, and thus at low speeds when the acceleration is highest, would lag further behind the airspeed than at higher speeds when the acceleration is less. That does not explain, however, why correcting the *airspeed* for this apparent bias results in better time-to-rotation estimates that do not use any GPS data. To determine the exact cause of this bias requires an additional experiment testing the airspeed sensor and GPS at several steady low speeds.

After correcting for GPS position errors and speed biases, the real-time takeoff distance predictor was reconstructed. Figure 35 and Figure 36 show the position and predicted distances for takeoffs at steady power settings of 90% and 60%. For the 90% power setting, shown in Figure 35, the real-time predictor initially under-predicted the takeoff distance, but quickly converged on the approximate distance within 150 feet.

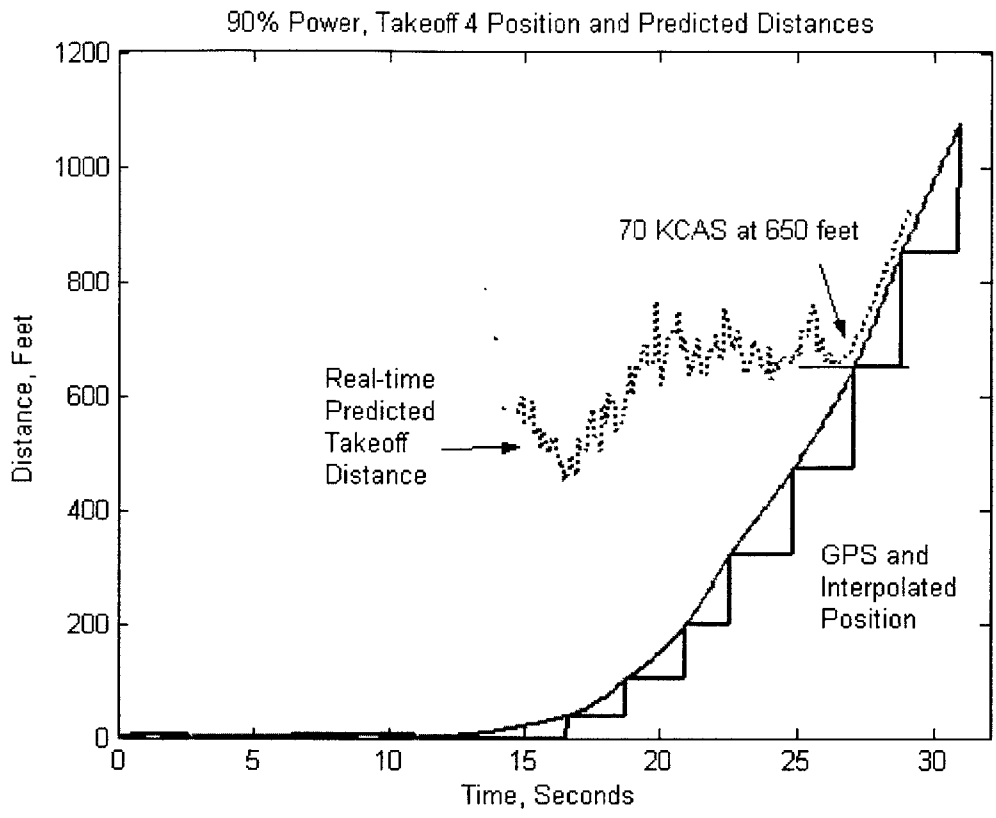


Figure 35: Position and Predicted Liftoff Distance vs. Time plot for 90% Power, Steady, Takeoff 4

Takeoff 5, shown in Figure 36, shows the opposite behavior, initially over-predicting the distance, then slightly under-predicting, and finally converging on the actual distance.

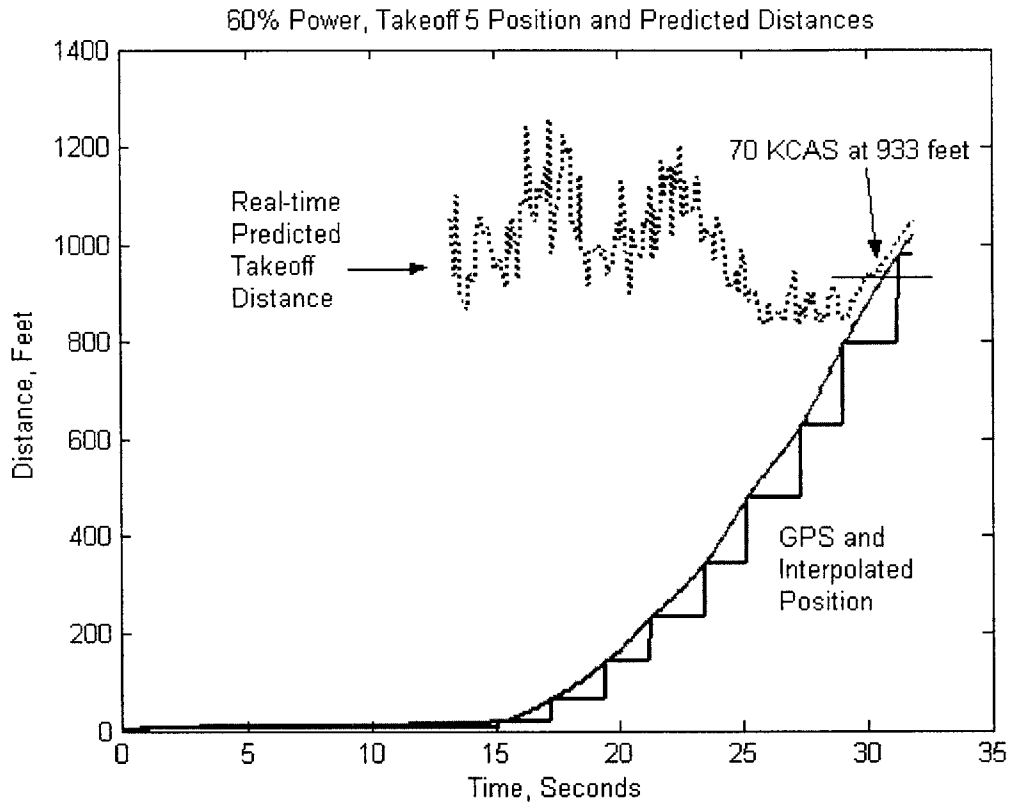


Figure 36: Distance vs. Time plot for 60% Power, Steady, Takeoff 5

The previous two takeoffs shown were both steady power takeoffs, representing steady deficiencies. The reconstructed real-time predictor was also able to observe and correct for discrete deficiencies, an example of which is shown in Figure 37. In this takeoff, the power was initially set to 100%, but at 40 KCAS, it was abruptly reduced to 70%. The initial prediction was low, around 500 feet, until the power was suddenly reduced about four seconds into the takeoff. At that point, the predicted liftoff distance shifted upward to within about 150 feet of the actual takeoff distance.

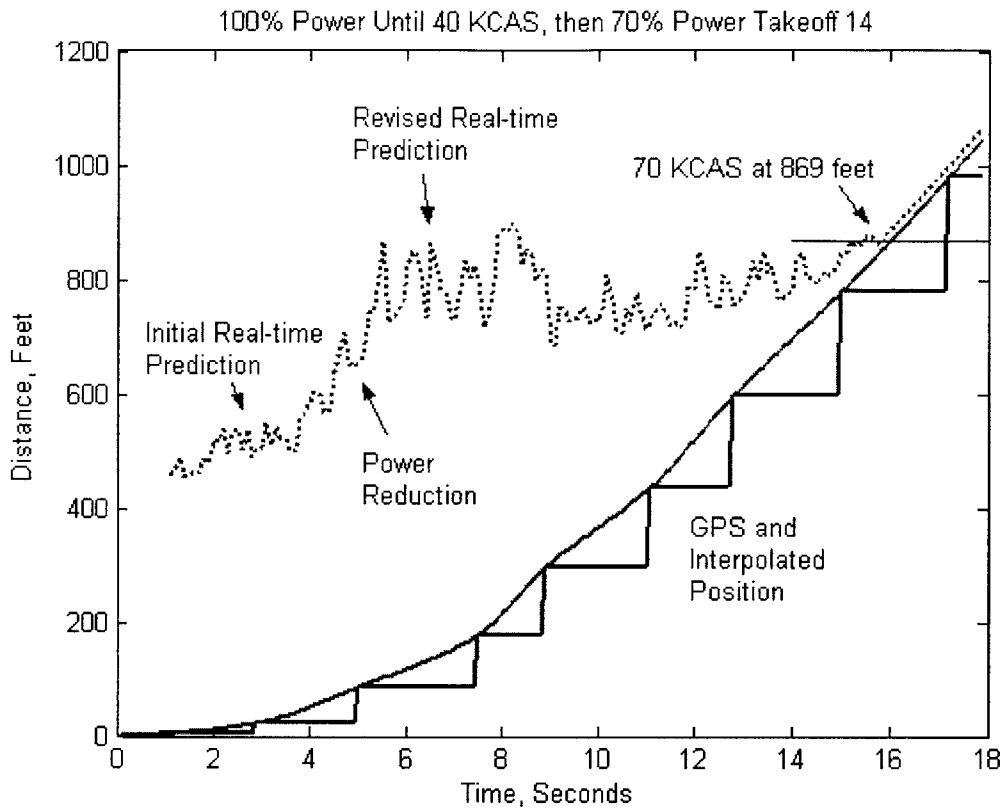


Figure 37: Position and Predicted Takeoff Distances during discrete performance deficiency takeoff

The overall capability of the real-time takeoff distance predictor can be seen in Figure 38. At low speeds near the beginning of takeoff, the real-time prediction is generally within +600/-200 feet of the actual distance. As the aircraft accelerated closer to rotation speed, the predictions begin to converge closer to the actual distance, within ± 200 feet of the actual distance by 55 KCAS. To improve accuracy on a future prototype, a more rigorous method for estimating the acceleration at rotation speed could incorporate a Kalman filter, much like that used in [7]. With a better acceleration model, the time-to-rotation estimate might then be more accurate, producing a better estimate of takeoff distance earlier.

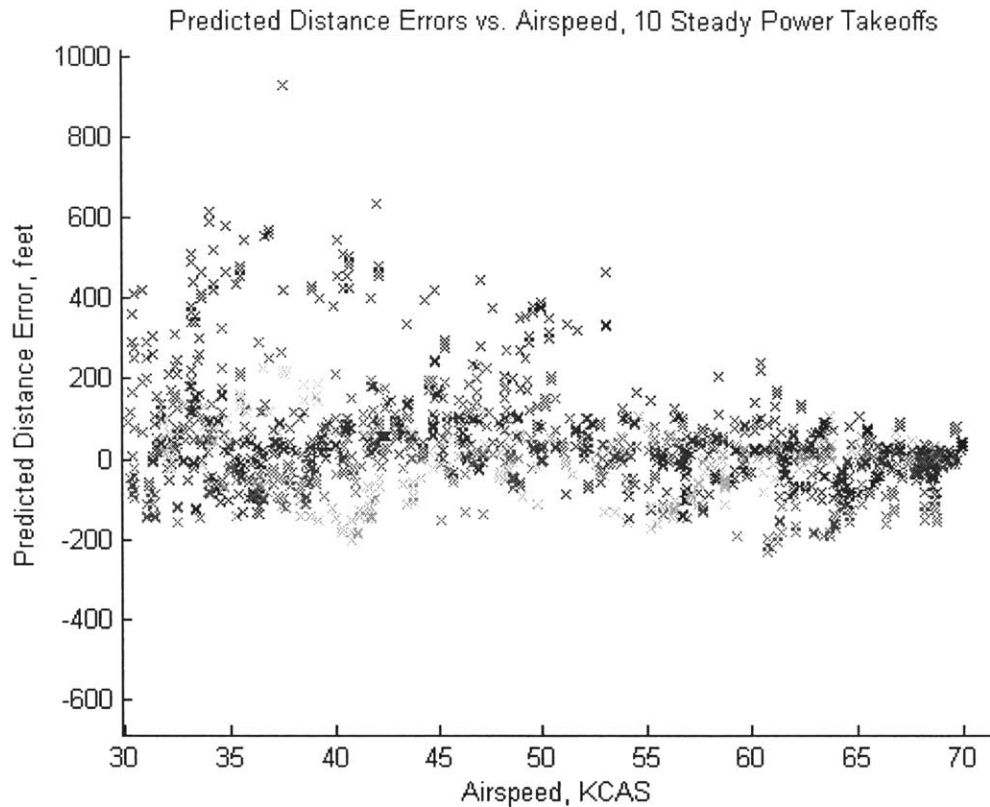


Figure 38: Difference between Predicted Distances and Actual Takeoff Distances vs. the airspeed when the predictions were made during all ten steady power takeoffs. By 55 KCAS, the predicted distance is generally within 200 feet of the actual takeoff distance.

3.7 Conclusions

The data gathered during the takeoff monitor flight tests point to three conclusions. First, calculating and displaying the published liftoff and obstacle clearance distances is useful to the pilot and straightforward to implement. While this prototype implemented the takeoff monitor on the PFD, an MFD would be a more natural home to the takeoff performance calculation. It would also incorporate well with a weight and balance calculation that could be conducted at start up of the MFD. A published distance calculator would need at least the wind speed and direction from the pilot and possibly the chosen runway. An even easier and possibly more useful system would simply compute takeoff distances for all the runways at the current airport and inform the pilot which were safe to takeoff from and which are not. Such a system might help pilots avoid choosing the wrong runway.

The second conclusion is that takeoff performance can be observed using acceleration and that steady deficiencies can be observed at the peak acceleration occurring at the very beginning of the takeoff. An acceleration criterion could be compared to the actual peak acceleration to provide the pilot with an easy “Go/No Go” indicator. Such a criterion could be derived two ways. A “required performance” approach would find the minimum peak acceleration required to takeoff on the current runway length distance given the drag characteristics of the aircraft. An “expected performance” approach would estimate the expected peak acceleration given the current weight, density altitude, runway slope, and surface type. Some combination of the two might help address both exceeding performance limits and performance deficiencies.

The third conclusion is that a real-time distance predictor is possible using the very simple constant average acceleration model, but only after correcting for GPS position errors and the airspeed/ground speed bias. A more accurate Differential GPS should solve the position error. The airspeed/ground speed bias should be explored further to determine where it originates, either in the air data computer or the GPS. If the source can be pinpointed, then a reliable correction could be included, perhaps similar to the rudimentary correction used here. With trustworthy GPS and airspeed, a Kalman filter could be used to estimate acceleration behavior and the time-to-rotation, and facilitating a better real-time takeoff distance predictor.

Chapter 4 Dynamic Stall and V-Speeds

Dynamic Stall and V-Speeds were designed and implemented on a PFD to address stall and takeoff climbout accidents. The *Dynamic Stall Speeds* are computed with respect to the weight and load factor during flight. The *Best Rate of Climb Speed* and *Best Angle of Climb Speed* are computed with respect to density altitude and weight, while the *Best Glide Speed* is computed with respect to weight.

To understand the design of the Dynamic Stall and V-Speeds prototype, the theory behind each speed is presented. The prototype was developed on a PFD and flight tested. Subject pilots found the Dynamic Stall and V-Speeds displays very useful in both maintaining awareness of stall margin and flying at optimal performance speeds.

4.1 Speeds Relevant to Flight

Every aircraft has a set of speeds related to its structural, aerodynamic, and performance limits. Some of these speeds are constant for an aircraft, some depend on loading or configuration, and some vary with aerodynamic conditions. It is the responsibility of the pilot to know each speed and how they vary during the course of the flight. In order to address stall and takeoff accidents, new ways were investigated to calculate and display four of these speeds; *Stall Speed*, *Best Rate of Climb Speed*, *Best Angle of Climb Speed*, and *Best Slide Speed*.

4.1.1 Stall Speed

By definition, maintaining flight requires avoiding stall. Physically, stall occurs when the critical angle of attack of the wing is exceeded and the airflow over the wing separates causing a significant loss in lift. As such, stall simply depends on the angle of attack of the wing and can occur at any airspeed and any attitude. Most general aviation aircraft, however, do not have any means of measuring angle of attack (a motivation for the Angle of Attack Estimators, described in Chapter 5) leading many pilots to think of

stall in terms of airspeed. This speed-based mental model of stall is furthered by the fact that airspeed indicators are marked with fixed stall speeds for flaps up and flaps down [2].

In 1g, un-accelerated flight, relating airspeed to angle of attack is sound. The lift generated by the wing is a function of the size and shape of the wing, the angle of attack, and the calibrated airspeed. For a given flap configuration, the size and shape of the wing are fixed, leaving a combination of angle of attack and airspeed to generate enough lift to support the weight of the airplane. At a higher angle of attack, the airplane can fly slower and still generate enough lift. At some point, however, the maximum angle of attack is reached, and the corresponding airspeed required at that angle of attack to generate enough lift to equal the weight is defined as the *stall speed*.

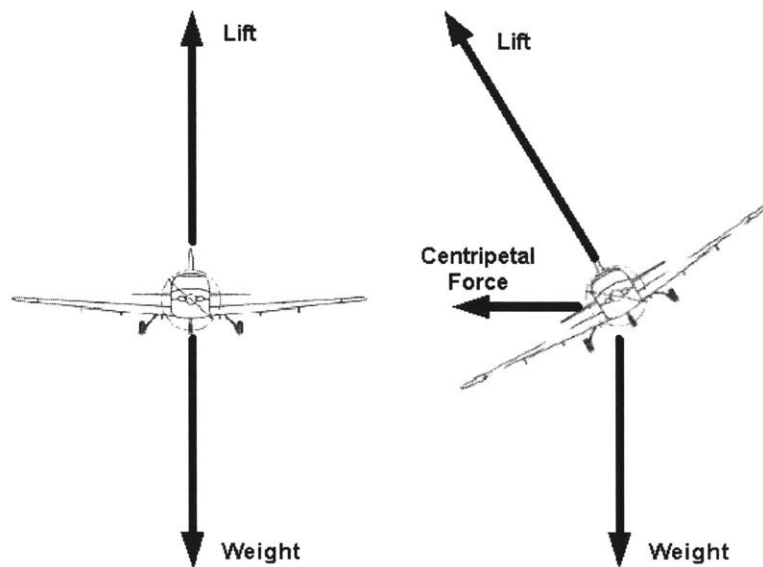


Figure 39: During a turn, more lift is required to support the weight and the centripetal force.⁷

Such a derivation of stall speed assumes the lift required equals the weight, which is true during straight and level flight. Some maneuvers, however, such as turns or pull-ups, require more lift than weight, thus increasing the stall speed. In a turn, as shown in Figure 39, the lift vector is tilted to the side, with the vertical component counteracting the weight, and the horizontal component providing the centripetal force to maintain the

⁷ Aircraft image from Cirrus SR22 Pilot's Operating Handbook

turn. This means that the total amount of lift required in a turn is higher than in straight and level flight. Since the critical angle of attack is a constant, the minimum airspeed required to maintain flight is higher. The change in stall speed for a Cirrus SR22 over increasing bank angle is shown in Figure 40.

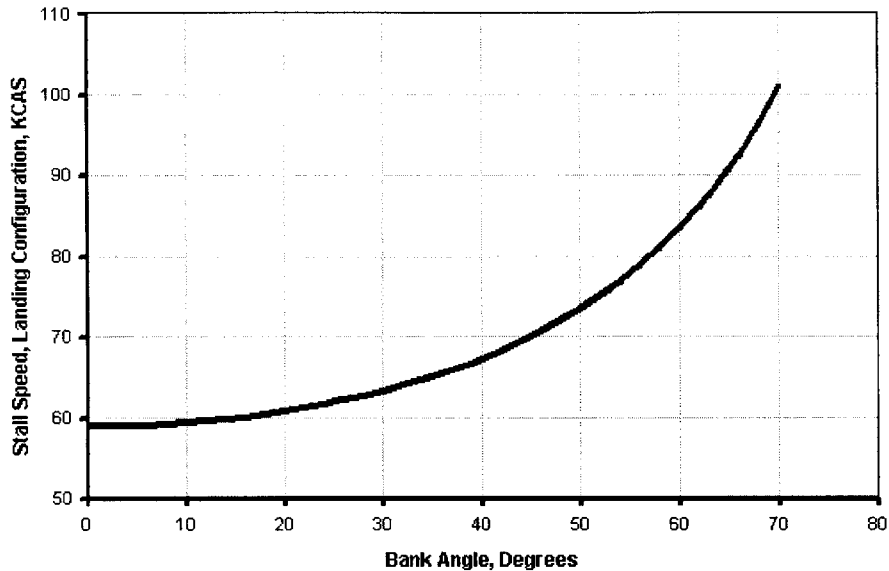


Figure 40: Flaps-down stall speed increasing with bank angle

It is precisely this increase in stall speed about which student pilots are instructed to be cautious and leave plenty of airspeed margin when making turns, especially in the traffic pattern. Despite these warnings, the “turn to final” stall is a common cause of accidents. As noted in Section 1.2 and in Figure 6, at least 80% of all stall/spin accidents over a ten-year period occurred at or below 1,000 feet above ground level. Forty-one percent of the fatal stall spin accidents over that same time period were classified as “maneuvering flight” indicating that the airplane was not flying straight and level at the time of the accident.

4.1.2 Climb Speeds

While stall and structural speeds are marked on the airspeed indicator, performance-based speeds are generally not. Instead, a pilot must study the Pilot’s Operating Handbook and memorize the speeds and the situations in which they apply.

An example of a table of performance speeds from the SR22 is shown below in Figure 41.

Section 4 Normal Procedures		Cirrus Design SR22
Airspeeds for Normal Operation		
Unless otherwise noted, the following speeds are based on a maximum weight of 3400 lb. and may be used for any lesser weight. However, to achieve the performance specified in Section 5 for takeoff and landing distance, the speed appropriate to the particular weight must be used.		
Takeoff Rotation:		
• Normal, Flaps 50%		70 KIAS
• Obstacle Clearance, Flaps 50%		78 KIAS
Enroute Climb, Flaps Up:		
• Normal		110-120 KIAS
• Best Rate of Climb, SL		101 KIAS
• Best Rate of Climb, 10,000		95 KIAS
• Best Angle of Climb, SL		78 KIAS
• Best Angle of Climb, 10,000		82 KIAS
Landing Approach:		
• Normal Approach, Flaps Up		90-95 KIAS
• Normal Approach, Flaps 50%		85-90 KIAS
• Normal Approach, Flaps 100%		80-85 KIAS
• Short Field, Flaps 100% (V_{REF})		77 KIAS
Go-Around, Flaps 50%:		
• Full Power		80 KIAS
Maximum Recommended Turbulent Air Penetration:		
• 3400 lb.		133 KIAS
• 2900 lb.		123 KIAS
Maximum Demonstrated Crosswind Velocity:		
• Takeoff or Landing		20 Knots
4-4		P/N 13772-001 Revision A2

Figure 41: V-Speeds in the Cirrus SR22 Pilot's Operating Handbook

Figure 41 lists two optimal performance speeds that are often used while climbing out after takeoff; the *Best Rate of Climb Speed*, referred to as V_X , and the *Best Angle of Climb Speed*, referred to as V_Y . Both are speeds for the optimal performance referred to by their names.

The *Best Angle of Climb* is defined as the angle at which an aircraft gains the maximum amount of altitude over a given distance. Because the maximum climb angle is defined geometrically, it is most useful when attempting to clear an obstacle, such as a tower at the end of a runway or terrain that suddenly appears in front of the airplane. The speed at which the best angle of climb occurs is very low and close to the stall speed. For

the SR22, the best angle of climb speed V_X is 78 KIAS at sea level, only 8 knots above the clean configuration stall speed of 70 KIAS.

The *Best Rate of Climb* is defined as the maximum amount of altitude an aircraft can steadily climb in a given amount of time. When clearing an obstacle is not critical, this climb speed is normally preferred after takeoff because it allows the pilot to achieve cruise altitude most quickly. The speed at which the best rate of climb occurs is also much higher than the best angle of climb speed, allowing the nose to point lower to the horizon, facilitating better visibility, as well as providing more margin between the climb speed and the stall speed. At sea level, the best rate of climb speed V_Y for the SR22 is 101 KIAS.

Mathematically, the best angle of climb speed is the speed at which the excess *thrust* is maximized, while the best rate of climb speed occurs when excess *power* is maximized [8]. For a theoretical fixed pitch propeller aircraft, the best angle of climb speed depends only upon the weight of a given airplane, and is constant over density altitude. For the SR22, a constant-speed propeller airplane, the published V_X values do in fact change with density altitude, but do so slowly. However, such a derivation is useful because it allows the assumption that V_X is at least linear, if not constant for the SR22. Thus, the best angle of climb speed for any given density altitude can be interpolated from the values published for sea level and 10,000 feet.

Likewise, the best rate of climb speed V_Y behaves linearly, decreasing with altitude, until V_X and V_Y converge at the theoretical absolute ceiling of the aircraft. As such, it can also be assumed that V_Y for a given density altitude can be interpolated from the values published for sea level and 10,000 feet.

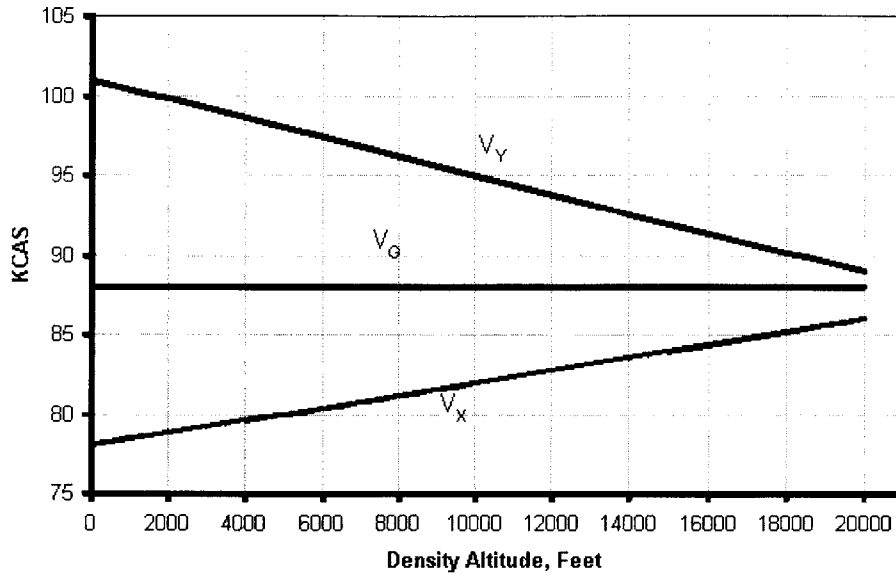


Figure 42: V-Speeds for a Cirrus SR22 changing over density altitude, at maximum gross weight, as interpolated from the pilot’s operating handbook. Best Glide Speed, V_G , does not change with density altitude.

4.1.3 Best Glide Speed

In the event of engine failure, maximizing potential range can be crucial when attempting to find an airport to land. To maximize the range, the pilot must quickly fly to the *Best Glide Speed*, V_G , and maintain it throughout the descent. The best glide speeds for two different weights of the SR22 are shown below in Figure 43.

Section 3 Emergency Procedures	Cirrus Design SR22
Airspeeds for Emergency Operations	
Maneuvering Speed:	
3400 lb	133 KIAS
Best Glide:	
3400 lb	88 KIAS
2900 lb	87 KIAS
Emergency Landing (Engine-out):	
Flaps Up	90 KIAS
Flaps 50%	85 KIAS
Flaps 100%	80 KIAS

Figure 43: Published Best Glide Speeds from a Cirrus SR22 Pilot’s Operating Handbook

Like the best angle of climb speed, the best glide speed is relatively low. For the Cirrus, the best glide speed is 87-88 KIAS depending on the weight, or 18 knots higher than the flaps up stall speed. At such low speeds, maintaining the best glide speed is not only important for extending range, but also for avoiding stall. Compounding the challenge is the fact that an engine-out is a time-critical, high workload situation. The pilot must quickly fly to and maintain the best glide speed, select an emergency landing site, attempt to restart the engine, communicate the situation to air traffic control, and if the engine does not restart, prepare for an emergency landing. Despite the workload during such an intense situation, the pilot must rely on memory to recall the glide speed, as it is usually not marked or placarded in the airplane except in the POH.

According to theory, the best glide speed is a function of the square root of the aircraft weight and is constant over density altitude [8]. From the empty weight to the maximum gross weight, the change in best glide speed with weight is approximately linear. Indeed, the Cirrus POH gives two values, 87 KIAS for 2900 lbs and 88 KIAS for 3400 lbs, leaving the pilot to interpolate between the two. Curiously, according to theory, the best glide speed should change with weight much more than the Cirrus POH indicates, but for this prototype, the published values were used.

4.2 Existing V-Speed Indicators

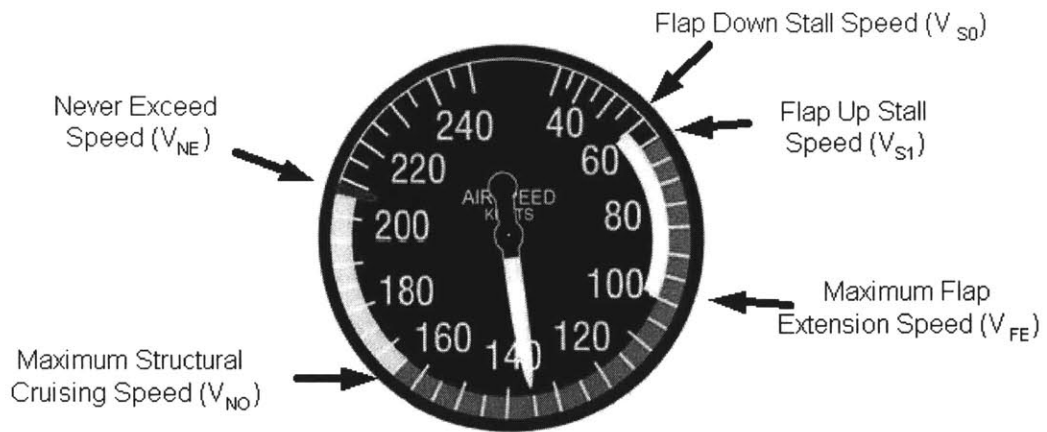


Figure 44: Traditional mechanical airspeed indicator with stall and structural speeds painted on.⁸

On a typical general aviation mechanical airspeed indicator, as shown in Figure 44, the stall speeds for a clean configuration (flaps and gear up, V_{S0}) and a landing configuration (flaps and gear down, V_{S1}) as well as structural limit speeds are shown as the end point of color bands. On mechanical airspeed indicators, these displayed stall speeds are fixed because they are simply painted on the airspeed indicator.

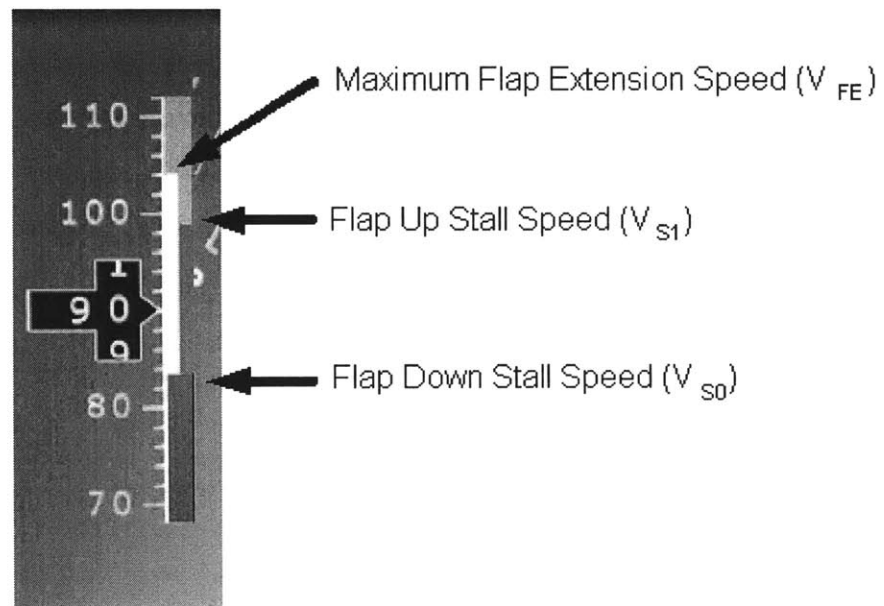


Figure 45: Stall and Structural Speeds on an electronic airspeed tape.

⁸ Airspeed indicator image from http://www.nappf.com/nappf_flight_instruments_files/image003.jpg

Integrated electronic displays in general aviation typically use a “tape” format instead of a “dial”, but generally repeat the colored arcs at fixed values scheme of the mechanical systems. In some products, the climb speeds are marked, but they are usually static values that do not adjust with density altitude. Only in larger transport aircraft are the stall speeds and V-speeds computed dynamically by the flight management system [24].

4.3 Prototype V-Speed System Design

In order to address stall, climbout, and engine-out accidents, the airspeed indicator of a PFD was modified to dynamically calculate and display the *flaps down stall speed*, the *flaps up stall speed*, the *best angle of climb speed*, the *best rate of climb speed*, and the *best glide speed*. The speeds are computed using pressure altitude, outside air temperature, weight, and load factor at the current instant of flight. A flow diagram of the Dynamic Stall and V-Speeds system is shown below in Figure 46.

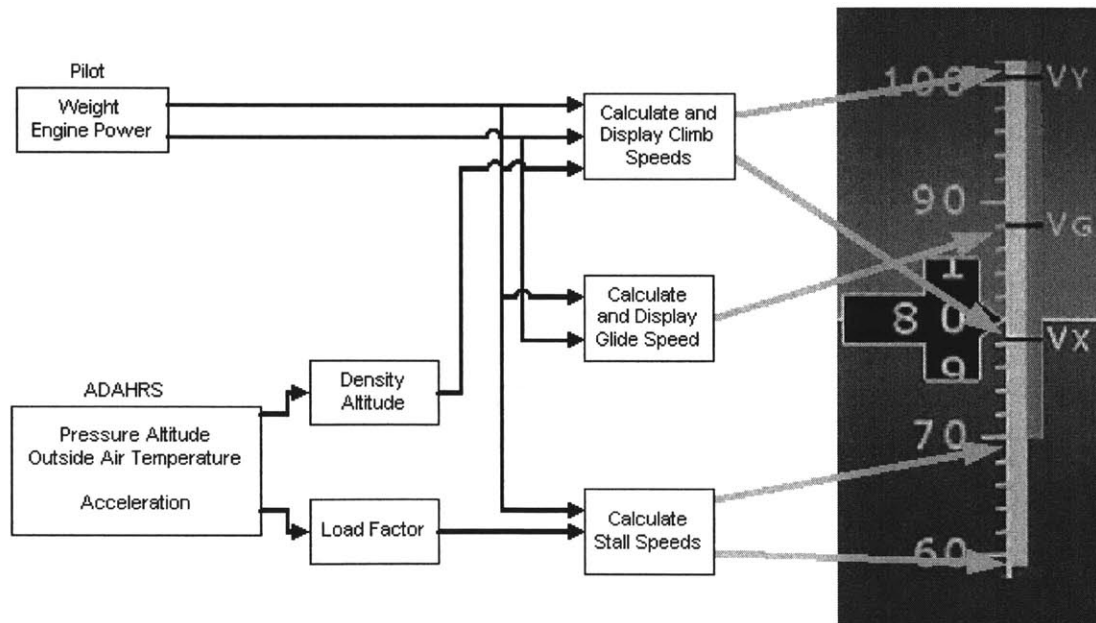


Figure 46: Dynamic Stall and V-Speed System Design

4.3.1 Stall Speeds

The standard stall speeds of the Cirrus for maximum gross weight at 1g flight are adjusted by two parameters: weight and load factor. Weight was input manually through

the laptop and transmitted to the PFD. Load factor was assumed to be the acceleration measured in the vertical direction in body axes. Thus the stall speeds were computed using Equation 3, where W is the current weight, W_0 is the maximum gross weight, and n is the load factor.

$$V_{dynamic\ stall} = V_s \sqrt{\frac{W}{W_0} n} \quad (3)$$

The computed flaps down stall speed and flaps up stall speed are then displayed in exactly the same way they are displayed on a fixed airspeed indicator, with the colored arcs. On the airspeed tape, the top of the lower red arc indicates the flaps down stall speed, and the bottom of the green arc indicates the flaps up stall speed. The locations of these arcs are then allowed to move as the stall speed changes with weight and load factor. Figure 47 shows the stall speeds increasing by a factor of 1.41 during a 60° bank and load factor of 2g.

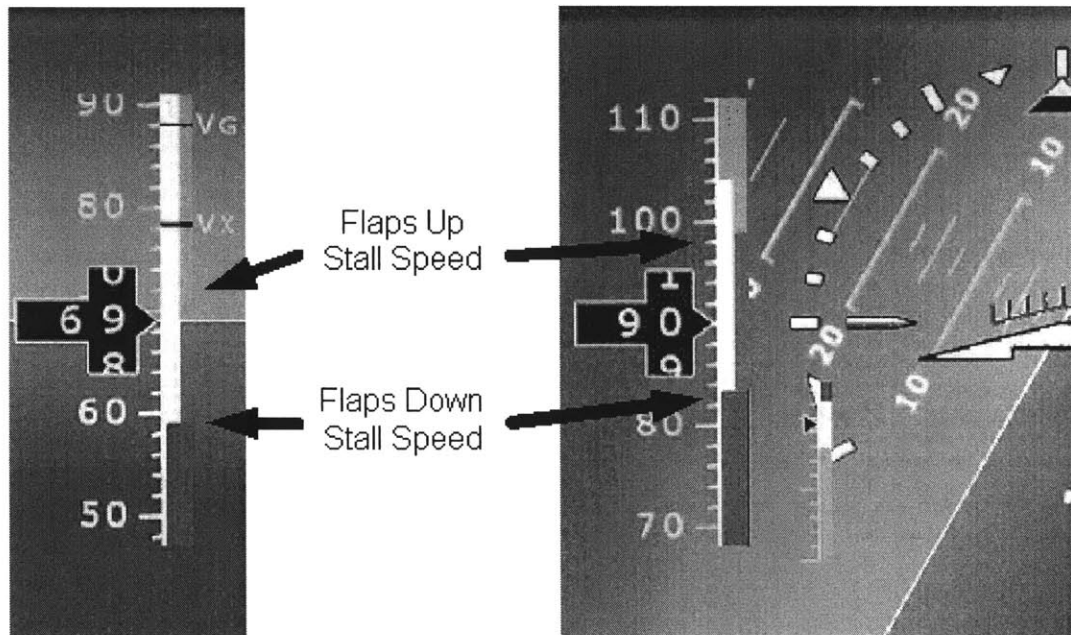


Figure 47: Increased stall speeds during a steep turn. Stall speed for flaps down, V_{s0} , is shown at the top of the red arc, and the flaps up stall speed, V_s , is shown at the bottom of the green arc.

4.3.2 Climb and Glide Speeds

The best angle of climb speed and the best rate of climb speed are linearly interpolated from the Pilot's Operating Handbook, based on the density altitude. The speeds are then adjusted by the weight. The best glide speed is only a function of the weight, and is computed with a linear interpolation of the Pilot's Operating Handbook values.

The climb and glide speeds are marked on the airspeed indicator with a black line and white text, as shown in Figure 48. They can be turned on and off at the Flight Test Engineer's command through the laptop, simulating the case where the climb speeds appear when the engine is at full power and the glide speed appears when the engine is at idle or not running.

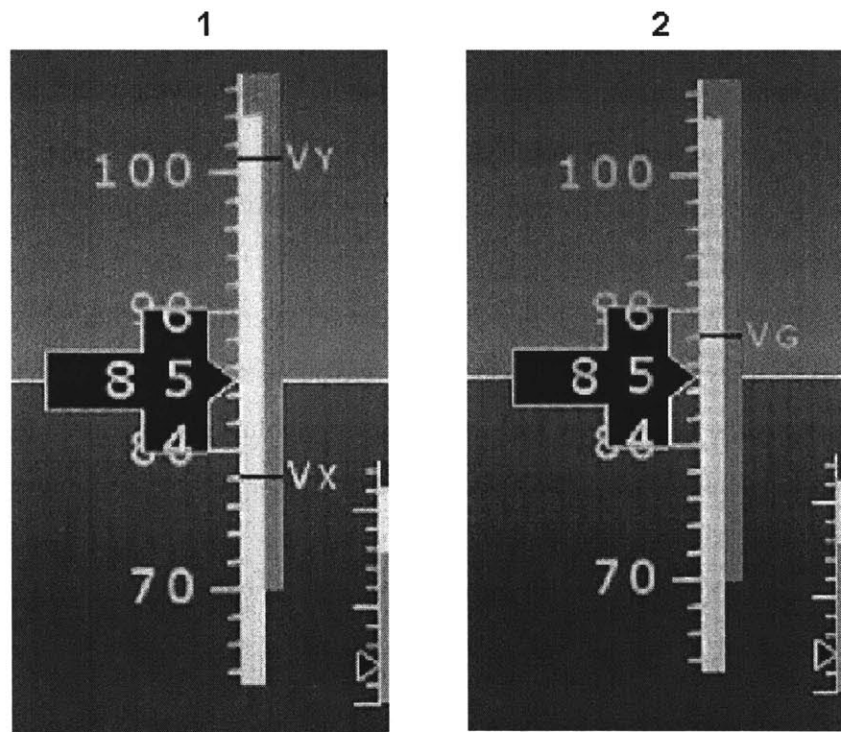


Figure 48: 1) Best Rate of Climb Speed, V_Y , and Best Angle of Climb Speed, V_X 2) Best Glide Speed, V_G

4.4 V-Speed Flight Tests

In a series of test flights, three subject pilots were asked to provide subjective feedback while using the displays in climbs, simulated engine-out situations, and the slow

flight environment. During and after the flight, comments were recorded detailing the usefulness or distraction caused by the speed displays. A list of the maneuvers used in the test protocol is shown in Table 4.

Table 4: V-Speeds Flight Test Maneuvers

<u>Maneuver</u>	<u>Relevant Speeds</u>
Takeoff Climbout	V_X, V_Y
Slow Flight, Straight and Level	V_S
Slow Flight, Climbing Turn	V_S
Slow Flight, Descending Turn	V_S
Slow Flight, Steep Turn	V_S
Chandelle	V_S, V_X
Simulated Engine-Out	V_G

The dynamic stall speed displays were evaluated by asking the pilots to avoid stall while performing various maneuvers in slow flight and an aggressive climb maneuver. The slow flight maneuvers included straight and level flight, climbing 90° turns, descending 90° turns, and a 360° steep turn at 45° of bank. For the aggressive climb maneuver, pilots performed a chandelle, where the objective is to gain as much altitude as possible while reversing direction.

Following each takeoff, the pilots were given the climb speed displays and allowed to use them as they desired. Similarly, two subject pilots performed simulated engine-out maneuvers, where they were required to establish and maintain the best glide speed while turning towards an emergency airport and proceeding through the Engine Restart and Forced Landing checklists.

Following each flight test, the subject pilots filled out a questionnaire and debriefed to record their reactions to the prototype displays.

4.5 Flight Test Results

Data from the Dynamic Stall and V-Speeds flight tests showed both performance benefit and pilot preference for the new displays. In general, the pilots were able to fly maneuvers in slow flight much closer to the dynamic stall speed with it being displayed than with only the static stall speed displayed. None of the pilots reported the stall speeds as distracting. The pilots also strongly preferred having the climb and glide speeds

displayed, citing them as both memory aids as well as helping them fly closer to their target speed.

4.5.1 Dynamic Stall Speed Maneuvers

The data plots for the Dynamic Stall and V-Speeds tests are all time histories of speed. Figure 49 is an example, showing the slow flight maneuvers flown by Subject Pilot 4.

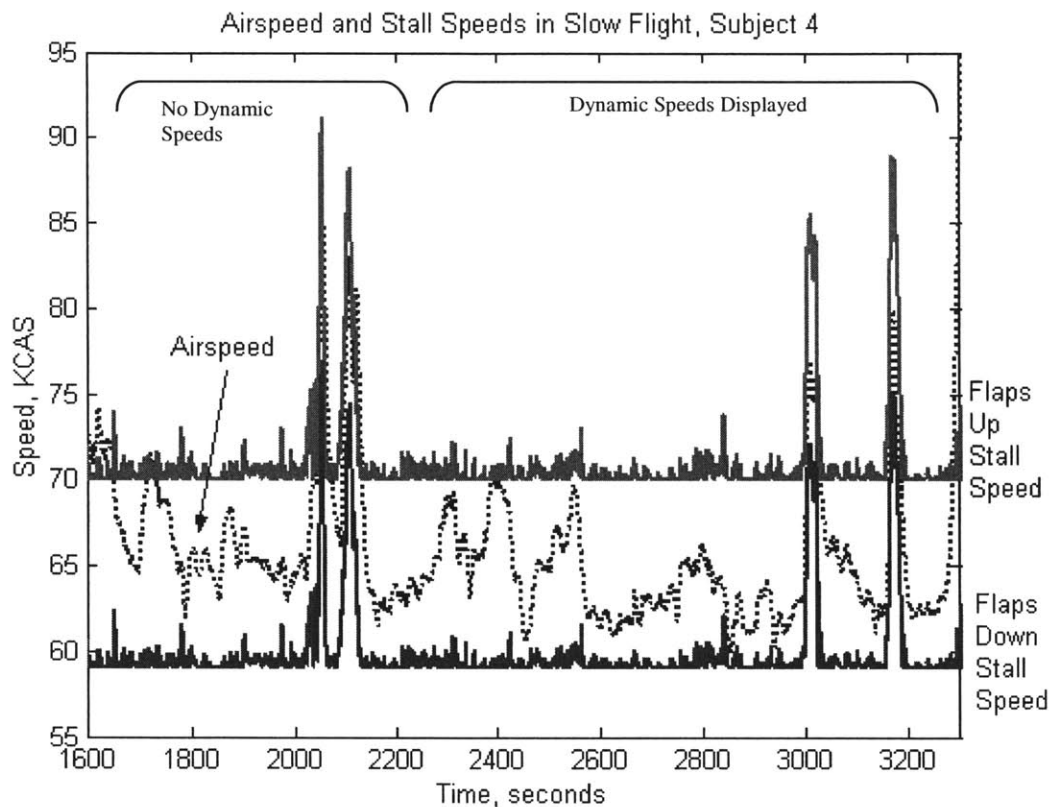


Figure 49: Airspeed and Stall Speeds in Slow Flight for Subject 4. Airspeed is the dotted line, flaps-up stall speed is the upper line based on 70 KCAS, and the flaps-down stall speed is the lower line based on 59 KCAS.

Time is shown in seconds from the start of the test flight. The dotted line is the aircraft's airspeed, while the two solid lines are the dynamic stall speeds. The upper stall speed is the Flaps Up Stall Speed. The lower stall speed is the Flaps Down Stall Speed. Most of the time, the flaps down and flaps up stall speeds fluctuate around their default values, 59 KIAS and 70 KIAS, respectively, as the aircraft was either in level or slowly accelerating flight. The fluctuation during these relatively un-accelerated portions of

flight was due to turbulence. The four peaks, where airspeed and the stall speeds increase significantly, were steep turns and will be examined in more detail. The plot is broken up into two sections, when the dynamic speeds were displayed and when they were not. In the portion of the plot representing when the dynamic speeds were not displayed on the airspeed indicator, the static stall speeds were displayed instead.

4.5.1.1 Un-Accelerated Maneuvers in Slow Flight

The portions of Figure 49 where the dynamic stall speed is approximately equal to the static stall speed represents maneuvers that were either un-accelerated or very slowly moving such that the load factor was approximately 1g. These maneuvers include straight-and-level and the climbing and descending turns, which were performed very slowly.

During straight-and-level and the slow climbing or descending turns, Subject 4 managed to maintain slow flight approximately 5 KIAS above the stall speed, with some fluctuation, with both the dynamic and fixed stall speeds displayed. This was expected because during un- or low-accelerated flight, the load factor is small and the dynamic stall speed is near the static stall speed. The slow flight speed plots for the other two subject pilots reflect this behavior, shown in Figure 50 and Figure 51.

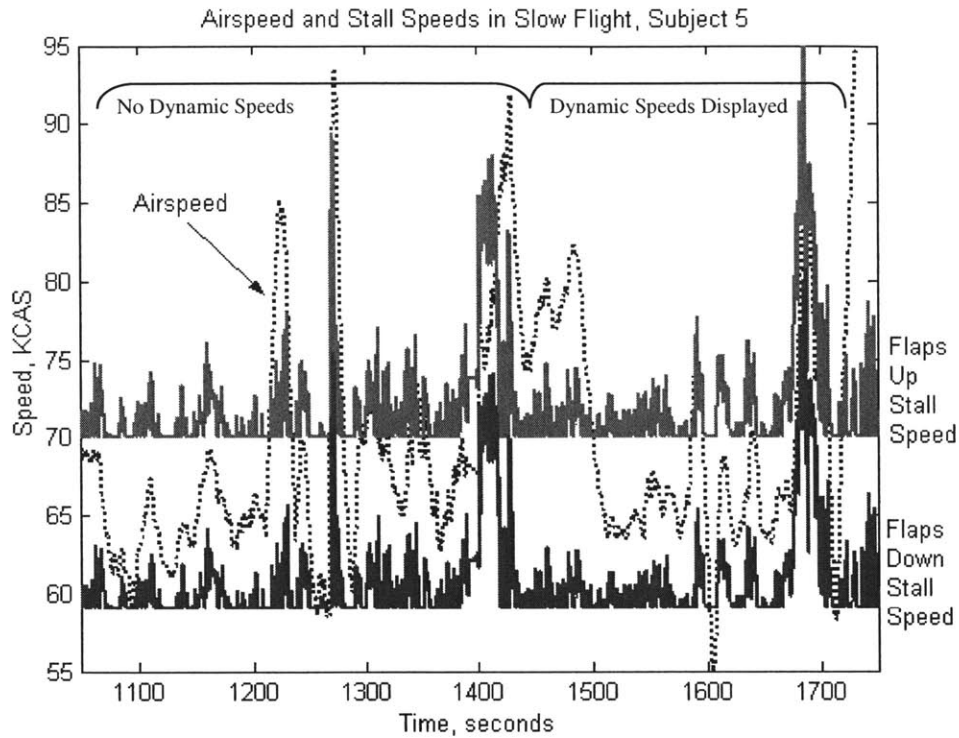


Figure 50: Airspeed and Stall Speeds during slow flight for Subject 5

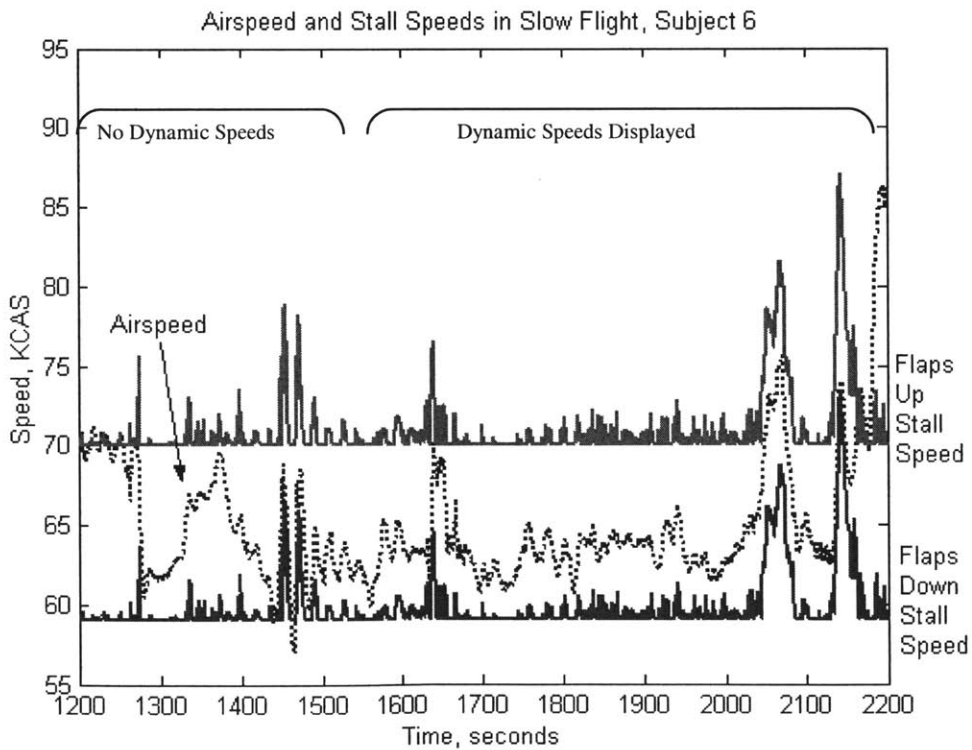


Figure 51: Airspeed and Stall Speeds during slow flight for Subject 6

4.5.1.2 Steep Turns in Slow Flight

During steep turns in slow flight, when the dynamic stall speed increased due to the increased load factor, subjects were able to fly closer to the dynamic stall speed while still avoiding stall when using the dynamic stall speed display than when using the static stall speeds.

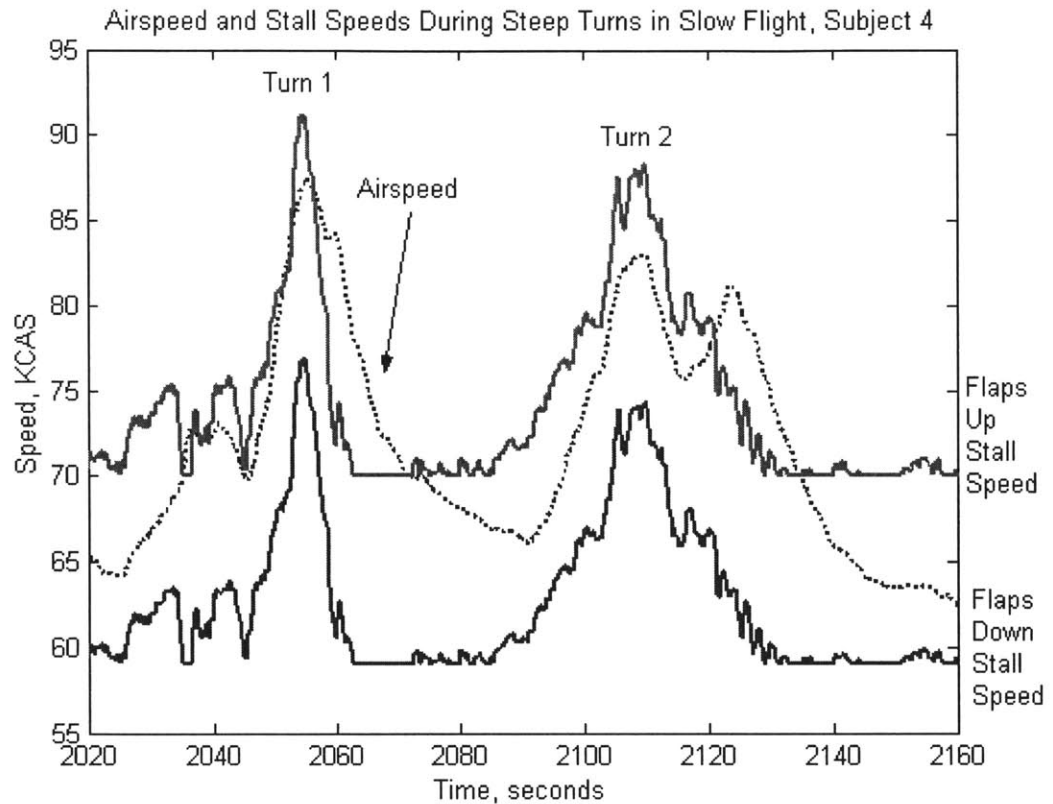


Figure 52: Two steep turns with fixed stall speeds displayed only, no dynamic stall speeds

Figure 52 shows the airspeed and the dynamic stall speeds during two steep turns in which only the static stall speeds were shown and not the dynamic stall speeds. The pilot avoided stall during both maneuvers and explained in debrief that he used the stall horn and airframe buffeting as his cues for stall margin in the absence of the dynamic stall speed indicator.

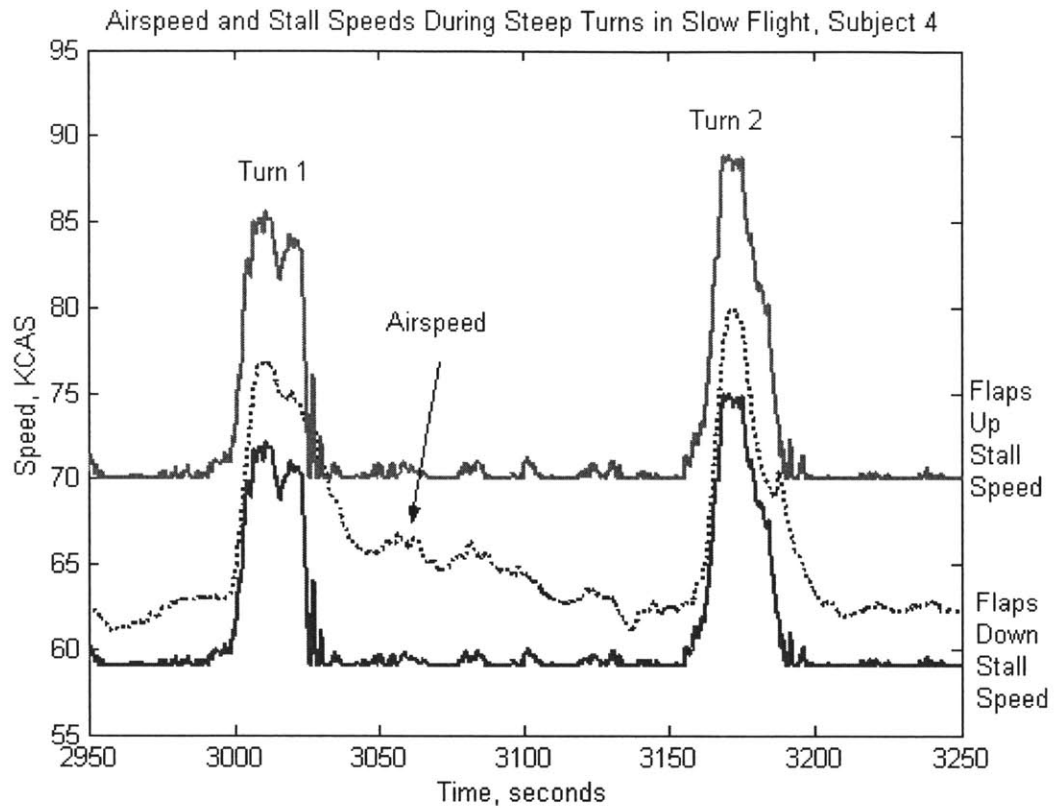


Figure 53: Two steep turns with dynamic stall speeds displayed

Figure 53 shows airspeed history of the same pilot performing two steep turns in slow flight with the dynamic stall speed displayed on the PFD. The pilot is able to maintain the steep turn while flying much closer to the dynamic stall speed. Subject 5 demonstrated the same improvement in performance with the dynamic stall speeds displayed compared to when only the static speeds displayed, as shown in Figure 54 and Figure 55.

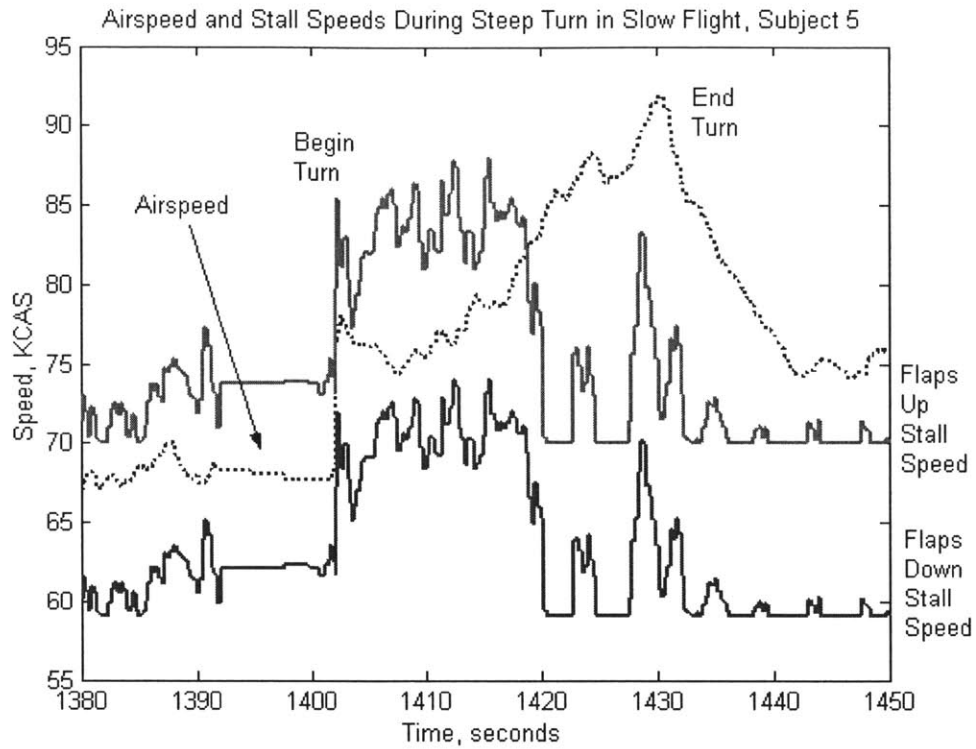


Figure 54: Steep turn in slow flight, static stall speeds displayed only, Subject 5

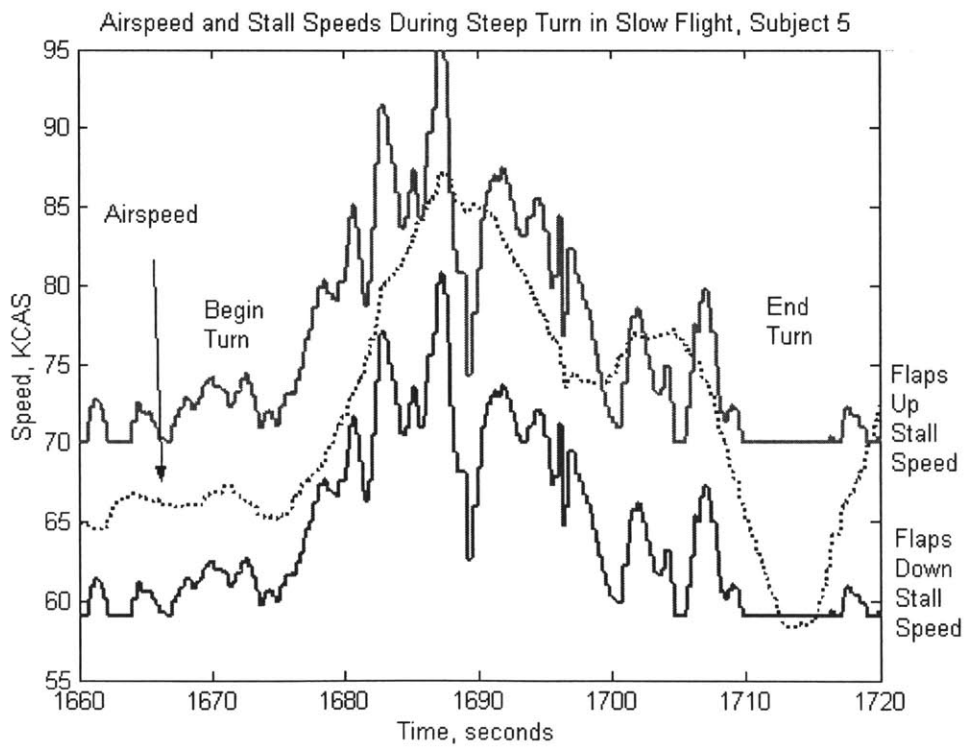


Figure 55: Steep turn in slow flight, dynamic stall speeds displayed, Subject 5

However, these performance improvements may also be attributed to learning, since neither subject pilot had any experience in this type of aircraft. Subject 6 only performed a steep turn with the dynamic stall speeds displayed, and thus has no baseline to compare to. However, the learning effect is very noticeable in Subject 6, as seen in Figure 56, where he performs his second steep turn much closer to the dynamic stall speed than during the first turn.

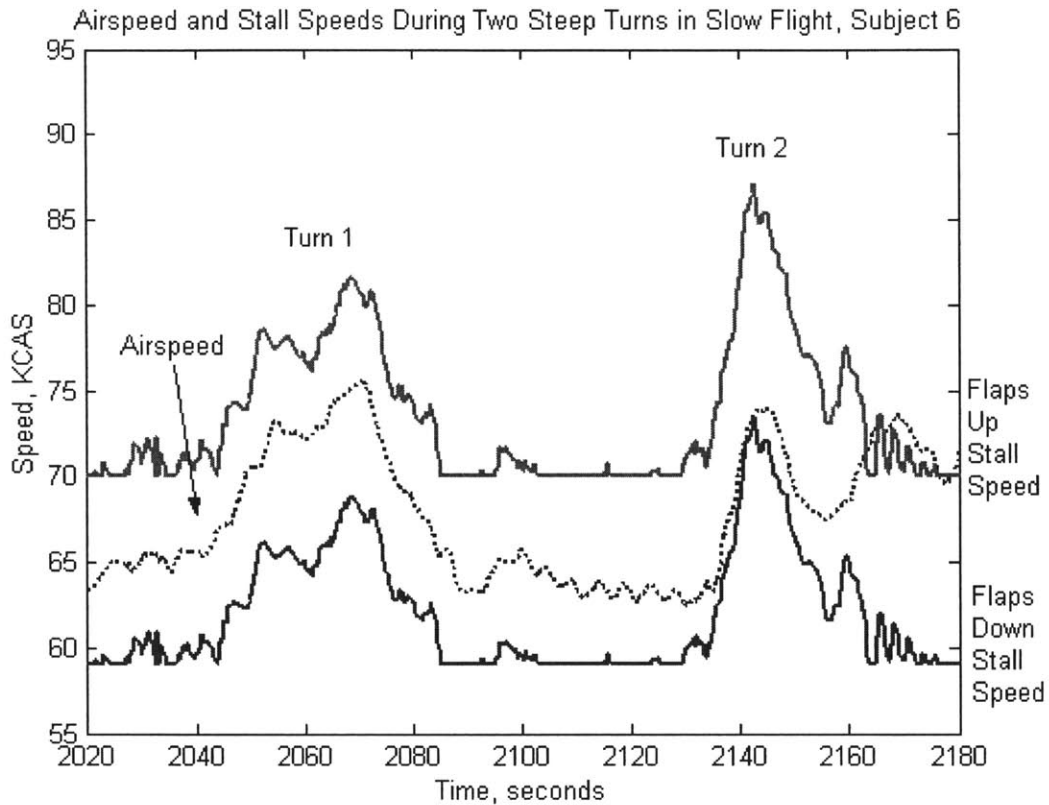


Figure 56: Two steep turns, both with dynamic stall speed displayed, Subject 6

4.5.1.3 Chandelles

Subjects 4 and 5 each performed two chandelles, one chandelle with only the static stall speed displayed and one with the dynamic stall speeds and climb speeds displayed. Subject 4 was able to perform the chandelles much more aggressively using the dynamic stall speed display than using the static stall speeds. Subject 5 did not demonstrate the same improvement. Both subjects performance in chandelles should be

taken lightly, however, since neither had any experience performing them before the flight tests.

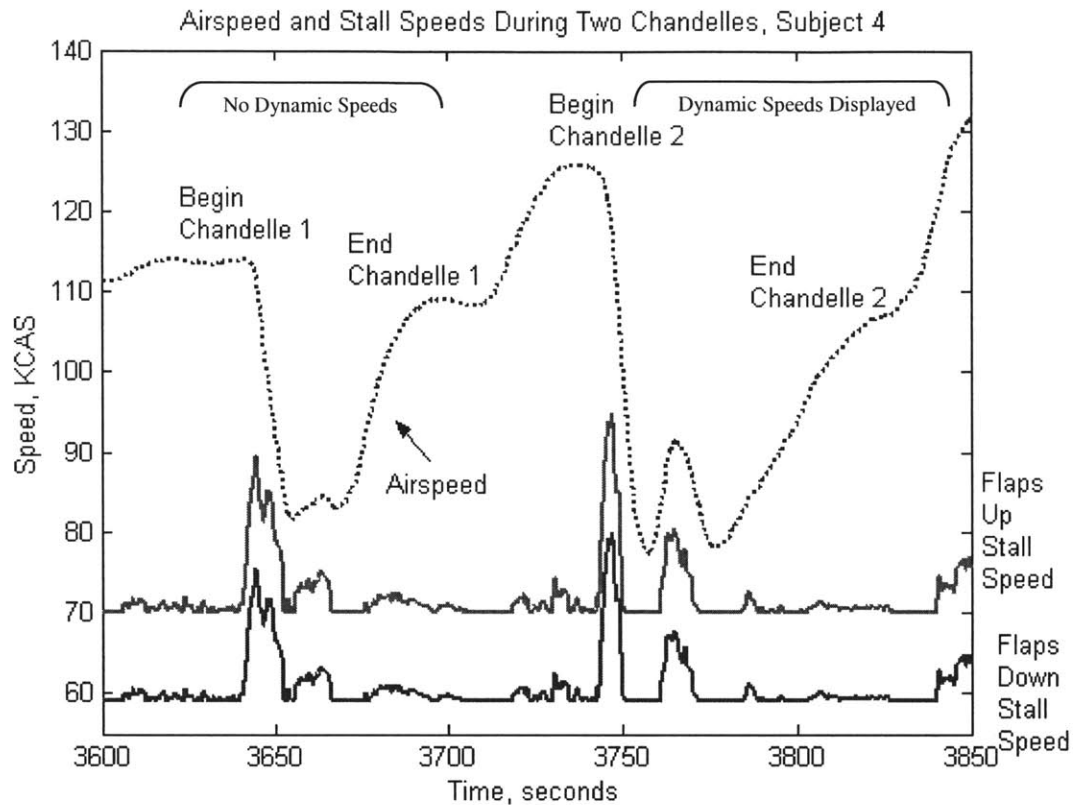


Figure 57: Two chandelles performed by Subject 4, the first with only static stall speeds, the second with the dynamic stall speed displays

Figure 57 shows two chandelles performed by Subject 4. During the first chandelle, only the static stall speeds were displayed. During the second chandelle, the dynamic stall speeds as well as the climb speeds were displayed. With the dynamic speeds, the pilot was able to perform the chandelle much more aggressively, completing the maneuver with less airspeed than using only the static stall displays. Furthermore, the pilot demonstrated a reaction to flying near stall when the dynamic stall speed increased abruptly at the end of the second chandelle by increasing speed as the stall speed rose.

The dynamic stall speed was not the only stall margin cue used by the pilots. Figure 58 also shows how the Subject 5 used other cues to determine stall margin, when at approximately 1940 seconds, the stall speed begins to increase. The pilot said he used

the stall horn and buffeting cues to infer that the stall margin was decreasing, and thus compensated by increasing airspeed.

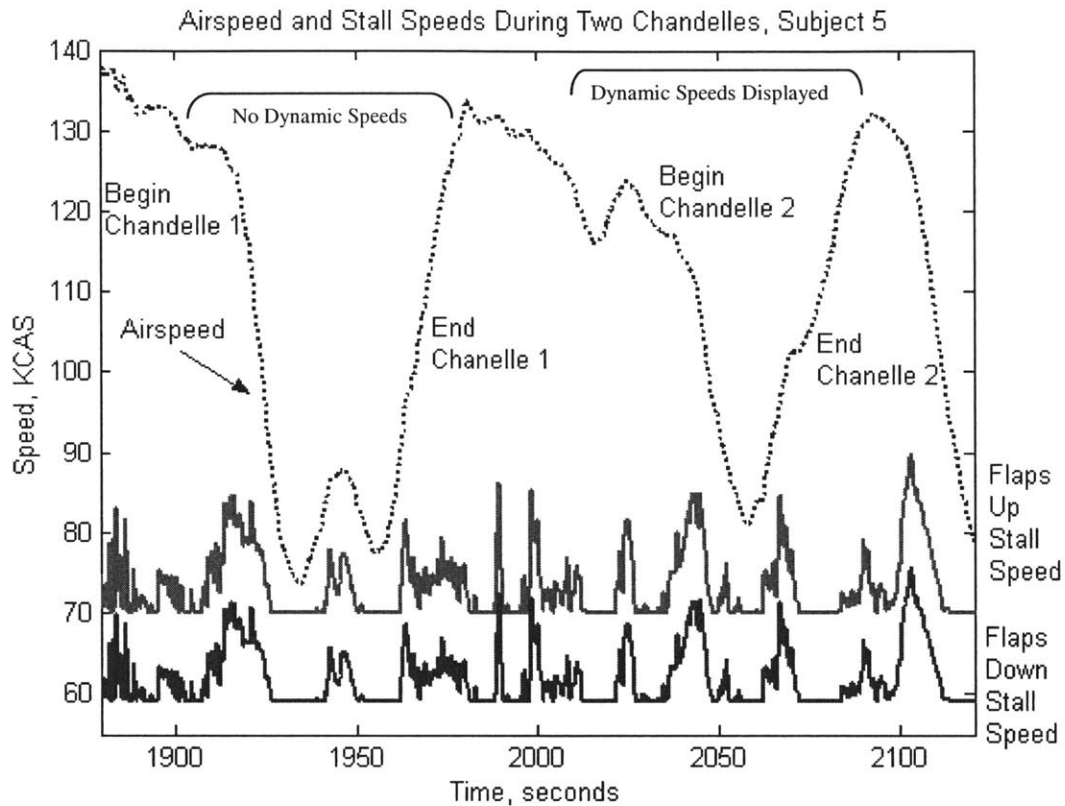


Figure 58: Chandelles with only static stall speed and with dynamic stall speeds for subject 5

4.5.1.4 Pilot Feedback on Dynamic Stall Speeds

All of the pilots who flew with the dynamic stall speed displays thought they were useful. Most of the pilots did not consciously notice the stall speed color arcs moving, but Pilot 4 commented that that was not necessarily bad. Instead, he trusted the location of the arcs as the region of stall and did not necessarily care that the actual speed had increased. This trust factor was further reinforced by the fact that the dynamic stall speeds corresponded with the region of buffeting as the aircraft flew close to the dynamic stall speed.

The pilots all used additional cues to determine stall margin. Most used the stall horn and the onset of buffeting as the primary stall margin cues, with the dynamic stall speeds as the secondary cue. Pilot 6 did use the dynamic stall speeds as the primary cue

during the steep turn, attempting to keep the airspeed between the red and green arcs when they moved upward as the load factor increased in the turn.

Pilot 1 expressed concern that using movable arcs may present misleading trend cues to the pilot. When not looking at the airspeed indicator directly, if the dynamic stall speed increased, causing the arcs to rise, the pilot might actually think the airspeed is dropping. However, while the actual airspeed may not be changing, the relative stall margin is, and it is a trend the pilot should be aware of. In that case, the trend cue provided by the dynamic stall indicator would help the pilot be more aware of the situation.

4.5.2 Climb Speed Maneuvers

During climbout after takeoff, the climb speeds were displayed and the pilots were left to use the V_X and V_Y cues as they saw fit. Only one subject pilot, Subject 6, attempted to fly at V_Y for the best rate of climb during climbout. The time history of airspeed and the best climb speeds are shown in Figure 59.

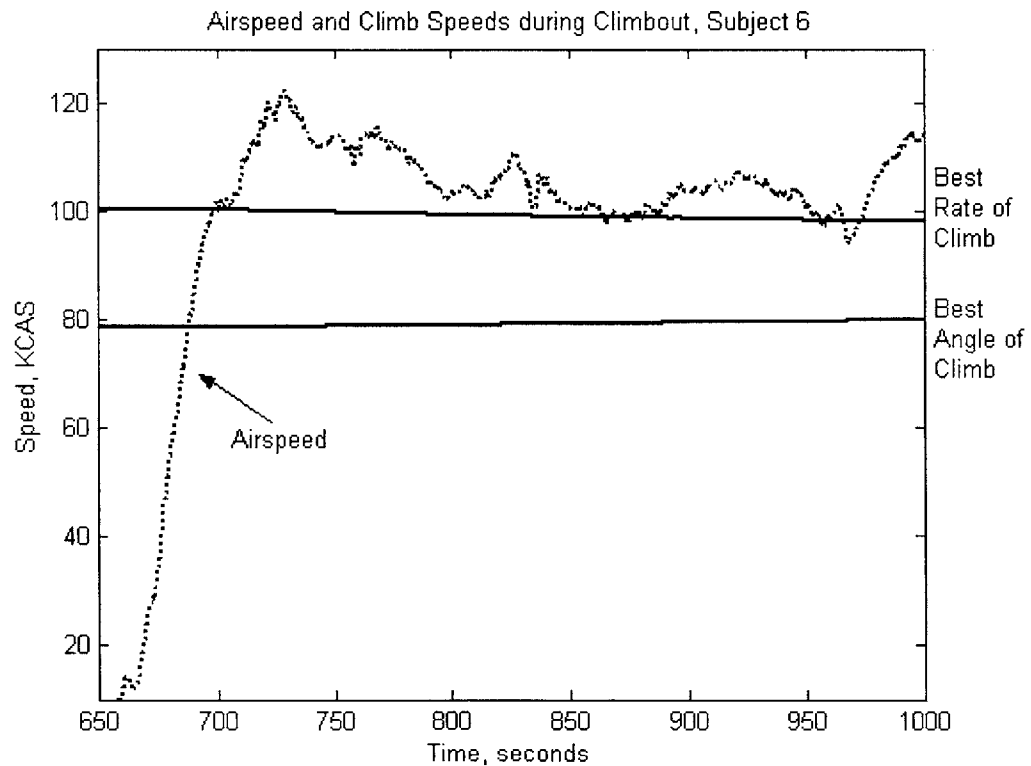


Figure 59: Speed During Takeoff and Climbout for Subject 6

All of the pilots thought that the climb speed markers were useful. None expressed any concern with distraction. One pilot did comment that while using the V_X marking during a chandelle, he noticed that his rate of climb was significantly diminished. For these prototypes, only the stall speeds were linked to load factor and not the climb or glide speeds because of concern that fluctuations in load factor would cause the V-speed markers to jitter and become distracting. In theory, however, the climb and glide speeds are all affected by load factor, so it could be explored whether to incorporate it into the weight fraction adjustment.

4.5.3 Glide Speed Maneuvers

Pilots 4 and 5 performed simulated engine-outs, where they had to quickly achieve and maintain the best glide speed V_G , select an emergency landing field, and go through the engine restart and forced landing checklists. Their time histories of airspeed, showing how closely they were able to maintain the best glide speed, are shown in Figure 60 and Figure 61.

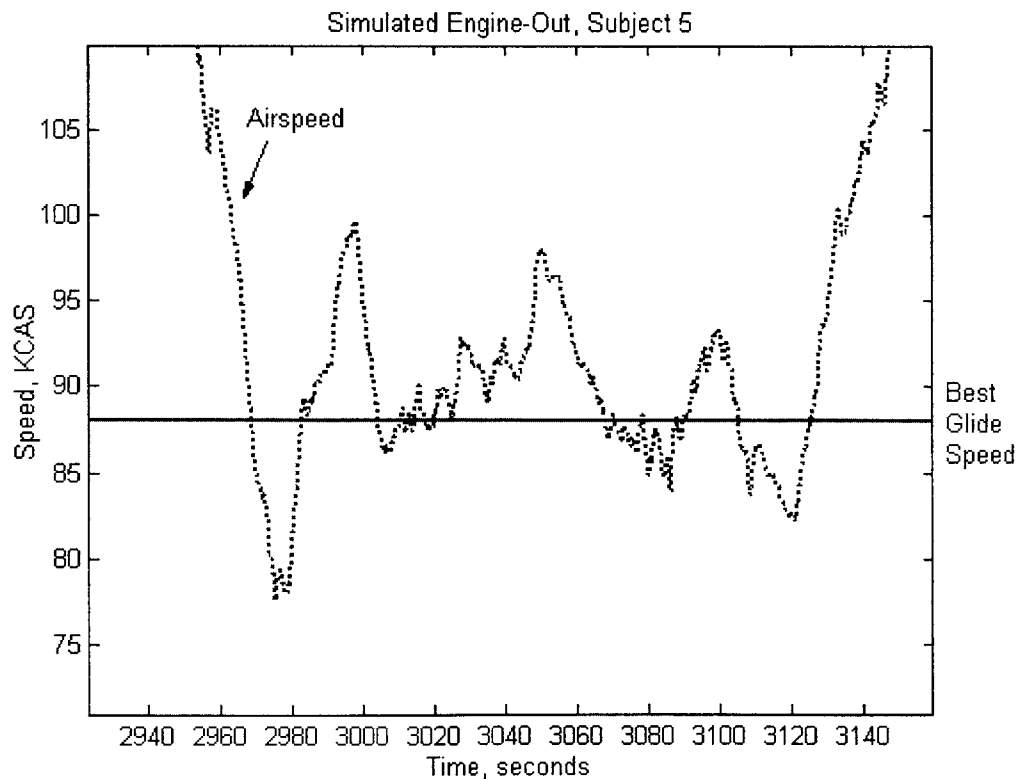


Figure 60: Airspeed and Best Glide Speed during simulated engine-out, Subject 5

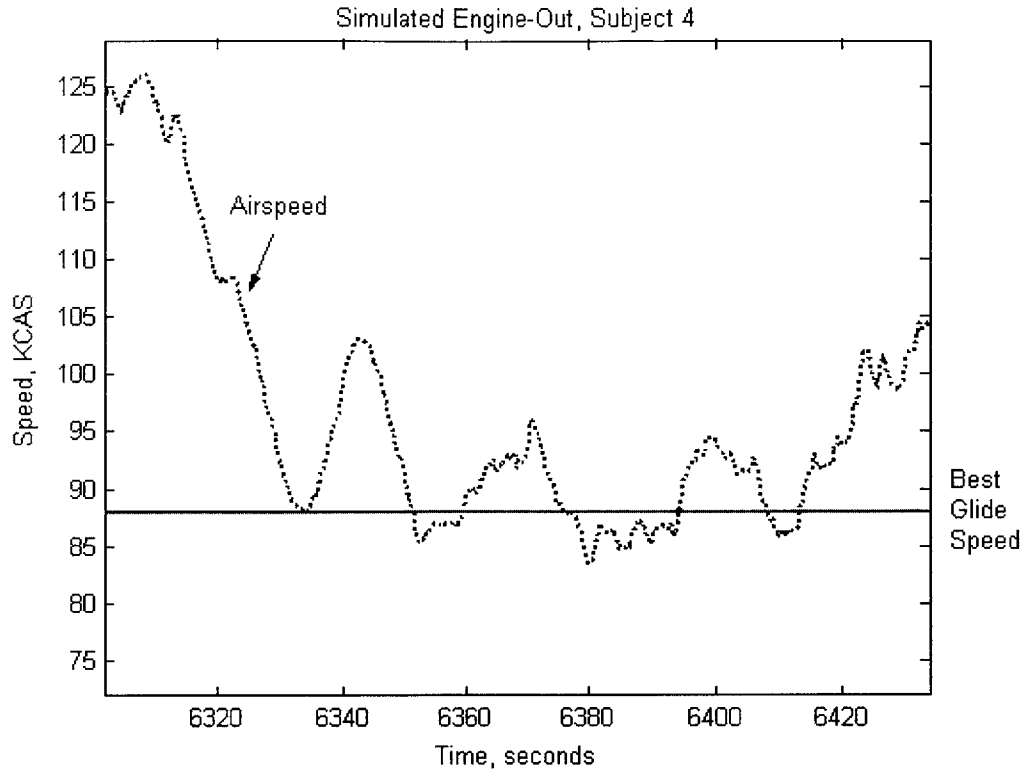


Figure 61: Airspeed and Best Glide Speed during simulated engine-out, Subject 4

Both subjects thought the V_G marking was a very useful cue, especially if the pilot does not remember the speed immediately. One pilot commented that maintaining V_G with the target speed displayed was not difficult once he got used to using an airspeed tape.

A pilot who did not fly with the prototype displays suggested the idea of placing the best glide cue on the vertical speed indicator instead of the airspeed. Doing so would allow the pilot to set the autopilot to fly the best glide vertical speed, freeing some of the pilot's attention resources which can be better focused on selecting a field and attempting an engine restart.

4.6 Conclusions

During the flight tests, the Dynamic Stall and V-Speed prototypes were observed to be useful to the pilots. Dynamic stall speeds appeared to help the pilots maintain better awareness of the stall margin. The most important factor in the dynamic stall speed, the load factor, is available in the standard ADAHRS data. Weight is not available presently,

but could be if a weight and balance were performed on the MFD. Until then, the dynamic stall should be implemented with load factor only.

The climb speeds should be implemented with the density altitude initially and then weight as it becomes available. It should be explored whether to also incorporate load factor into the climb speeds to provide more accurate targets during accelerated climbs, such as chandelles.

The best glide speed, which depends solely on weight, should be implemented as a range of speeds between the maximum weight and the low weight listed in the Pilot's Operating Handbook until weight becomes available. The human factors of this should be studied, however, to see if pilots would understand that they should choose their target based on their weight instead of flying to the center of the range.

In order to avoid cluttering the airspeed indicator, the glide speed should only be displayed during an engine-out, while the climb speeds should only be displayed during full power climbs. To implement this de-cluttering scheme, algorithms for detecting engine-outs and full power will need to be developed. Some combination of tachometer, manifold pressure, fuel flow, alternator amperes, or other engine data could be used.

Chapter 5 Angle of Attack Estimator

An *Angle of Attack Estimator* was designed and implemented on a PFD to help a pilot maintain awareness of stall margin. Two estimation methods were used. The *Speed-based Method* computed the lift required for flight and used a simple aerodynamic model to compute the necessary angle of attack. The *Angle-based Method* measured the angular difference between the aircraft attitude and the flight path angle to estimate the angle of attack. The angle of attack estimates were then displayed on a traditional gauge and with a *Pitch Limit Indicator* on the attitude indicator. The background and design of the estimators and displays are described, followed by a description of tests conducted to evaluate them.

Flight tests demonstrated that the speed-based method produced angle of attack estimates that corresponded well with a reference vane in all angles of attack except very high angles. The angle-based method was able to estimate the general trends of angle of attack, but the flight path angle measurement introduced excessive high frequency noise to the estimator. Pilots reported that the speed-based estimator combined with the pitch limit indicator provided a useful stall avoidance cue that was consistent with the dynamic stall speed on the airspeed indicator.

5.1 Angle of Attack and Stall

As described in Section 1.2.1, stall contributed to 10% of all accidents and nearly 14% of all fatal accidents between 1993 and 2000. While many pilots hold to the myth that stall is primarily related to speed, stall is instead a purely geometric issue. Any aerobatic pilot can attest that stall can occur at any attitude and any airspeed if the critical angle of attack is exceeded.

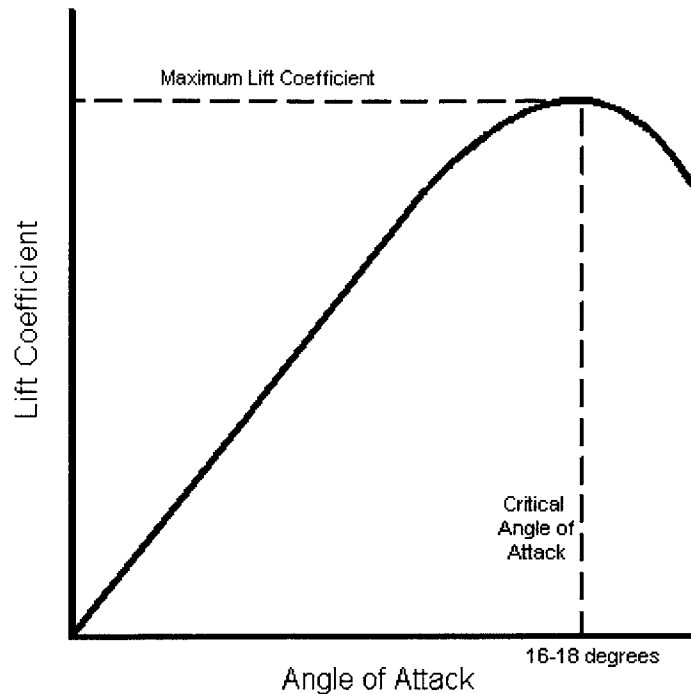


Figure 62: Lift Coefficient vs. Angle of Attack and the critical angle of attack where stall occurs

A typical wing generates lift as a function of the airspeed, air density, shape and size of the wing, and the angle at which the air flows over the wing. This angle is the *Angle of Attack*. As shown in Figure 62, when angle of attack increases, so does lift in a linear fashion. However, at approximately 16-18 degrees angle of attack, the maximum amount of lift is reached. Pushing the angle of attack beyond this critical angle results in separation of the flow around the wing causing a sudden drop in lift, known as *stall*. If aware of when the wing is approaching the critical angle of attack, the pilot can take action to avoid the impending stall.

5.2 Previous Angle of Attack Systems

Despite the fact that angle of attack is a fundamental performance parameter, it is not required to be measured in flight and very few general aviation aircraft are equipped to do so [2]. On military and commercial aircraft, however, angle of attack sensors are more common. The traditional way to measure angle of attack is with a vane that aligns itself with the airflow. On commercial jets, where the engines are under the wings or at the rear of the aircraft, the vanes can be mounted in the fuselage near the nose. On

propeller driven aircraft, the vane must be away from the propeller wake, typically mounted on a boom under or ahead of the wing. Vane systems tend to be expensive, in the \$20,000 range for certified systems, because they involve mechanical moving parts with sensitive sensors that protrude out from the aircraft. Another method for measuring angle of attack avoids the potential problems of moving parts by measuring the pressure distribution on the top and bottom of the wing. This method is less widely used, but is available in both certified and experimental equipment.

To avoid the expense and maintenance of angle of attack vanes or pressure sensors, several attempts were made in the 1970's and 80's to estimate angle of attack from other known measurements. Once such system was developed by an Air Force engineer and flight tested on an F-15 [25]. The Air Force system, like the others, was a lift estimation system, whereby the amount of lift required for the aircraft to be in its current state is estimated, and then the necessary angle of attack for generating that lift is computed using an aerodynamic model of the wing. The Air Force system was demonstrated to be accurate within 0.5 degrees of a reference "truth" measurement, but also required extensive calibration and tuning with the reference system before it could be used confidently.

5.3 Prototype Angle of Attack Estimators

Two angle of attack estimation methods were developed and prototyped for flight tests on a primary flight display. The "Speed-based" method estimates the required lift and the associated angle of attack. The "Angle-based" method estimates angle of attack from the angular difference between where the aircraft is pointed and the direction the aircraft is moving.

5.3.1 Speed-based Estimator

The speed-based system estimates the amount of lift required for flight in the current state and the angle of attack required to generate that lift at the current airspeed. Lift required is calculated by multiplying the current weight by the load factor as measured by the vertical accelerometer. The flow diagram of the speed based estimator is depicted in Figure 63.

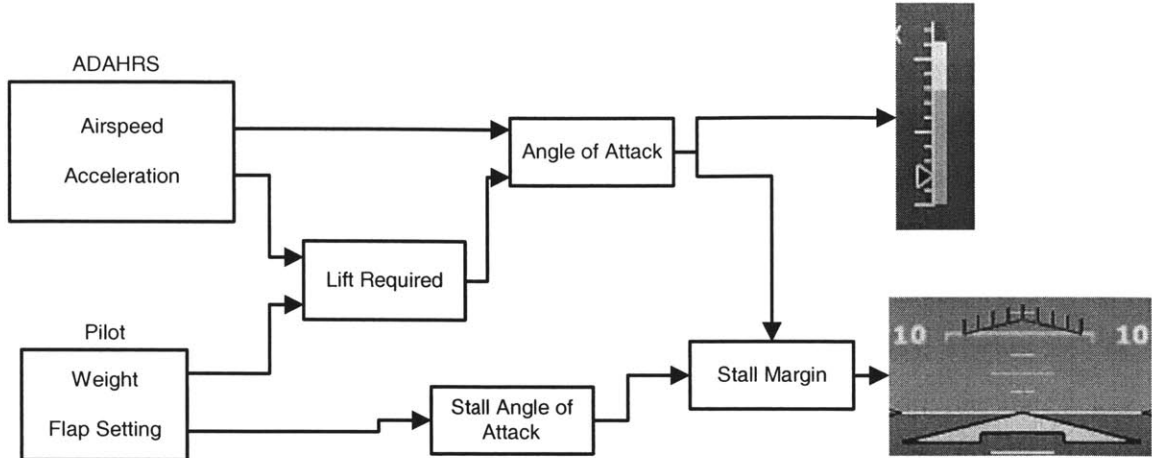


Figure 63: Information flow diagram for the speed-based method

Knowing the amount of lift required and the current airspeed, a simple linear model of the lift coefficient - angle of attack relationship was used to compute the angle of attack. In a mathematical formula, the speed-based method looks like Equation 4, where n is the load factor, W is the weight, and V_{CAS} is the calibrated airspeed. The remaining terms are constants: e is the Oswald efficiency factor of the wing, AR is the aspect ratio, ρ_0 is the standard sea-level air density, and S is the wing area.

$$\alpha = \frac{1 + \frac{2}{eAR} \frac{nW}{\rho_0 S \pi V_{CAS}^2}}{\rho_0 S \pi V_{CAS}^2} \quad (4)$$

The speed-based method has several possible sources of error. First, the method requires an accurate weight estimate. Inaccurate weight estimates are amplified by the slow speed. For example, at 70 KIAS, the estimator will have 0.5 degrees of error for every 100 pounds of weight estimate error, where as at 110 KIAS, the error is only 0.2 degrees per 100 pounds.

Another source of error is that the lift model is a very simplified, and does not account for trim, lift from the horizontal stabilizer, or for center of gravity effects. Moreover, it is impossible to infer the necessary aerodynamic constants without significant flight testing.

5.3.2 Angle-based Estimator

On most general aviation glass cockpits, a weight estimate is not available. To avoid using weight, as well as an aerodynamic model for the wing, the angle-based estimator was developed. The angle-based estimator uses only the geometry of attitude and the flight path vector where the angle of attack is defined as the angular difference between where the aircraft is pointed and where the aircraft is going, as depicted in Figure 64.

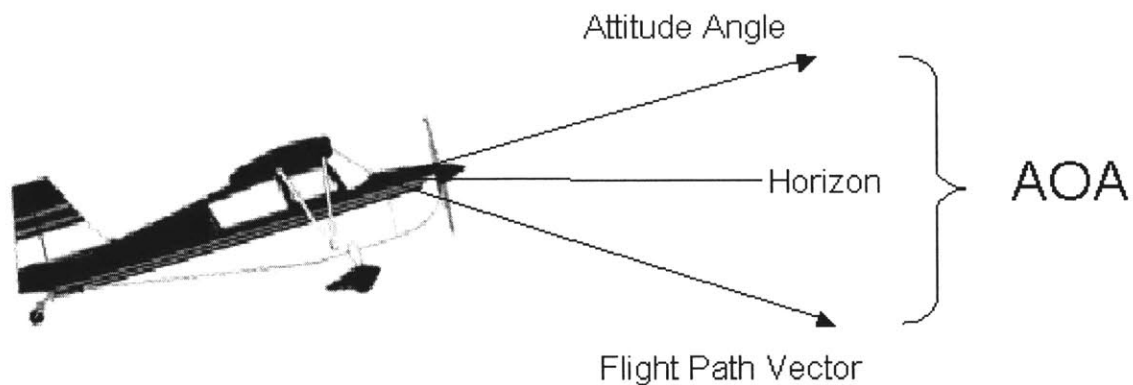


Figure 64: The Angle AOA method finds the geometric difference between the direction the aircraft is pointed and the direction the aircraft is moving⁹

The direction the aircraft is pointed is measured directly from the pitch and roll angles from the ADAHRS. Because angle of attack is with respect to the airmass, the flight path vector is composed of the airspeed and the vertical speed. Since the standard vertical speed measurement is heavily filtered and has a significant lag, an “instantaneous” vertical speed estimator is used to complementarily filter changes in barometric altitude and accelerations in the up-down direction. The flow diagram of the angle-based estimation method is shown in Figure 65.

⁹ Aircraft image modified from <http://www.pilotfriend.com/aircraft%20performance/champion/gallery.htm>

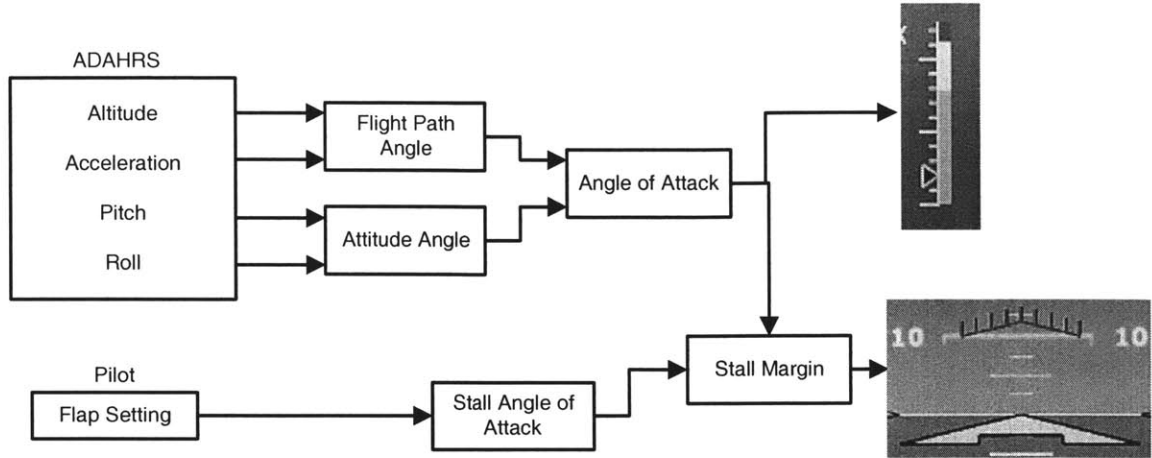


Figure 65: Information flow diagram for the angle-based method

First, flight path angle γ must be calculated based on the instantaneous vertical speed \dot{h} , and true airspeed V_{TAS} , shown in Equation 5.

$$\gamma = \sin^{-1} \frac{\dot{h}}{V_{TAS}} \quad (5)$$

The angle-based method must also account for the difference between the zero-lift angle of attack and the attitude. Since deploying flaps changes the camber, and thus the zero-lift angle of attack of the wing, the flap setting must be accounted for in the angle-based estimator. The equation for the angle-based estimator is thus shown in Equation 6, where θ is the pitch angle, γ is the flight path angle, ϕ is the roll angle, and α_0 is the zero-lift angle of attack for the current flap setting.

$$\alpha = \frac{\theta - \gamma}{\cos \phi} - \alpha_0 \quad (6)$$

The angle method also has its own sources of error, primarily due to the vertical speed component of the flight path angle. First, vertical speed measures static pressure change, and thus cannot observe any vertical wind. Like the weight error in the speed-based method, vertical wind errors are larger at lower airspeeds than at higher airspeeds. At 70 KIAS, for every 500 feet/min of vertical wind, the angle of attack estimate will be off by 4 degrees, whereas at 110 KIAS, it will only be off by 2.6 degrees. There is no way around the vertical wind problem short of installing a pitot tube to measure the vertical wind.

The second problem with the vertical speed is the associated lag. The instantaneous vertical speed filter was designed to reduce this lag, but it cannot eliminate it. Steady flight in smooth air would not result in any errors, but flight during maneuvers or turbulence causes noise in the angle-based method.

The final source of error is that the roll angle will amplify any other errors. For a given pitch and flight path angle, if the aircraft rolls 60 degrees, then the angle of attack and any errors in the estimate will be twice as large as if the wings were level.

5.4 Prototype Angle of Attack Displays

The speed-based and angle-based method estimates were displayed on the primary flight display in two ways; on a traditional gauge with tape with pointer and on a Pitch Limit Indicator. Both of the displays are shown in Figure 66.

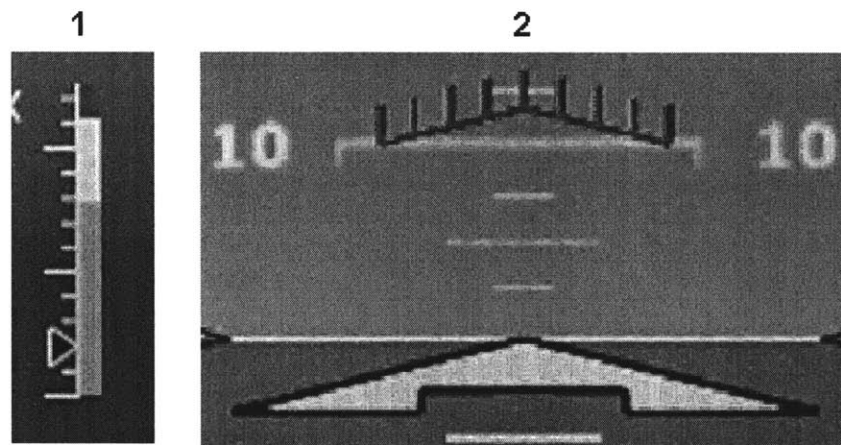


Figure 66: 1) Traditional-design angle of attack indicator 2) Pitch Limit Indicator

The traditional gauge was situated to the lower right of the airspeed tape. A black pointer moves along a white scale marked with ticks in two degree increments, and major tick marks every 10 degrees. The color bands correspond to the speed-based angle of attack estimates at 1g load factor with maximum gross weight at the flaps up and flaps down stall speeds. The green band meets the white band where the flaps up stall occurs and the white band meets the red band where the flaps down stall occurs, reflecting the color coding of the airspeed tape.

The Pitch Limit Indicator is displayed as a red rake that descends toward the aircraft reference symbol as the stall margin shrinks. The shape of the PLI is derived

from the Society of Automotive Engineers standard [26]. The stall margin shown between the aircraft reference and the PLI rake is the difference between the stall angle of attack and the current angle of attack. Since the angle of attack at stall depends on the flap setting, the PLI adjusts itself according to the flap setting delivered to the PFD from the laptop.

5.5 Angle of Attack Flight Tests

Flight tests were conducted with two objectives. First, the accuracies of the speed-based and angle-based estimators were compared to reference angle of attack vane. Second, feedback from the subject pilots was gathered to assess the usability of the traditional AOA gauge and the Pitch Limit Indicator as stall margin indicators.

Table 5: Angle of Attack Flight Test Maneuvers

Maneuver	Flap Configuration	Speed (KIAS)
Straight and Level	Clean	75 for 1 min
Straight and Level	Clean	80 for 1 min
Straight and Level	Clean	100 for 1 min
Straight and Level	Clean	120 for 1 min
Straight and Level	Clean	146 for 1 min
Straight and Level	Clean	Accelerate from 70 to 146
Straight and Level	Clean	Decelerate from 146 to Stall
Straight and Level	Clean	Slow Flight
Straight and Level	Clean	Power-off Stall
Straight and Level	Landing	Slow Flight
Straight and Level	Landing	Power-off stall
Climbing Turn	Landing	Slow Flight
Descending Turn	Landing	Slow Flight
Abrupt Pull Up/Push Down	Clean	130
Steep Turn	Clean	130
Chandelle	Clean	130
Lazy-8	Clean	130

In order to test the accuracy of the estimation methods, a series of steady and unsteady maneuvers were flown, listed in Table 5. In straight and level flight, a set of constant speeds was flown for one minute each to cover the slow and fast regimes of flight. To sweep through the entire speed range, a level acceleration from near stall to

maximum level cruise speed, followed by a level deceleration to a power-off stall was conducted. Slow flight was performed in both clean and landing flap configurations.

Because the angle-based estimator relies on flight path and the speed-based estimator uses the load factor, unsteady maneuvers were also performed. In slow flight, this consisted of climbing and descending turns. At the maneuvering speed, an abrupt pull up and push down, a steep turn, a chandelle, and a lazy-8 were performed.

5.6 Flight Results

To evaluate the accuracy of the angle-based estimator and the speed-based estimator, the time histories of each estimator were compared with the time history of the reference angle of attack vane for the series of steady and unsteady maneuvers listed in Table 5. Because the values of the zero-lift angle of attack, the lift-coefficient slope, and the vane potentiometer gain were not known exactly, the two estimators and the vane were calibrated after the flight testing.

5.6.1 Constant Speed, Constant Altitude

The most basic maneuvers performed were the constant speed, constant altitude maneuvers. Four different speeds were flown (75, 80, 100, 120 KIAS), all with flaps up. The vane and estimator outputs are shown in Figure 67.

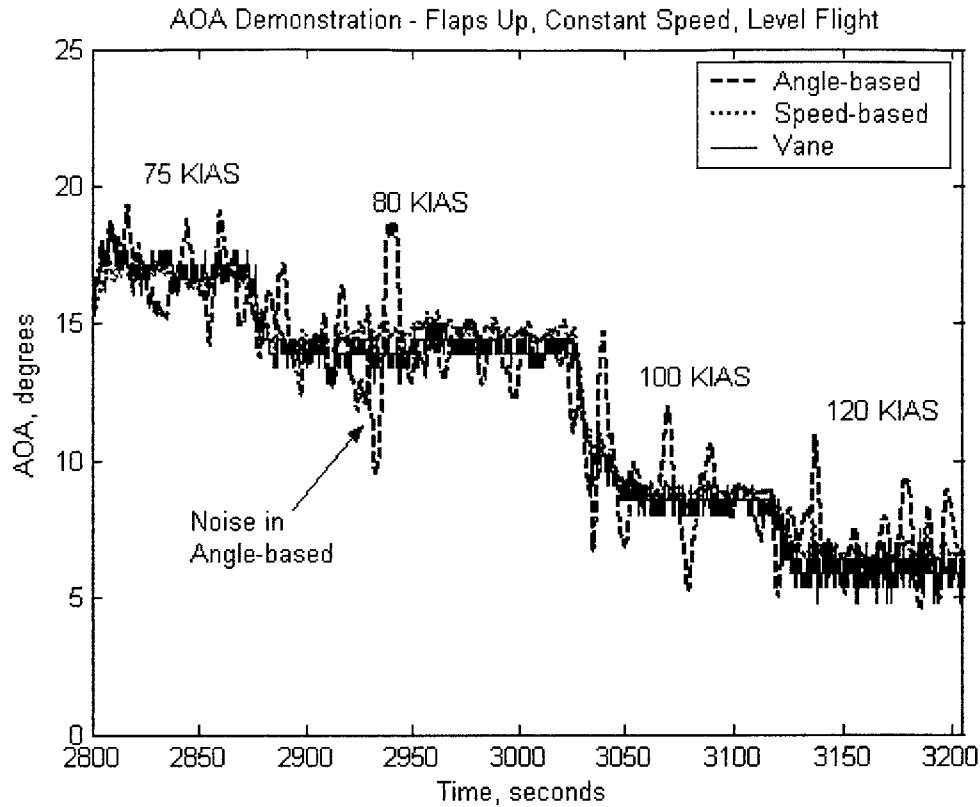


Figure 67: Adjusted vane and estimator outputs at constant altitude, constant speeds

At constant altitude and constant speed, the speed-based estimator was consistent with the vane in both high and low frequencies. The angle-based estimator, on the other hand, followed the general, low frequency trend of the vane, but displayed (relatively) higher frequency noise. Flight conditions on the day of the test included moderate convective turbulence. Since the angle-based estimator relied on a flight path angle estimate that incorporated accelerometer measurements, the high frequency noise reflected the turbulence during the flight as picked up on the accelerometers.

5.6.2 Acceleration and Deceleration at Constant Altitude

Accelerating from near stall speed to maximum level speed and then decelerating back until performing a power-off stall, shown in Figure 68, demonstrated the same trends as the constant speed, constant altitude maneuvers.

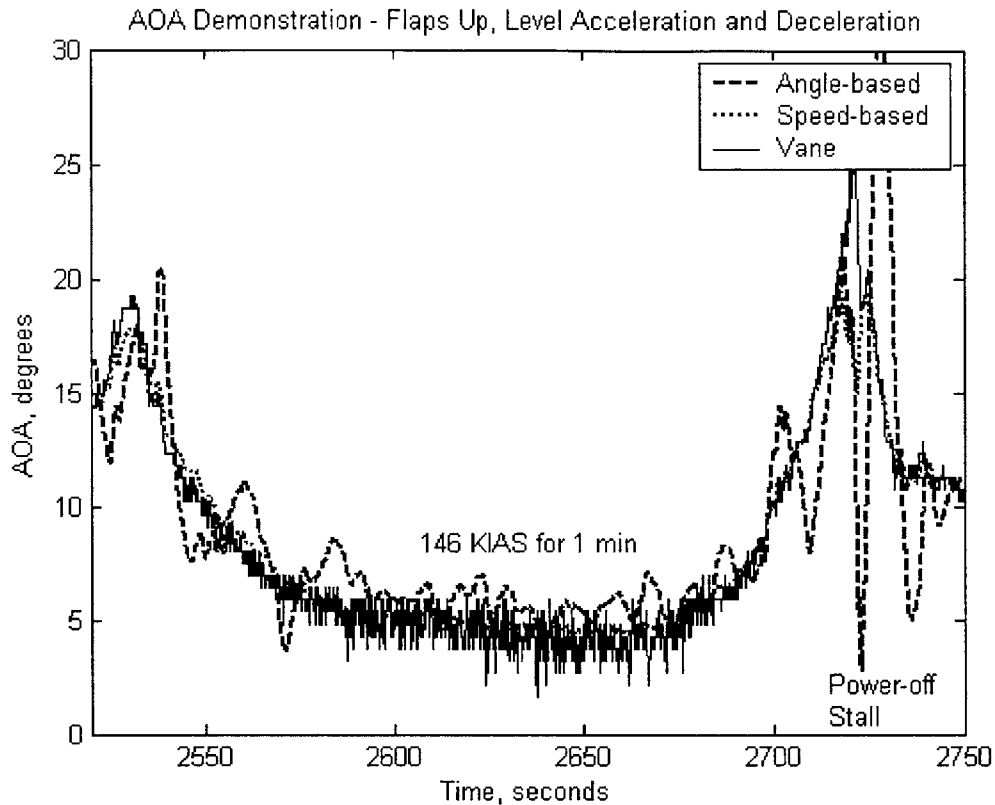


Figure 68: Constant altitude acceleration from slow flight to maximum level cruise, followed by deceleration until power-off stall

During the maneuver, the speed-based estimator closely tracked the vane, while the angle-based estimator tracked the general trend but with high frequency noise. At the point of stall, however, the angle-based estimator error became more pronounced. The power-off stall shown in Figure 68 at 2720 seconds is zoomed in upon in Figure 69.

5.6.3 Power-off Stalls and Slow Flight

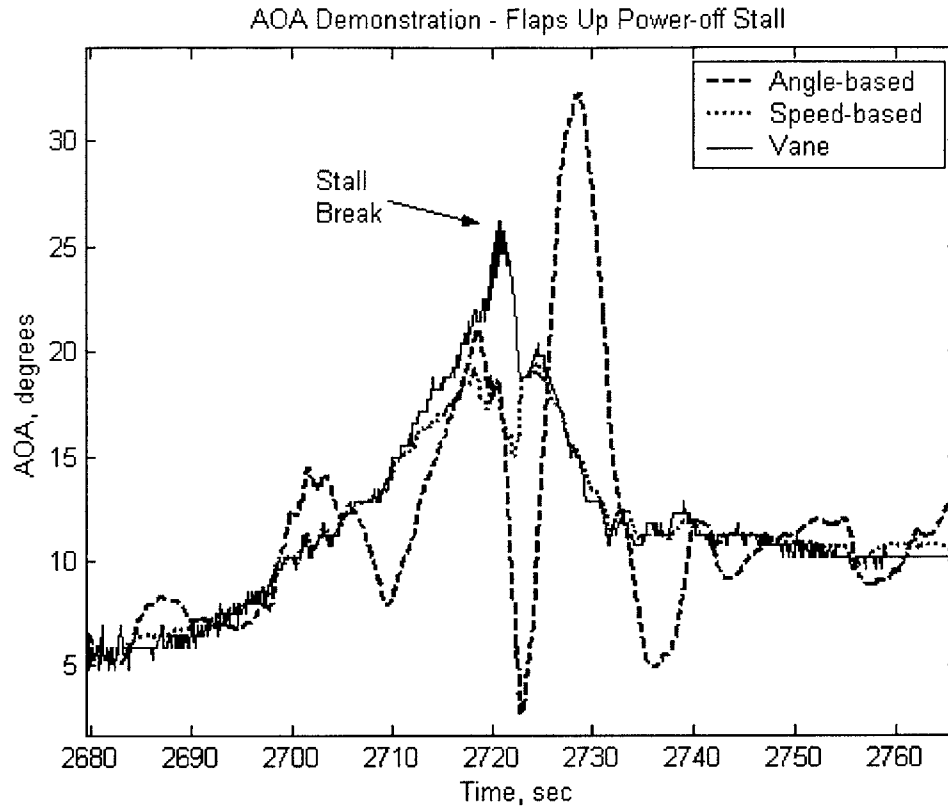


Figure 69: Power-off stall, flaps up.

At the point of stall, the angle-based estimator swung wildly and did not stabilize around the vane measurement until the aircraft had completely recovered from the stall. The speed-based estimator also departed from the vane as the stall approached. There are some caveats, however. The vane shows stall occurring at over 25° angle of attack whereas the actual stall angle of attack for the aircraft is closer to 18° . Also, from the cockpit during the flight, the speed-based estimator used with the pitch limit indicator appeared to show stall occurring just as the margin disappeared.

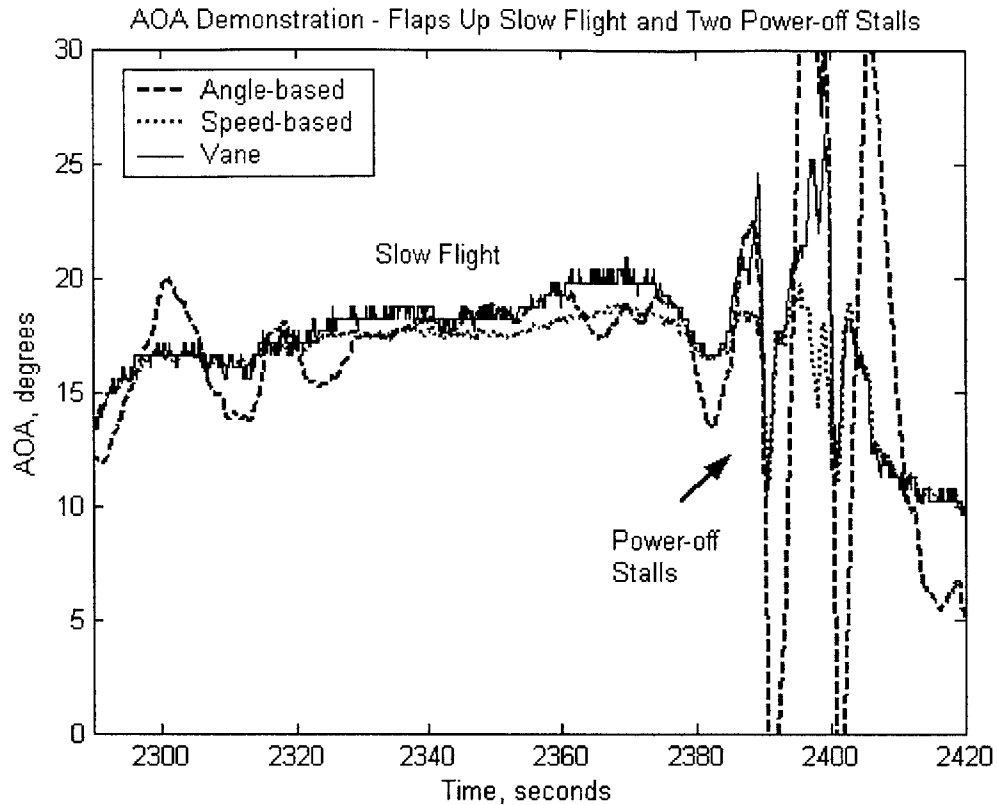


Figure 70: Slow flight and two power-off stalls with flaps up

Figure 70 shows the same behavior during slow flight and two power-off stalls with the flaps up. The speed-based estimator mostly tracked the vane until the vane began approaching 20° at about 2350 seconds. The angle-based estimator tracked the general trend well during slow flight, but fluctuated heavily during the entry to slow flight and the stall. A close-up of the two power-off stalls is shown in Figure 71.

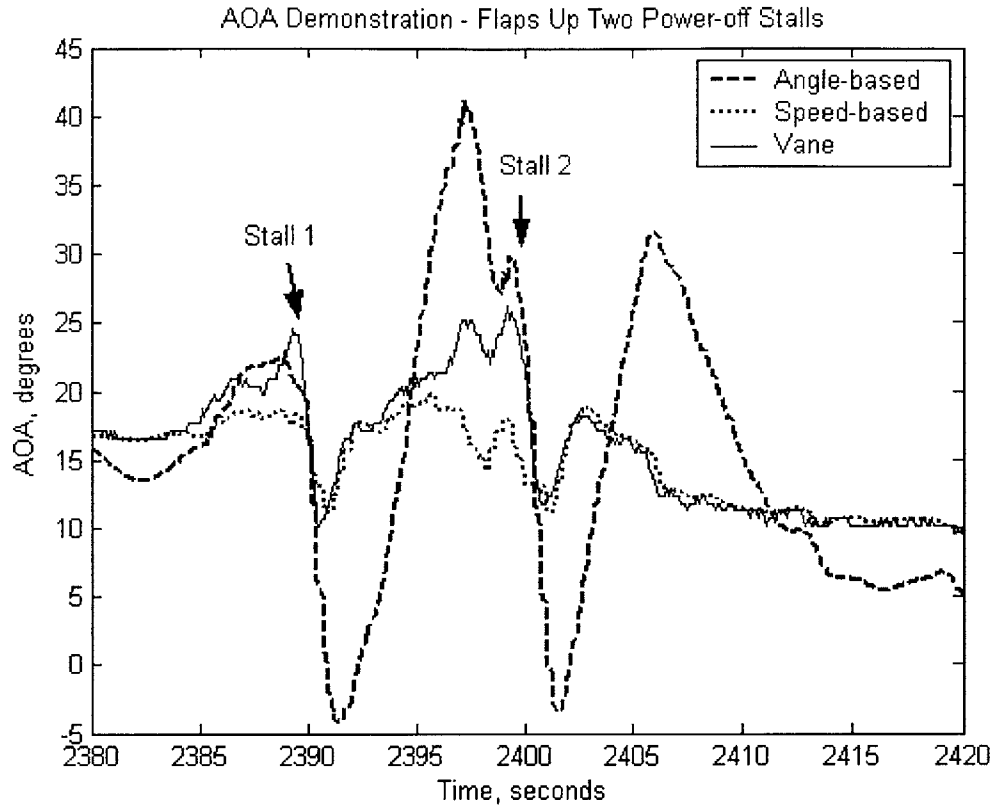


Figure 71: Close-up of two power-off stalls after slow flight with flaps up

Slow flight was also performed with flaps down, shown in Figure 72. As with the flaps up configuration, the speed-based estimator tracked the vane well, while the angle-based estimator fluctuated around the general trend. During the constant altitude portion of the slow flight with flaps maneuver, the angle-based estimator had much smaller errors than it did during the climbing and descending turns, demonstrating the difficulty with accurately and quickly measuring the flight path angle.

During the power-off stall, shown in close-up in Figure 73, the angle-based estimator diverged. The speed-based estimator also separated from the vane, but again, caution is due because the vane measured over 30° angle of attack at stall, well beyond the normal stall angle of 18° .

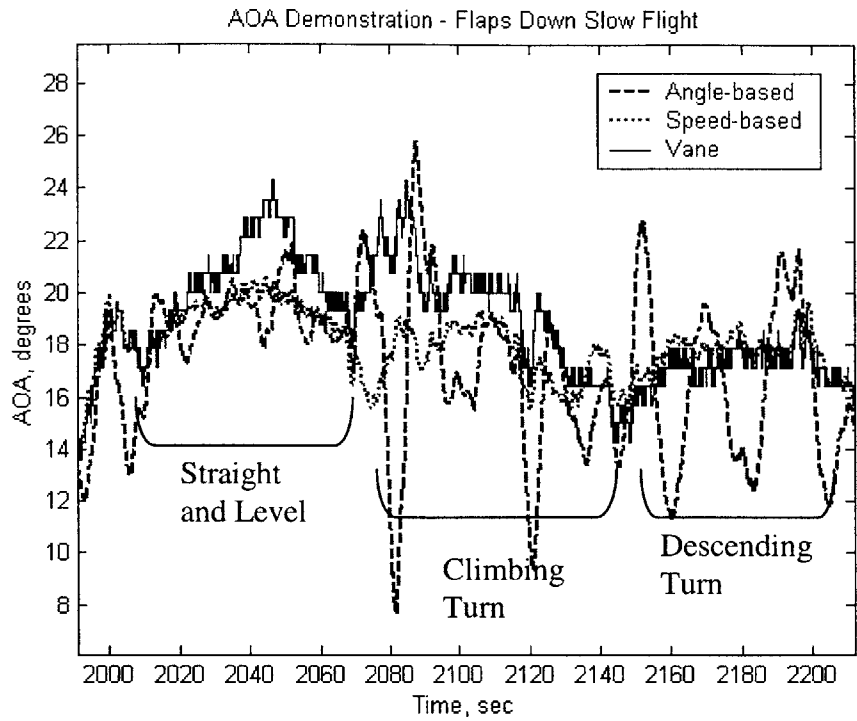


Figure 72: Slow flight, flaps down

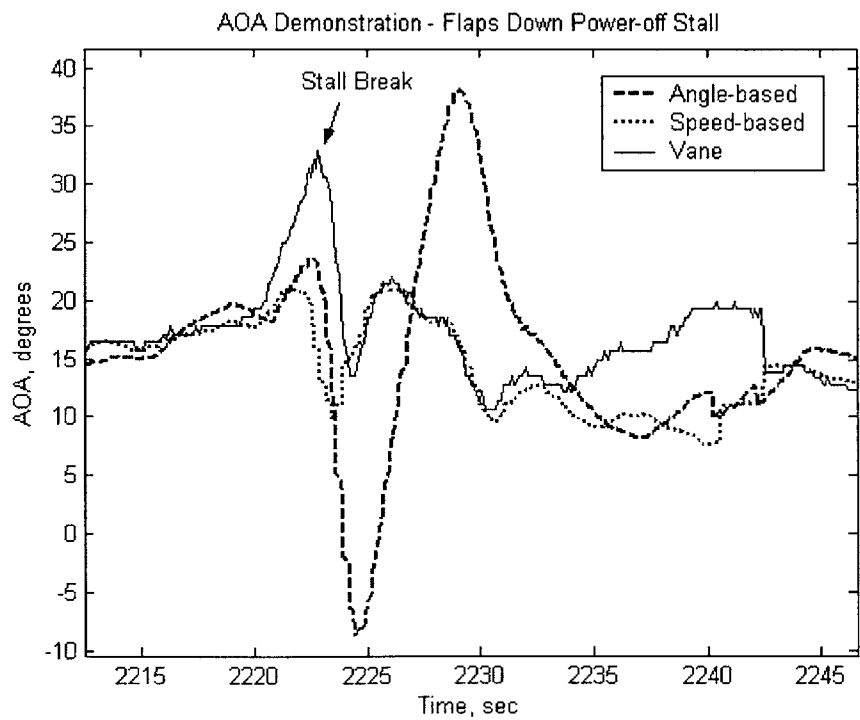


Figure 73: Power-off Stall in slow flight, full flaps down

5.6.4 Abrupt Pull Up/Push Down

The abrupt pull up/push down was used to test the angle-based estimator's sensitivity to sudden changes in flight path angle. As expected from the steadier maneuvers, the angle-based estimator fluctuated wildly during the two pull up/push down maneuvers, as shown in Figure 74. As the pilot pulled suddenly on the stick, the pitch angle increased quickly, but the measured flight path angle lagged behind, resulting in excessively large estimated angles of attack at the beginning of the maneuver. During the push down, the opposite effect took place, when the pitch dropped faster than the measured flight path angle, resulting in large negative estimated angles of attack.

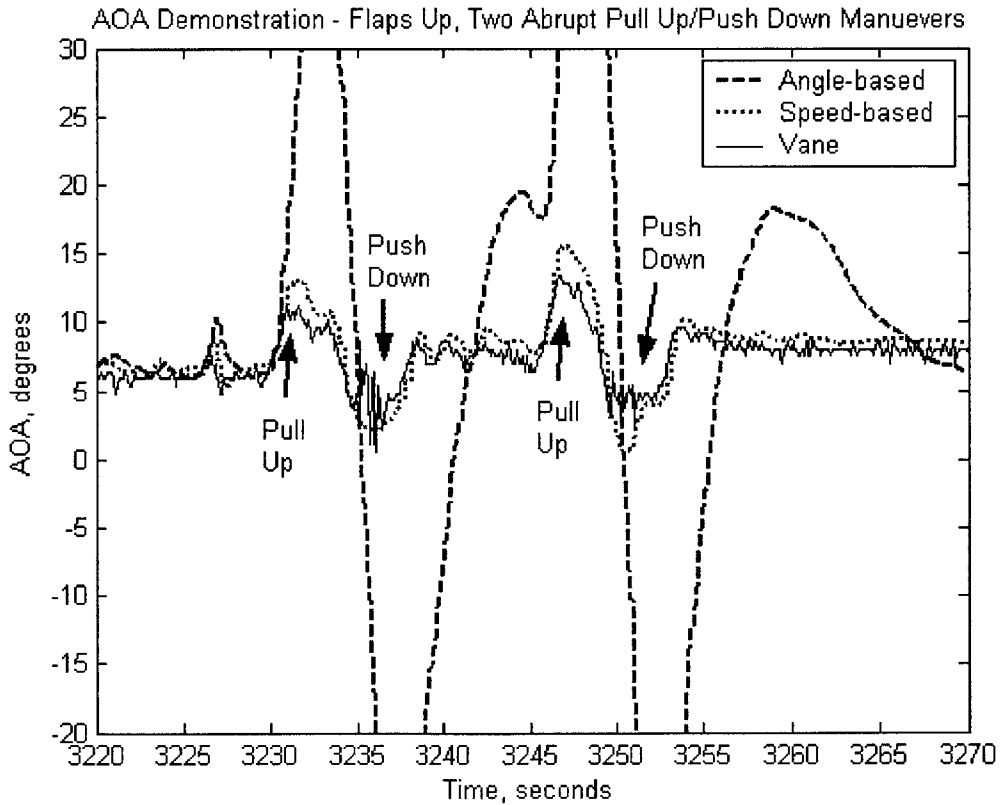


Figure 74: Two pull up/push down maneuvers, flaps up

5.6.5 Steep Turns

Two steep turns were performed, one to the left, the other to the right, shown in Figure 75. During the steep turns, the angle-based estimator fluctuated as it had in all the other maneuvers. Interestingly, the speed-based estimator, which estimated the angle of

attack to be less than the measurement from the vane during the stall maneuvers, estimated a higher angle of attack than the vane during the steep turns.

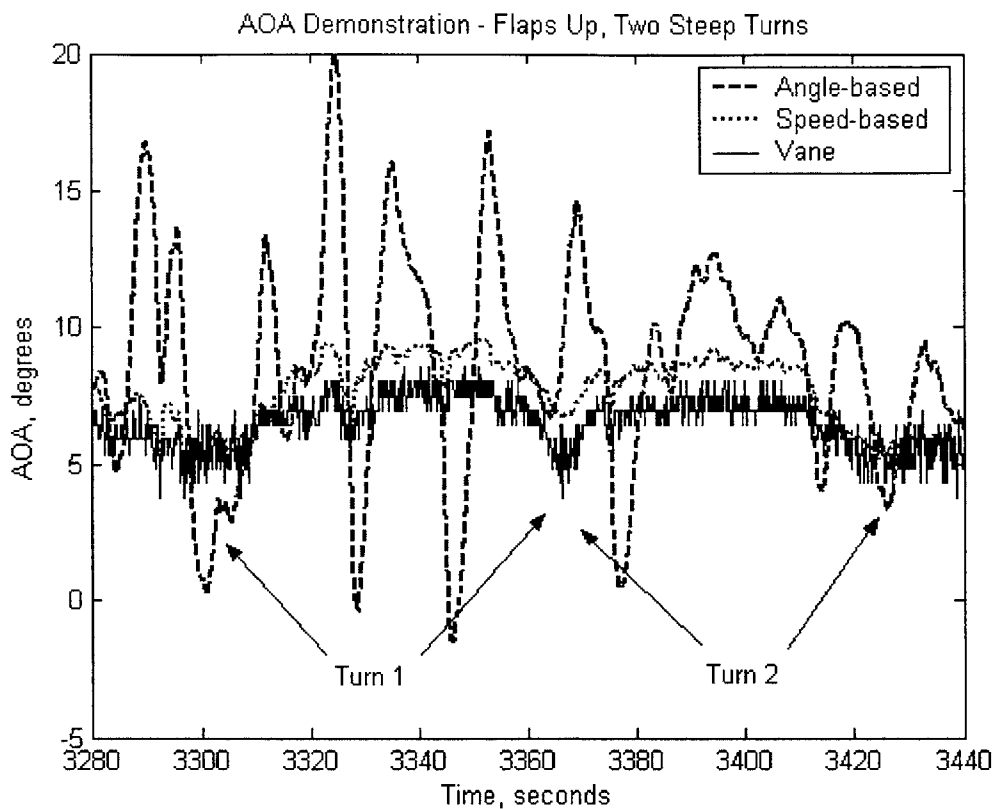


Figure 75: Two steep turns, flaps up.

5.6.6 Chandelle

One chandelle was performed to combine rapid changes in altitude and flight path angle, along with a turn, and high angle of attack at the end of the maneuver. The angle of attack plot for the chandelle is shown in Figure 76. The speed-based estimator, like in the other maneuvers, tracked the vane closely until the vane measures a high angle of attack, when the speed-based estimator estimated lower than the vane. The angle-based estimator also fluctuated widely, initially estimating high as the pilot pulled back hard on the stick during the beginning of the maneuver. Then, as the flight path angle caught up with the pitch, the pilot relieved the back pressure, lowering the pitch below the lagging flight path angle.

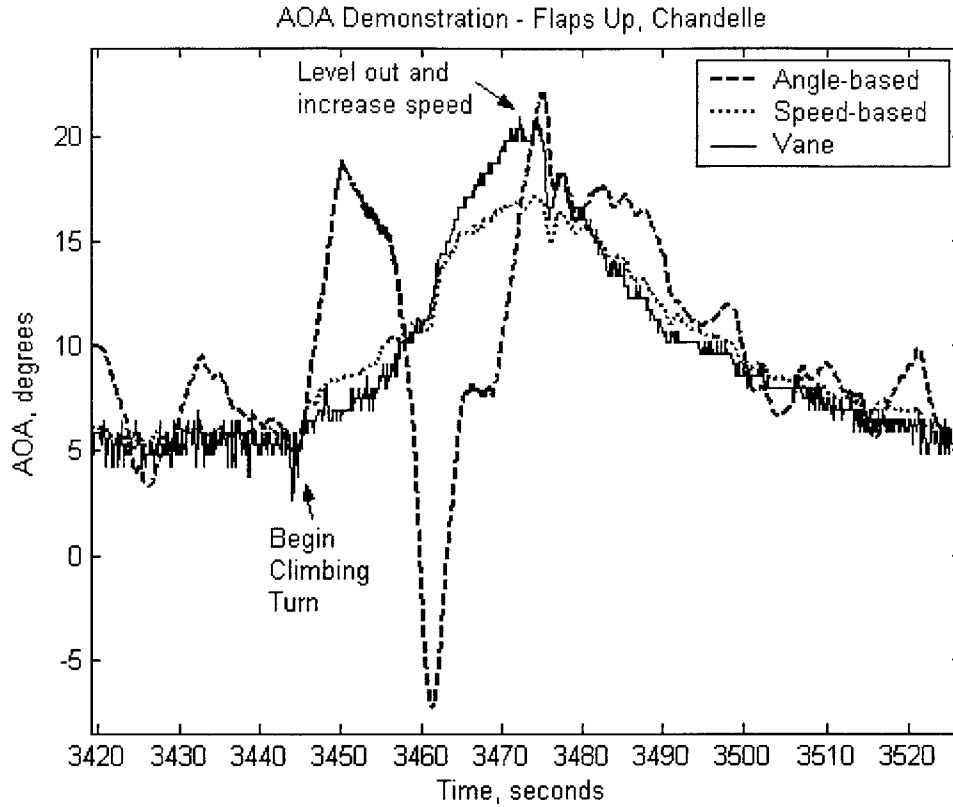


Figure 76: Chandelle, flaps up

5.6.7 Lazy-8

One lazy-8 was performed for the same reason as the chandelle; to test the estimators while changing pitch, flight path angle, roll angle, and load factor. The angle of attack plot is shown in Figure 77. The speed-based estimator tracked very closely to the vane during the entire maneuver. The angle-based estimator demonstrated the same flight path angle lag as during the chandelle, estimating a high angle of attack initially when the pitch rises faster than the flight path angle, then turning negative as the pitch moves below the flight path angle before it can adjust.

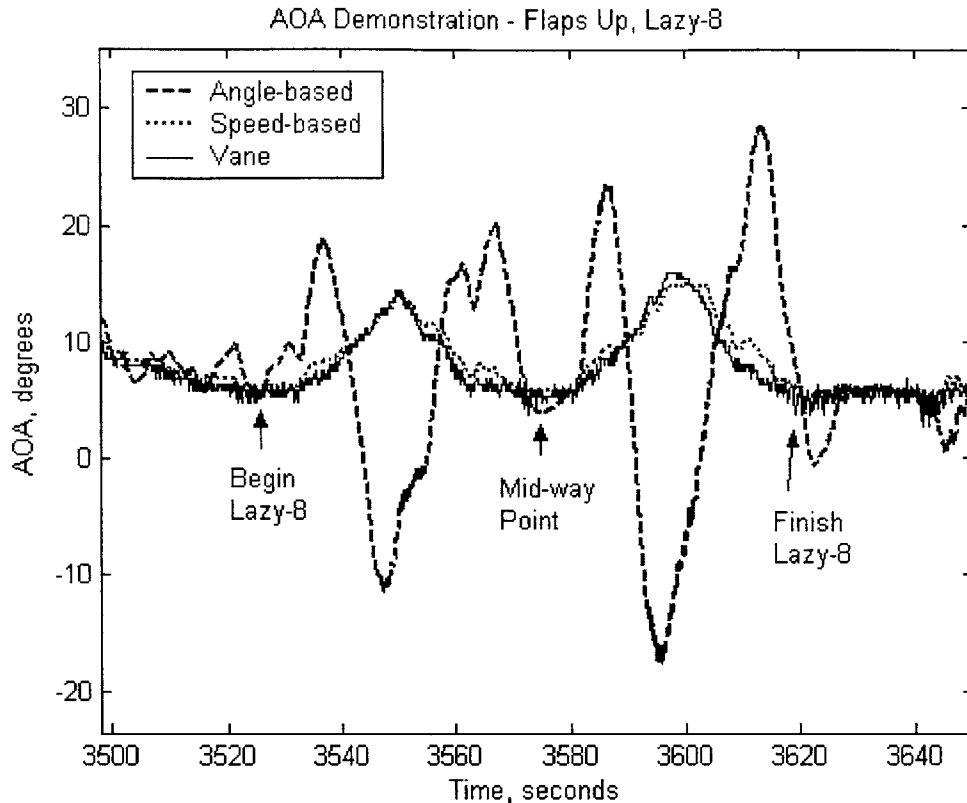


Figure 77: Lazy-8, flaps up

5.6.8 Pilot Feedback on the Pitch Limit Indicator and AOA Gauge

During the maneuvers, pilots were shown both the pitch limit indicator and the AOA gauge. Both used the same estimator as their source at any given point, which alternated between the angle-based and the speed-based estimators.

When using the angle-based estimator, none of the pilots trusted its angle of attack estimate, and thus ignored the indicators. They found the speed-based estimator much more useful and trustworthy. In particular, several reported they preferred using the speed-based estimator with the pitch limit indicator. It was more difficult to observe the actual estimated angle of attack using the PLI, but they were more interested in margin to stall than the actual angle.

The pilots also all said that the PLI should not be displayed all of the time, but instead should only appear as the angle of attack begins to approach stall. At low angle of attack, the margin changes little and it might even be deceptive because the aircraft can pitch well beyond the supposed pitch limit because it has enough energy to do so. One

suggestion was to cue the indicator when airspeed dropped below 1.3 times the dynamic stall speed, much like the Boeing pitch limit indicator [27].

5.7 Conclusion

The speed-based estimator, combined with the pitch limit indicator, is a useful stall avoidance device, even if it is not exactly the angle of attack. In most cases, the speed-based estimator corresponded well with the vane, but it tended to drift away from the vane at high angles of attack. It is unclear whether the speed-based estimator or the vane was more representative of the “true” angle of attack, as the vane was only roughly calibrated. A more detailed follow-on study should perform a much more rigorous calibration of the reference vane to enhance confidence in its measurement. With a fully calibrated vane, the wing lift model could be refined through further flight testing, adding to the estimator’s accuracy. A more accurate weight estimate that changes with fuel burn would also improve the accuracy of the speed-based estimator.

The angle-based estimator did not accurately estimate angle of attack due to lag in the flight path angle derived from an instantaneous vertical speed estimator. The angle-based estimator did, however, show that the general trend of the angle of attack can be determined. It might be possible to use a different instantaneous vertical speed algorithm to reduce the lag, although such an algorithm would rely heavily on the accelerometers, and thus be susceptible to accelerometer noise and turbulence. Even so, the theoretical issue that it cannot account for vertical wind would probably render the angle-based estimator inaccurate even with the best flight path angle estimate possible.

The traditional AOA gauge received a lukewarm response from the pilots involved, with the one exception who liked it also being the former military aviator who was used to flying with angle of attack. Most of the pilots did, however, like using the pitch limit indicator. They felt it served best as a stall margin indicator rather than a method for determining angle of attack. In this sense, the PLI acted as a different format for the exact same information displayed on the dynamic stall speed indicator, but also translated it from speed to pitch for the pilot, and thus reinforced the proper mental model for stall.

Chapter 6 Unusual Attitude Alerting

Unusual Attitude Alerting was designed and implemented on a PFD to aid in the recovery from spatial disorientation. Two types of alerts were used, *Command* alerts that instructed the pilot on the actual recovery procedure and *Informative* alerts that reported the situation, but left the recovery procedure to the pilot. A background on spatial disorientation and verbal alerting systems is presented, followed by the design and test procedures used to evaluate the unusual attitude alerting prototypes.

In flight tests where subject pilots performed simulated instrument recoveries after being disoriented, both alert types were compared to a non-specific alert instructing the pilot only to recover. The pilots found the specific alerting useful, the Command alerts being most useful.

6.1 Spatial Disorientation

As described in Section 1.2.3, spatial disorientation is rare, but almost always fatal. In general, a pilot may become disoriented through illusions in the visual system, vestibular system, or the somatosensory system [6]. The visual system obtains information through the eyes and helps maintain orientation by looking for directional cues, such as horizons. The vestibular system is the set of biological accelerometers in the inner ear, where accelerations are detected by the motion of fluid past very sensitive hairs in ear canals. Finally, the somatosensory system is made up of the nerves all around the body that sense pressure differentials, such as when the body is pressed down in the seat as a result of G-forces.

Most of a person's information about their orientation is derived from the visual system, while the vestibular and somatosensory systems function as high-rate sensors. An illusory horizon, most commonly occurring at night, can induce disorientation, while a clear horizon serves as a steady reference point with which to reset the other systems as they drift.

The vestibular and somatosensory systems are high rate accelerometers, thus prone to drift, and are typically corrected by referring to the visual horizon. In the absence of a horizon, as occurs during flight in IMC, a pilot must learn to trust the instruments over his senses or risk illusions that can be disorienting the pilot. Two well-known illusions are “the leans” and “the graveyard spiral”, both of which result from the fact that the vestibular system cannot sense slow turns well. A pilot may get the leans, the most common of all disorientation illusions, by slowly entering a turn without the vestibular system detecting it. If the aircraft rolls back to straight and level quickly, the pilot will feel like the aircraft is now banking the opposite direction. If the pilot trusts his senses over the instruments, he may try to bank the aircraft back to what was mistakenly perceived as straight and level.

The graveyard spiral also results from the inability to detect slow banking motion. The aircraft enters a shallow bank without being detected by the pilot’s vestibular system, and the aircraft begins to descend. The pilot, thinking that the wings are still level, adds back pressure in an effort to regain altitude. But being in a bank, the back pressure tightens the spiral, resulting in a steeper bank and more altitude loss. Unless the pilot uses the instruments to roll back to level, the spiral will diverge until it becomes a high-speed steep dive into the ground.

Spatial disorientation can also occur in the pitch axis as well as in roll. The “Inversion Illusion” occurs during a sudden change from a climb attitude to straight and level, causing the vestibular illusion of tumbling backwards.

When the pilot is well trained to trust the instruments, spatial disorientation can usually be avoided. Unfortunately, some pilots make the fateful decision to continue flying visually as they enter IMC, accounting for 41% of all spatial disorientation accidents between 1994 and 2003. Eighty-three percent of those accidents involved VFR-rated pilots, but instrument training does not completely eliminate the risk, as evidenced by the remaining 17% that involved instrument rated pilots.

Spatial disorientation accidents can also occur in VMC, accounting for 33% of all spatial disorientation accidents in 1994-2003. Sixty-six percent of those accidents occurred at night. The remaining 26% of all spatial disorientation accidents occurred during IFR flight in IMC, at least 46% of which involved instrument failures.

After becoming disoriented when the instruments are functional, the pilot must trust the instruments, otherwise he risks flying into an *Unusual Attitude* and losing control of the aircraft. The leans or a graveyard spiral may induce a steep bank. In heavy disorientation, when the visual cues from the instruments and the vestibular cues conflict, and the pilot may become so confused that he cannot make a recovery decision. A third vote from another sensory system, the audio system, may be possible to break the tie and help the pilot recover correctly from unusual attitudes and spatial disorientation.

6.2 Audio Altering

Audio alerting is widely used in aviation, more so in military and commercial aviation than in general aviation. Some audio alerting systems are simple tones, others are voices that convey complicated messages. The most common audio alert, and one that can be useful during spatial disorientation, is the stall horn. Acting as a crude but effective angle of attack sensor, the stall horn is typically a simple mechanical device that buzzes when the airflow over the leading edge of the wing exceeds an angle of attack limit. The stall horn is very effective in helping pilots know when they are approaching the stall threshold.

More advanced audio alerting systems use speech to convey information. In general aviation, the most common are traffic and ground proximity alerts. Most traffic alert systems will provide simple verbal alerts, such as “Traffic! Traffic!” while more advanced systems provide specific data, such as “Traffic 6 o’clock! Low! One mile!” [28].

Human factors research has demonstrated the value of speech commands in urgent commands and advisories [29]. In particular, two studies showed that combining a visual display with a voice warning resulted in faster response times than a visual display and non-speech warning. Combining specific speech advisories or commands in conjunction with the attitude indicator can help break the cognitive freeze induced by spatial disorientation and aid in recovery to a straight and level attitude.

6.3 Prototype Unusual Attitude Alerting

In order to address the problem of spatial disorientation, an auditory alerting system that provides specific verbal information to aid in recovery from an unusual attitude was prototyped and flight tested. Using pitch and roll information obtained from the PFD, the verbal cues are triggered whenever a pitch or roll limit is exceeded. When an alert is called, it can either be played as a *Command* or an *Informative* statement.

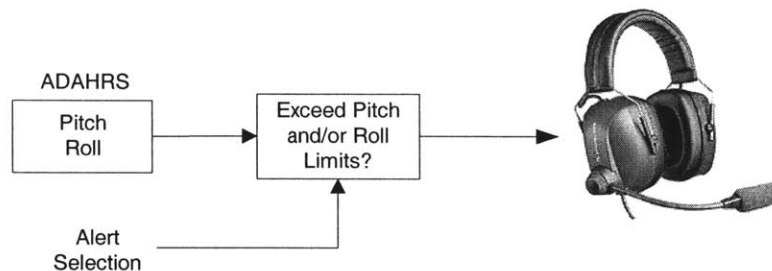


Figure 78: Unusual Attitude Alerter System Design¹⁰

The basic functionality of the unusual attitude alerter is shown in Figure 78. Since the PFD does not have an audio interface, the alerter was implemented on the laptop computer, which reads ADAHRS telemetry from the PFD. When a pitch or roll limit is crossed, an alert is created and queued to play over the intercom through the laptop sound card. For this prototype, pitch and roll limits slightly less than the aerobatic limits were used:

- Pitch $+20^{\circ}/-10^{\circ}$
- Roll $\pm 45^{\circ}$

The pitch and roll alerts, when used in combination, were played in the order of recovery priority. A high pitch alert always sounds first, then an excessive roll alert, followed by a low pitch alert. Figure 79 demonstrates this as well as the *Informative Statement* and *Command* types of alerts that the operator may select on the laptop. The attitude depicted on the left is a low pitch attitude and an excessive roll to the right. Since excessive roll takes priority over a low pitch attitude, the informative statement is “Steep Right Bank! Nose low!” Conversely, the attitude depicted on the right is a high

¹⁰ Headphones image from http://www.aircraftspruce.com/menus/av/headsets_sennheiser.html

pitch attitude and an excessive roll to the left. Since high pitch takes priority over roll, the command is "Push Down! Roll Right!"

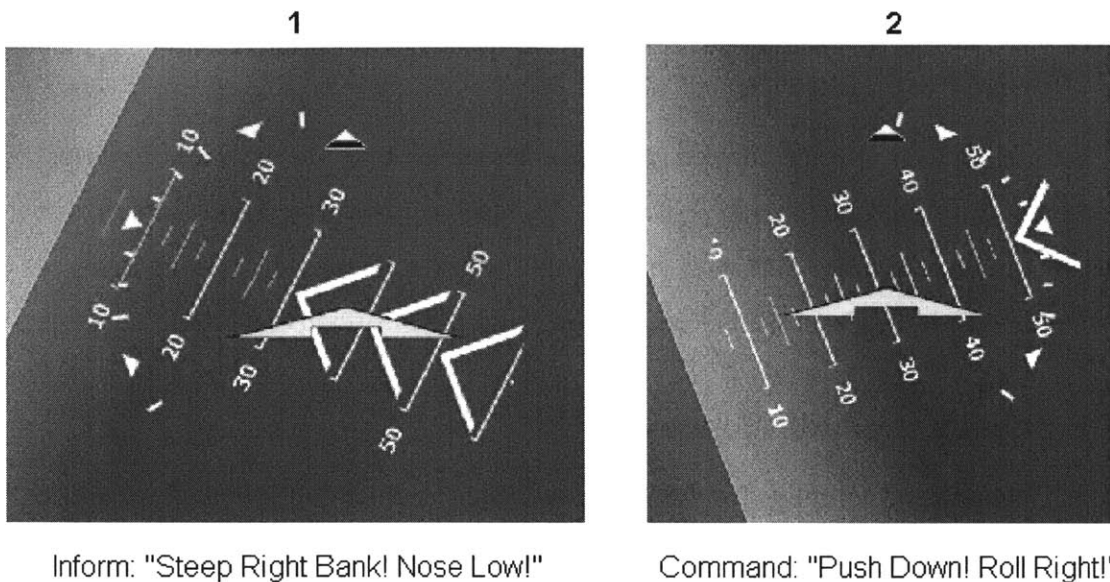


Figure 79: 1) Informative alert 2) Command alert

6.4 Unusual Attitude Alerting Flight Tests

In order to evaluate the usefulness and usability of a verbal unusual attitude alerting system, the prototype was flight tested by comparing four subject pilots' unusual attitude recoveries performed with and without the specific command and informative statements.

Each unusual attitude test flight consisted of a Pilot-In-Command (PIC), a Subject Pilot, and a Flight Test Engineer (FTE). The subject pilots wore foggles to simulate instrument conditions. The subject pilot then closed his eyes and lowered his head. The PIC then asked the subject pilot to perform a series of maneuvers, such as a standard rate turn or a pitch change or some number of degrees, which the subject pilot attempted while flying blind. Eventually, the aircraft entered an unusual attitude, as defined by the pitch and roll limits. At that point, the subject pilot heard an alert over the intercom, and then opened his eyes and recovered using the PFD displays and the alert.

Three different alerts were used. The command set, such as "Pull Up! Roll Left!", the informative set, such as "Nose low! Steep Right Bank!", and a default alert

that simply said “Your airplane.” The “your airplane” alert let the pilot know when he could open his eyes and recover, but did not provide any information about the actual attitude.

6.5 Flight Test Results

Four subject pilots performed simulated instrument unusual attitude recoveries using the unusual attitude alerting prototype. Each subject performed three sets of unusual attitude recoveries, one with the default “Your Airplane” alert serving as a baseline, one with the Command alerts, and one with the Informative alerts.

6.5.1 Unusual Attitude Maneuvers

The pitch and roll plots for the “Your Airplane” segment of Subject 4 recoveries is shown in Figure 80. The other two subject pilots’ performance plots look roughly the same.

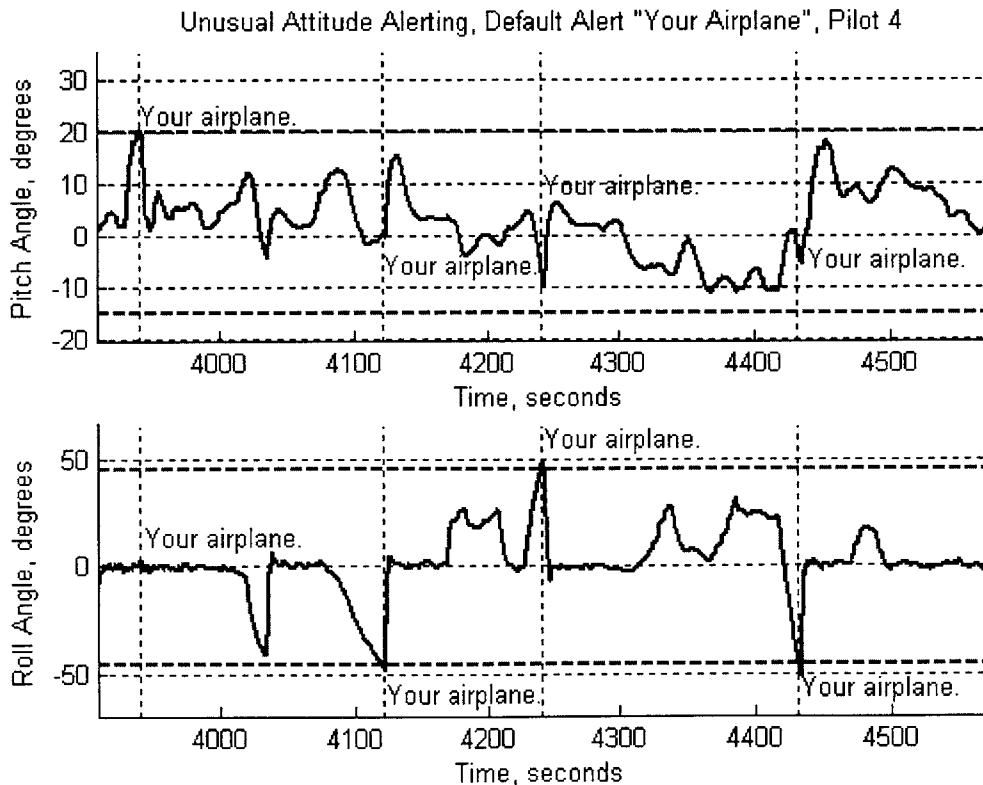


Figure 80: Default Unusual Attitude Alert, Subject 4

The pitch angle time history is shown on the top, and the roll angle time history is shown on the bottom. The pitch and roll thresholds for triggering the unusual attitude alerts ($+20^{\circ}/-15^{\circ}$ pitch, $\pm 45^{\circ}$ roll) are depicted with the dashed horizontal lines on both pitch and roll plots. When an alert was triggered, a vertical dashed line is shown along with the text of the auditory alert.

From these plots of the default “Your Airplane” alerts, it can be seen that Subject 4 initially had a high pitch warning at approximately 3930 seconds. The second alert was triggered by an excessive left bank at approximately 4120 seconds, followed by an excessive right bank at about 4340 seconds. The last alert was triggered again by an excessive left bank occurring at about 4430 seconds.

These plots also show the recovery decision made by the pilot after the alert. Here the pilot makes the correct decision for all the alerts, and quickly returns to wings level and pitch within $+10^{\circ}/-5^{\circ}$.

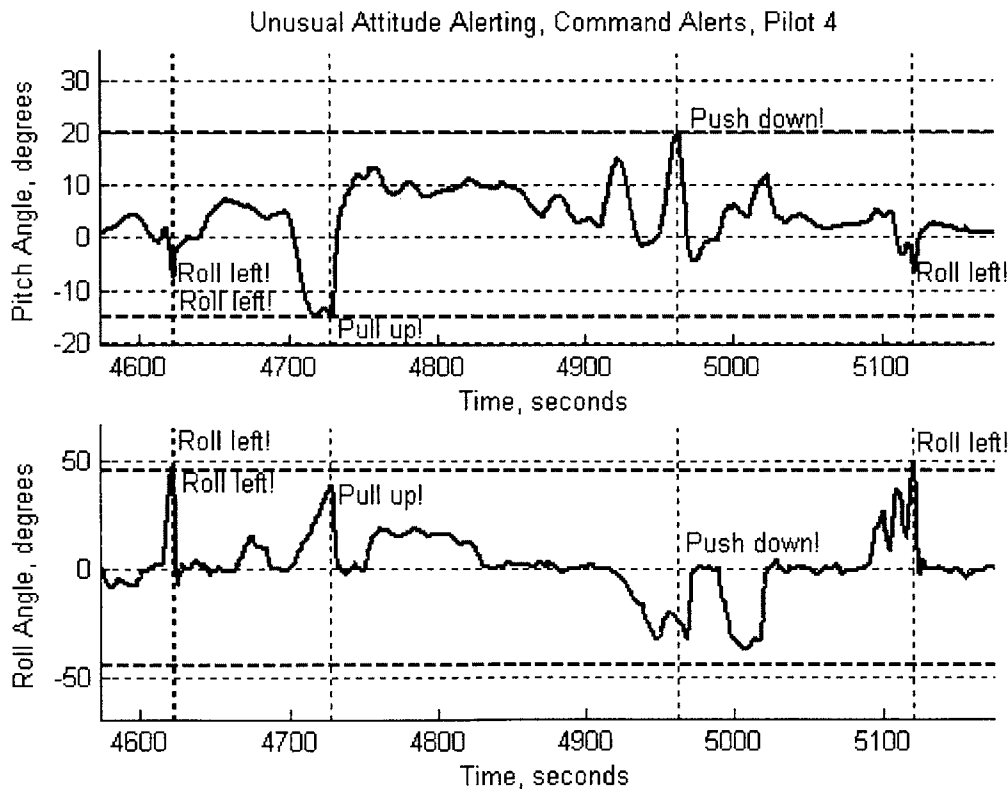


Figure 81: Command Unusual Attitude Alert, Subject 4

Figure 81 shows the same plotting format for the Command alert segment of Subject 4's unusual attitude recoveries. The first alert provides an example of a repeated alert. When the roll exceeded 45° to the right for longer than it took to play the "Roll Left!", the alert was repeated a second time, after which the roll was within the limits and the alert ceased playing.

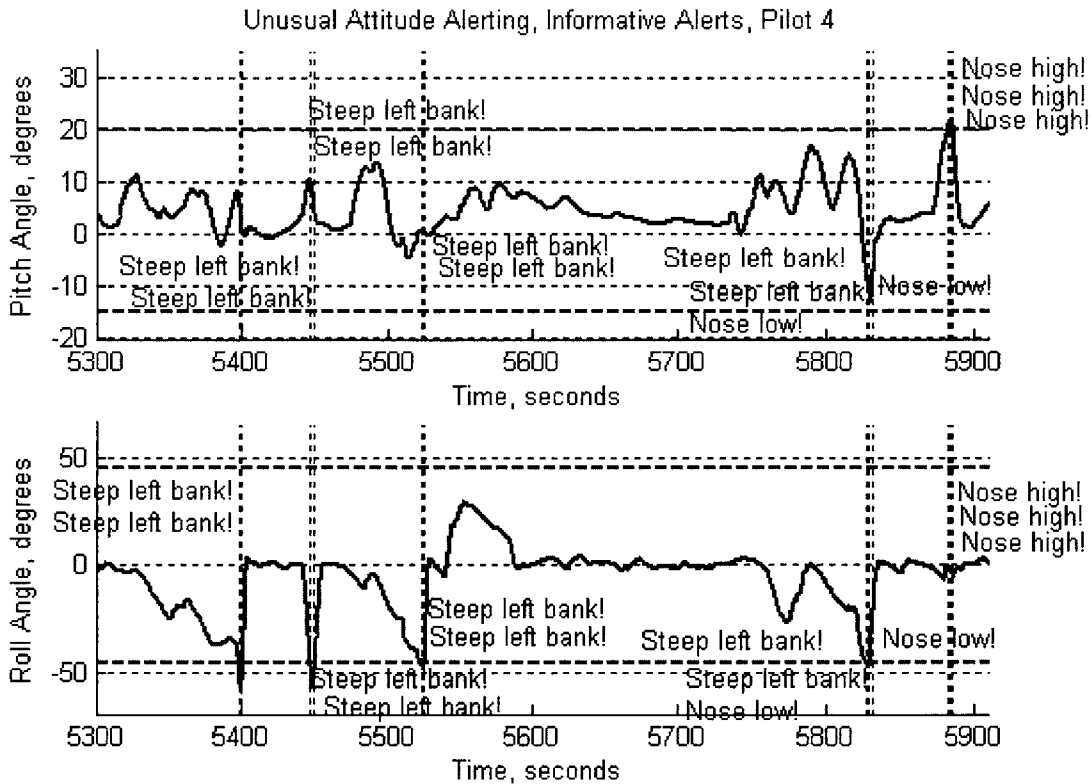


Figure 82: Informative Unusual Attitude Alert, Subject 4

Figure 82 depicts the Informative unusual attitude alerts, and shows additional repeated alerts as well as a combination alert. At approximately 5830 seconds, the aircraft was banking excessively to the left, resulting in a "Steep Left Bank!" alert. Then, while the excessive bank condition still existed, the nose was pitched down too low as well. The combination alert "Steep Left Bank! Nose Low!" was then played. The pilot responded with the correct recovery order, first rolling out of the bank, then pulling the nose up.

6.5.2 Pilot Feedback

All of the subject pilots believed the specific Command and Informative alerts were more useful in aiding recovery than the unspecific “Your Airplane” alert. Pilot 3 believed the alerts “may be helpful for a distracted pilot, definitely would be helpful for a disoriented pilot.”

All of the pilots preferred the Command alerts to the Informative alerts, including the pilot who predicted before the flight that he would prefer the Informative alerts. While all the pilots commented that they never used the auditory alert alone to recover, Pilot 4 explained that the command alerts “pre-loaded” the decision he was about to make, but he still had to interpret the instruments to determine the best recovery procedure.

Pilot 1, who served as PIC during some of the unusual attitude flights but not as a Subject Pilot, was the only one who said he would prefer an alert that only told him to “Check Attitude” and prompt the pilot to look at the attitude indicator and use it to recover. Several others commented that an operational system would also need some way to mute it when a pilot does not want to hear the alerts, for instance, when practicing steep turns.

One pilot observed the limited nature of the prototype during a recovery where the pitch was high as well as the bank. The Command alert would be “Push Down! Roll Left!”, even though the proper procedure is to let the aircraft yaw to bring the nose down, then roll out of the bank.

6.6 Conclusion

Auditory alerts were observed to be useful in aiding pilots recovering from unusual attitudes induced by spatial disorientation. The pilots preferred Command alerts to Informative alerts, but an Informative system would be easier to deploy. A system using Informative alerts could be simply adapted from the prototype, with the only changes being additional support for inverted flight and the ability to mute the system.

A Command alerts system, the type preferred by most subject pilots, needs more development to be more intelligent about recovery technique. Extremely steep attitudes or inversions require different recovery procedures than the simple commands used in

this prototype. The Command system of this prototype also does not have any way to measure or command power setting. In standard unusual attitude recovery procedure, power is added during a high pitch attitude, while power is reduced during a low pitch attitude. To remedy this, some combination of power and airspeed, possibly stall margin, could be incorporated to formulate more precise recovery commands.

Chapter 7 Summary of Conclusions

This thesis demonstrated the potential of several prototype enhancements to a PFD that can improve general aviation safety in the areas of takeoff and climbout, stall, and spatial disorientation.

Assisting the pilot in performing published takeoff distance calculations is a simple and effective way to help prevent accidents caused by exceeding performance limits of an aircraft. Such a system should be implemented on an MFD and incorporated with a weight and balance calculation to obtain the most accurate takeoff distance predictions. Additionally, takeoff performance deficiencies can be detected as early as the peak acceleration immediately after throttle-up. Comparing the peak acceleration to a “required peak acceleration” for lifting off within the runway distance or to an “expected acceleration” based on flight conditions could provide simple “Go/No Go” cues to the pilot early in the takeoff. Predicting takeoff distance in real-time was also shown to be possible within ± 200 feet by 55 KCAS using a simple constant average acceleration assumption. A more rigorous acceleration prediction algorithm using the same general design could improve the accuracy of the prediction further.

Displaying dynamic stall, climb, and glide speeds were all very useful to the subject pilots. By allowing the flaps down and flaps up stall speeds to move with weight and load factor on the airspeed indicator, pilots were more aware of their margin for stall, especially during accelerated maneuvers such as turns. Likewise, displaying the best rate of climb speed, best angle of climb speed, and best glide speed was also useful to pilots as memory aids and targets. Adding too many speed targets can clutter the airspeed indicator, however, so the climb and glide speed displays should be cued to engine power, such that the climb speeds display only when the engines are at full power and the glide speed displays only in an engine-out situation.

The speed-based angle of attack estimator and the pitch limit indicator were observed to be a useful stall avoidance aid that is also consistent with the dynamic stall

speeds on the airspeed indicator. With some calibration, the speed-based estimator calculated an approximate angle of attack very close to the angle of attack measured from a vane.

Finally, verbal unusual attitude alerting was observed to be useful for aiding recovery during disorientation. The alerts supplemented the attitude indicator and helped the pilot decide the recovery technique. Alerts that Command the recovery were preferred by the pilots, but a Command system is also the most complicated to implement, requiring more robust recovery procedures to cover the wide array of possible attitudes as well as engine power settings.

Appendix A – Previous Takeoff Monitor Displays

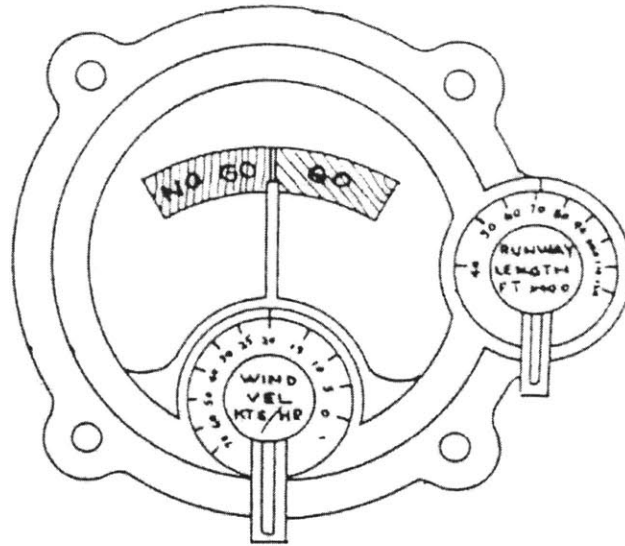


Figure 83: An analog Go/No Go acceleration-based indicator, reproduced in [12]

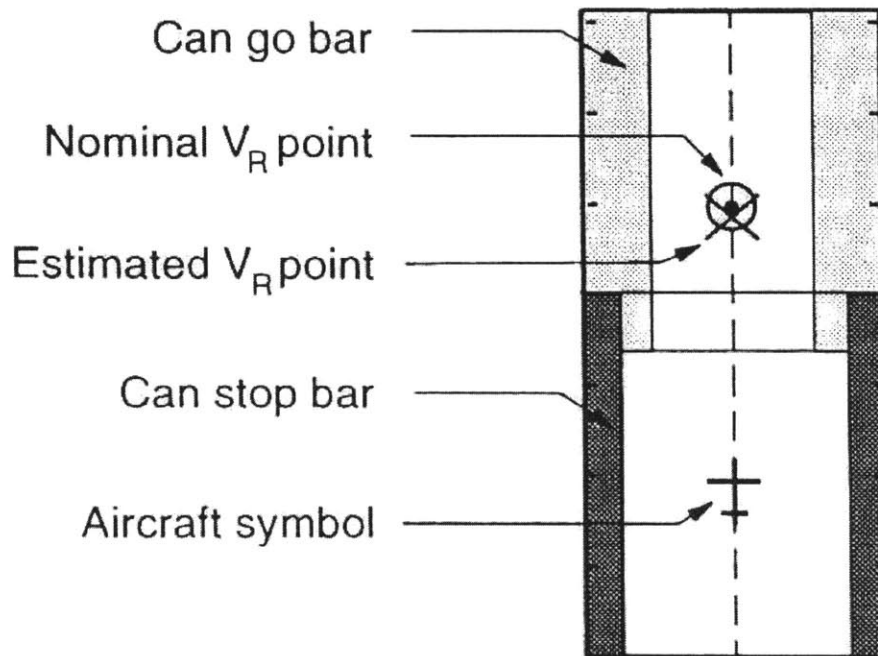


Figure 84: Khatwa's TOPM display, reproduced in [12]

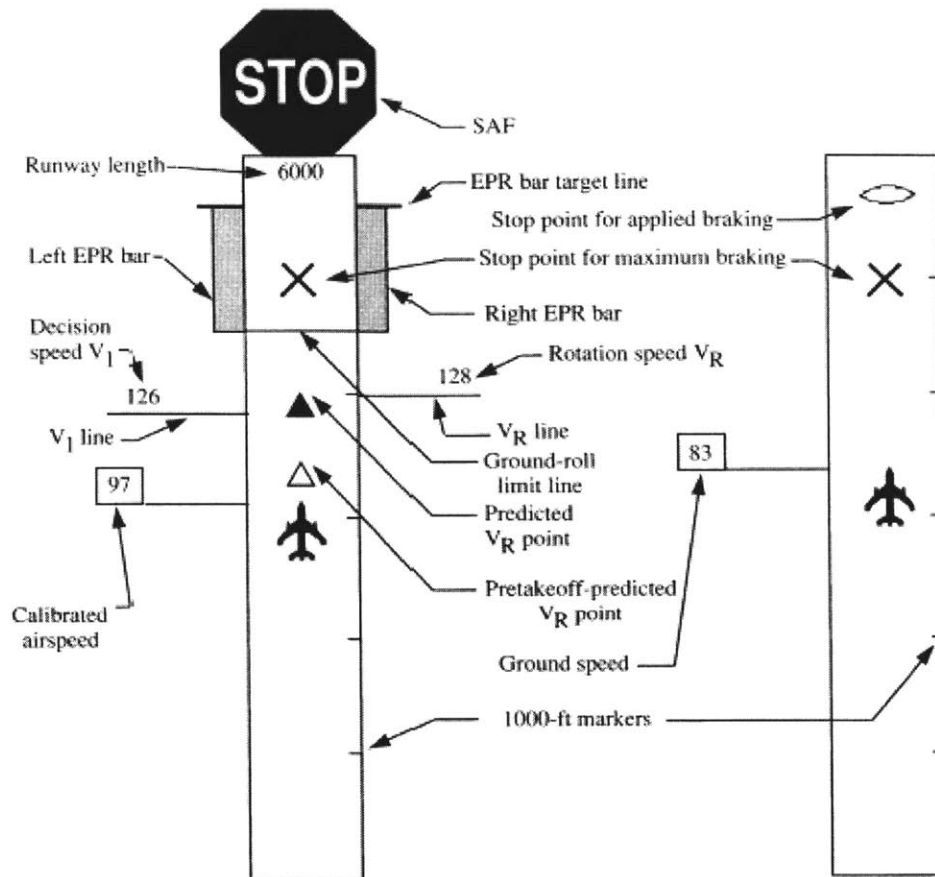


Figure 85: NASA Langley's TOPM to be displayed on the HSI. Left side is what is displayed while accelerating, right side is displayed if braking [30].

Works Cited

1. "Technically Advanced Aircraft: Safety and Training" AOPA Air Safety Foundation, 2005. <http://www.aopa.org/asf/publications/topics/>
2. "Stall/Spin: Entry point for crash and burn?" AOPA Air Safety Foundation. 2003. http://www.aopa.org/asf/publications/topics/stall_spin.pdf
3. AOPA Air Safety Foundation *2003 Nall Report*
<http://www.aopa.org/asf/publications/03nall.pdf>
4. AOPA Air Safety Foundation *2002 Nall Report*
<http://www.aopa.org/asf/publications/02nall.pdf>
5. AOPA Air Safety Foundation *2001 Nall Report*
<http://www.aopa.org/asf/publications/01nall.pdf>
6. "Spatial Disorientation: Confusion that Kills" AOPA Air Safety Foundation Safety Advisor, Physiology No. 1, 2004.
7. Pinder, S.D., Crowe, T.G., Nikiforuk, P.N. "A Lumped Parameter Model of Turboprop Aircraft Operating on Gravel Runways" AIAA A01-37327, 2001.
8. Lowry, John T. *The Performance of Light Aircraft*. Reston, VA: AIAA. 1999.
9. 2000 GA Accident Aircraft Data Used in Annual Review.
<http://www.nts.gov/aviation/Stats.htm> Accessed 29 Apr 2005.
10. Khatwa, R. "The Development of an Efficient Takeoff Performance Monitor (TOPM)." Proceedings ICAS 92 Beijing, Vol 1, 1992. 219-241.
11. NTSB Identification DCA82AA011. National Transportation Safety Board. "Aviation Accident Synopses" <http://www.nts.gov/ntsb>. Accessed 19 Mar 2005.
12. Zammit-Magnion, D., Eshelby, M. "Display requirements for enhanced situational awareness during takeoff" *Enhanced and Synthetic Vision 2002*. Jacques G. Verly, Ed. Proceedings of SPIE Vol. 4713, 2002.
13. Society of Automotive Engineers. Aerospace Standard AS-8044. "Takeoff Performance Monitor (TOPM) System, Airplane, Minimum Performance Standards For" 1987.
14. Khatwa, R., Verspay, J.J.L.H. "Flight Simulator Evaluation of Takeoffs Conducted With and Without a Takeoff Performance Monitor (TOPM)" Proceedings ICAS 94 Anaheim, Vol 2, 1994. 1328-1339.

15. Srivatsan, R., Downing, D.R., Bryant, W.H. "Development of a Takeoff Performance Monitor" NASA Technical Memorandum 89001, N86-21591, August 1986.
16. Khatwa, R. "The Development of an Efficient Takeoff Performance Monitor (TOPM)." Proceedings ICAS 92 Beijing, Vol 1, 1992. 219-241.
17. Wallace, L.E. "Airborne Trailblazer – Two Decades with NASA Langely's 737 Flying Laboratory," NASA SP-4216, 1993.
18. McKenna, J.T. "NASA Develops System to Monitor Aircraft Performance on Takeoff" *Aviation Week & Space Technology* 13 Nov 1989. pg 43-50.
19. Milligan, M.W., Zhou, M.M., Wilkerson, H.J. "Monitoring Airplane Takeoff Performance: Prototype Instrument with Learning Capability" *Journal of Aircraft* Vol. 32, No. 4, 1995, pp. 768-772.
20. Pinder, S.D., Crowe, T.G., Nikiforuk, P.N. "A Practical Investigation of a Takeoff Performance Monitor for Turboprop Aircraft" AIAA A01-37086, 2001.
21. Craig, D.R. "Two Takeoff Monitor Display Designs" MIT 16.422 Final Project (unpublished), 2004.
22. Garmin: GNS 430 Specifications. <http://www.garmin.com/products/gns430/spec.html> Accessed 6 May 2005.
23. Garmin: GPS 92 Specifications. <http://www.garmin.com/products/gps92/spec.html> Accessed 6 May 2005.
24. Airbus A320 Pilot Manual.
25. Zeis, Joseph E. "Angle of Attack Estimation Using an Inertial Reference Platform" AIAA 88-4351-CP.
26. Society of Automotive Engineers. ARP4102/7 Appendix A. "Electronic Display Symbology for EADI/PFD" 1988.
27. Cashman, J.E., Kelly, B.D., Nield, B.N. "Operational Use of Angle of Attack on Modern Commercial Jet Airplanes." *Aero Magazine* Seattle:Boeing Commercial Airplanes Group. October 2000.
28. Ryan International Corporation: Products: Traffic: 9900BX. http://www.ryaninternational.com/products/traffic_9900BX.html Accessed 6 May 2005.
29. Stokes, A.F., Wickens C., Kite, K. *Display Technology: Human Factors Concepts*. Warrendale, PA: Society of Automotive Engineers. 1990.

30. Middleton, D.B., Srivatsan, R. "Evaluation of a Takeoff Performance Monitoring System Display" *Journal of Guidance* Vol. 12, No. 5, 1989, pp. 640-646.